Consistent modelling of transport processes and travel times - coupling soil hydrologic processes with StorAge Selection functions

Robin Schwemmle[1] and Markus Weiler[2]

[1]Albert-Ludwigs-University Freiburg
[2]University of Freiburg, Germany

February 27, 2023

Abstract

Understanding the transport processes and travel times of pollutants in the subsurface is crucial for an effective management of drinking water resources. Transport processes and soil hydrologic processes are inherently linked to each other. In order to account for this link, we couple the process-based hydrologic model RoGeR with StorAge Selection (SAS) functions. We assign to each hydrological process a specific SAS function (e.g. power law distribution function). To represent different transport mechanisms, we combined a specific set of SAS functions into four transport model structures: complete-mixing, piston flow, advection-dispersion and advection-dispersion with time-variant parameters. In this study, we conduct modelling experiments at the Rietholzbach lysimeter, Switzerland. All modelling experiments are benchmarked with HYDRUS-1D. We compare our simulations to the measured hydrologic variables (percolation and evapotranspiration fluxes and soil water dynamics) and the measured water stable isotope signal (18O) in the lysimeter seepage for a period of ten years (1997-2007). An additional virtual bromide tracer experiment was used to benchmark the models. Additionally, we carried out a sensitivity analysis and provide Sobol indices for soil hydrologic model parameters and SAS parameters. Our results show that the advection-dispersion transport model produces the best results. And thus, advective-dispersive transport processes play a dominant role at Rietholzbach lysimeter. Our modelling approach provides the capability to test hypotheses of different transport mechanisms and to improve process understanding and predictions of transport processes. Overall, the combined model allows a very effective simulation of combined flux and transport processes at various temporal and spatial scales.

Consistent modelling of transport processes and travel times – coupling soil hydrologic processes with StorAge Selection functions

Robin Schwemmle[1] and Markus Weiler[1]

[1]Hydrology, Faculty of Environment and Natural Resources, University of Freiburg, Freiburg, Germany

Corresponding author: Robin Schwemmle (robin.schwemmle@hydrology.uni-freiburg.de)

Key Points:

- Transport processes and the selection of appropriate StorAge Selection (SAS) functions depend on the considered soil hydrological processes
- Using a coupled-SAS approach representing advection-dispersion tranport by power law distribution function explains the transport of ^{18}O and bromide in a grassland lysimeter better than other transport representations
- The complete-mixing transport based on uniform SAS functions and a coarse vertical discretization may lead to errors in tracer arrival
- Choice between static or time-variant StorAge Selection differently affects parameter sensitivity of hydrologic model and transport model

Abstract

Understanding the transport processes and travel times of pollutants in the subsurface is crucial for an effective management of drinking water resources. Transport processes and soil hydrologic

processes are inherently linked to each other. In order to account for this link, we couple the process-based hydrologic model RoGeR with StorAge Selection (SAS) functions. We assign to each hydrological process a specific SAS function (e.g. power law distribution function). To represent different transport mechanisms, we combined a specific set of SAS functions into four transport model structures: complete-mixing, piston flow, advection-dispersion and advection-dispersion with time-variant parameters. In this study, we conduct modelling experiments at the Rietholzbach lysimeter, Switzerland. All modelling experiments are benchmarked with HYDRUS-1D. We compare our simulations to the measured hydrologic variables (percolation and evapotranspiration fluxes and soil water storage dynamics) and the measured water stable isotope signal (^{18}O) in the lysimeter seepage for a period of ten years (1997-2007). An additional virtual bromide tracer experiment was used to benchmark the models. Additionally, we carried out a sensitivity analysis and provide Sobol indices for hydrologic model parameters and SAS parameters. Our results show that the advection-dispersion transport model produces the best results. And thus, advective-dispersive transport processes play a dominant role at Rietholzbach lysimeter. Our modelling approach provides the capability to test hypotheses of different transport mechanisms and to improve process understanding and predictions of transport processes. Overall, the combined model allows a very effective simulation of combined flux and transport processes at various temporal and spatial scales.

Plain Language Summary

Knowledge about transport velocities of solutes through the soil is fundamental for an effective protection of drinking water resources from different pollution sources. We subsume transport velocities by the concept of travel times which is time from entering to leaving the soil. The calculation of travel times is based on the combination of a model representing the soil-vegetation-

atmosphere continuum and model representing the dynamics of solute ages based on probability distributions. The predictive accuracy of our calculations are satisfactory and travel times can be effectively estimated in space and time.

1 Introduction

Understanding the underlying transport processes of solutes, such as nitrate or pesticides, in soils is crucial for an effective management of drinking water resources. Thereby, solute transport and soil hydrologic processes, including percolation of soil water, root water uptake or runoff generation processes, are inherently linked to each other (e.g. Hrachowitz et al., 2016, Sprenger et al., 2019). The quantification of solute transport is still challenging and a unified approach considering flow and transport processes is still missing. Travel times are a widely used concept to enable the quantification of transport processes. They describe the time period of water parcels from entering (e.g. by infiltration) to leaving (e.g. by evapotranspiration, groundwater recharge) a system (e.g soil). Travel time distributions can inter alia be used to disentangle slow (e.g. transport through soil matrix) from fast transport (e.g. transport through macropores) (Benettin et al., 2015b; Sprenger et al., 2019).

In order to simulate water-bound transport of solutes in soil, two types of models can be discerned. On the one hand, physically-based transport models (e.g. Hansen et al., 2012; Köhne et al., 2004; Larsbo and Jarvis, 2005; Sternagel et al., 2019) provide information at high spatial and temporal resolution and important insights into process understanding of solute transport, once they are realistically parameterized. However, realistic parameterization requires detailed information on the modelled system (e.g. soil properties), which are usually not available in adequate spatial resolution. Moreover, estimation of solute breakthroughs or travel times requires the application of particle tracking which is computational expensive (e.g Brinkmann et al., 2018). On the other hand,

66 travel-time-based transport models try to include the calculation of travel times in their modelling
67 procedure and the empirical linkage between travel times and solute transport provide useful in-
68 formation about the soil transport patterns. However, they also simplify the transient processes of
69 solute transport in soils. In recent years, travel-time-based transport models using StorAge selec-
70 tion (SAS) functions (Rinaldo et al., 2015) have particularly emerged in solute transport studies
71 (e.g. Asadollahi et al., 2020; Asadollahi et al., 2022; Kumar et al., 2020; Nguyen et al., 2022;
72 Rigon and Bancheri, 2021). They can be distinguished into pure-SAS (e.g. Benettin and Bertuzzo,
73 2018) and coupled-SAS approaches (e.g. Heße et al., 2017). Pure-SAS models rely on measured
74 storage states (e.g. soil water content) and input/output fluxes (e.g. streamflow) and represent un-
75 derlying hydrologic processes in a lumped way, whereas coupled-SAS models link simulated
76 fluxes and storages from hydrologic models with SAS functions. A prerequisite for coupled-SAS
77 models is an appropriate model structure, i.e. a model structure that contains all relevant hydro-
78 logical processes of the considered hydrological system. Unlike pure-SAS models, coupled-SAS
79 models only require a upper boundary condition (e.g. precipitation, potential evapotranspiration)
80 and can be applied as lumped (e.g. Hrachowitz et al., 2013) or spatially-distributed predictions
81 (e.g. Jing et al., 2020).
82 Since Botter et al. (2011) has introduced the master equation, pure-SAS models have widely been
83 applied at the plot scale (e.g. Asadollahi et al., 2020; Asadollahi et al., 2022; Queloz et al., 2015)
84 and catchment scales (e.g. Benettin et al., 2015a; Benettin et al., 2017; Harman, 2015; Wilusz et
85 al., 2020). Thereby, pure-SAS models successfully reproduced measured solute or stable isotope
86 concentrations in lysimeter seepage or streamflow. Due to spatial heterogeneity, travel times at
87 plot scale derived by pure-SAS models differed from those at catchment scale (Queloz et al., 2015).
88 At the plot-scale, pure-SAS modelling experiments with isotope and flourobenzol tracers modeled

found that tracer transport is realistically explained if soil water percolation was dominated by old water (Asadollahi et al., 2020; Asadollahi et al., 2022; Queloz et al., 2015).

In contrast to pure-SAS models, coupled-SAS models were applied mainly applied at the catchment scale (e.g. Benettin et al., 2017; Jing et al., 2020; Kumar et al., 2020; Nguyen et al., 2022; Yang et al., 2019) to predict conservative (e.g. deuterium) and non-conservative solute transport (e.g. nitrate). In these studies, simulations were compared to measured concentrations at the catchment outlet. Those integrate all processes and hence only allow for a non-direct, spatially-implicit analysis of internal transport processes (e.g. groundwater recharge). Furthermore, using a non-conservative instead of a conservative tracer blurs the analysis of underlying transport processes due to inherent interaction between transport and biogeochemical processes. To date, coupled-SAS models have neither been applied at the plot scale nor evaluated with plot-scale observations.

In this study, we couple the soil hydrologic model RoGeR (Runoff Generation Research; Steinbrich et al., 2016) with SAS functions. We assign SAS functions to each implemented hydrologic process and test different transport hypotheses (e.g. piston, advection-dispersion) represented by different model structures, each evaluated by a sensitivity analysis using the Sobol method. We use bromide and isotope data from the Rietholzbach lysimeter in Switzerland (Menzel and Demuth, 1993; Seneviratne et al., 2012b). Similar to other studies investigating travel times at the plot scale (e.g. Asadollahi et al., 2020; Sprenger et al., 2016), we provide a benchmark comparison with HYDRUS-1D.

We will address three main research questions: (i) What are the sensitivities of hydrologic model parameters and SAS parameters for the different transport model structures using a coupled-SAS

approach? (ii) Which transport model structure explains isotope and bromide transport at the Rietholzbach lysimeter most realistically? (iii) What are the advantages of a coupled-SAS transport model compared to a physically-based transport model?

2 Study site

The Rietholzbach lysimeter is situated within the pre-alpine Rietholzbach research catchment, Switzerland (Hirschi et al., 2017; Seneviratne et al., 2012b). The lysimeter is located at an elevation of 755 m above sea level and climatic characteristics can be summarized by an average air temperature of 7.1 °C, average annual precipitation of 1459 mm and annual actual evapotranspiration of 560 mm. The weightable lysimeter container is filled with the local gleyic cambisol and has an entire depth of 2.5 m (Figure 1). A 0.5 m thick layer of sand and gravel at the bottom of the lysimeter enables free drainage. The 3.14 m^2 lysimeter surface is covered by grass, which is cut at similar times as the surrounding grassland. We use hydrometeorological data and bi-weekly bulk samples of the stable water isotope oxygen-18 ($\delta^{18}O$) in precipitation and lysimeter seepage from Seneviratne et al. (2012b). Data gaps in $\delta^{18}O$ of precipitation have been filled with data from nearby GNIP station St. Gallen (GNIP, 2023) and using Piso.AI (Nelson et al., 2021). Additional model evaluation was possible by including data from a bromide tracer experiment (Menzel and Demuth, 1993) carried out from November 1991 to February 1993. Due to data availability, our study investigates bromide transport the period from November 1991 to February 1993 (see Sect. 3.4) and bromide and ^{18}O transport for the period from January 1997 to December 2007 (see Figure 1).

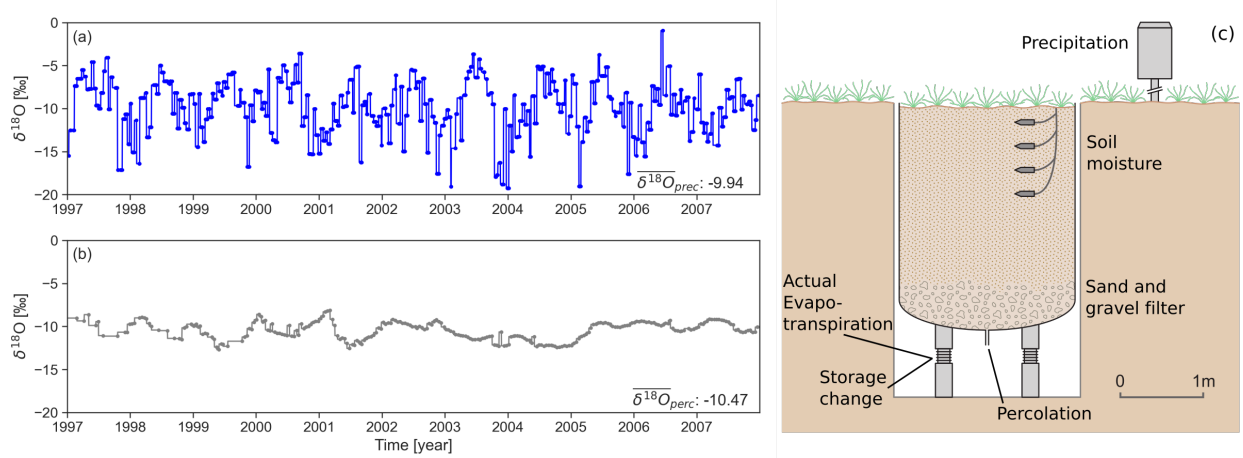

Figure 1. (a) Bi-weekly measured $\delta^{18}O$ in precipitation and (b) measured $\delta^{18}O$ in lysimeter seepage at Rietholzbach lysimeter. (c) Cross-section of Rietholzbach lysimeter with measured variables (modified from Seneviratne et al. (2012b)). Storage change and actual evapotranspiration are derived from measured lysimeter weight change. Air temperature and global radiation were measured at the nearby are measured at the nearby weather station (not shown).

3 Methods

3.1 Representation of soil hydrologic processes using the hydrologic model RoGeR

As stated above, realistic process-oriented hydrological modelling should be the prerequisite for successful coupled-SAS approaches. Here, we use the RoGeR model (Steinbrich et al., 2016), which was developed from the soil hydrological model IN^{3}M (Weiler, 2005) to calculate hydrologic fluxes and storage volumes. These fluxes and storage volumes were then coupled with the SAS functions. In RoGeR, hydrologic fluxes and storage dynamics are simulated with an adapted temporal resolution (time steps of 10 minutes for high rainfall intensities, hourly time steps for low rainfall intensities or snow melt, and daily time steps for dry periods). The model requires precipitation (mm/10 minutes), daily air temperature (°C) and daily potential evapotranspiration (mm/day) data as input. We corrected the original precipitation data according to Richter (1995) to account for systematic errors due to wind uncercatch in the measurement of precipitation. Po-

147 tential evapotranspiration is calculated after Makkink (Makkink, 1957) with daily average air tem-
148 perature (°C) and daily average global radiation (MJ/m^2). Model parameters are listed in Table 1.
149 The hydrologic processes considered in this study are summarizes as:

150 - **Surface water storage:** Surface water storage comprises an interception storage. Storage pa-
151 rameters are land cover specific and seasonally time-variant.
152 - **Soil water storage:** Soil water storage is divided into an upper (i.e. root zone) and lower
153 storage (i.e. subsoil). Soil hydraulic parameters are derived using a Brooks-Corey scheme
154 (Brooks and Corey, 1966). The two soil storage layers have the same soil hydraulic param-
155 terization.
156 - **Evapotranspiration:** Evapotranspiration is limited by energy (i.e. potential evapotranspira-
157 tion) and water availability (i.e. soil water content). Evapotranspiration occurs sequentially
158 from top to bottom (interception evaporation, soil evaporation and transpiration). Soil evapo-
159 ration is represented by the Stage I – Stage II scheme (Or et al., 2013). Transpiration (i.e. flux
160 by root water uptake) is limited to vegetation/land cover specific root depth. The seasonal
161 variation of ground cover (e.g. deciduous trees) are quantified by a transpiration coefficient.
162 - **Interception:** Interception storage is represented by a single bucket. Liquid and solid precip-
163 itation fill the storage and the interception storage spills over if storage exceeds total storage
164 capacity. Evaporation empties the interception storage.
165 - **Snow accumulation/Snow melt**: Solid precipitation (air temperature below 0 °C) accumu-
166 lates in the interception storage or at the ground surface. Snow melt is calculated by a degree-
167 day approach and by a delayed release of melt water.
168 - **Infiltration:** Water infiltrates into the soil matrix, into macropores or shrinkage cracks. Matrix
169 infiltration is implementend by a modified Green-Ampt approach (Green and Ampt, 1911;

Peschke, 1985). Infiltration through macropores is represented by the approach from Weiler (2005) and requires excess of soil matrix infiltration. Macropore infiltration depends on density, length of vertical macropores and saturated hydraulic conductivity. Depending on the parameterization, macropore infiltration can attain shares up to 70 % of total infiltration. Infiltration through shrinkage cracks is adopted from Steinbrich et al. (2016) and depends on clay and soil water content. Water exchange from macropores/cracks is realized with a geometriy-dependend solution of horizontal infiltration by a Green-Ampt approach (Steinbrich et al., 2016)

Table 1. Hydrologic model parameters, their lower and upper parameter boundaries for the Monte-Carlo (MC) sampling and Saltelli (SA) sampling, and the final parameter sets of the best 100 simulations (average ± standard deviation). Usable porosity, fraction of large pores and fraction of fine pores are auxillary parameters used to set meaningful parameters for air capacity of soil and and plant available field capacity.

Hydrologic model parameter		**Unit**	**Parameter boundaries**		**Best parameter(s)**
			MC	**SA**	
Land use/Land cover	lu_id	-	8		8
Makkink coefficient	$c1_{PET}$	-	0.55 - 0.65	0.5 - 0.7	0.61 ± 0.03
Makkink coefficient	$c2_{PET}$	mm day^{-1}	-0.2 - 0.0	-0.4 - 0.2	-0.09 ± 0.05
Density of vertical macropores	ρ_{mpv}	m^{-2}	10 - 300	1 - 400	202 ± 70
Length of vertical macropores	l_{mpv}	mm	50 - 1500	1 - 2000	879 ± 165
Soil depth	z_{soil}	mm	2200		2200
Effective porosity[1]	θ_{eff}	-	0.15 - 0.35		0.21 ± 0.04
Fraction of large pores	f_{lp}	-	0.1 - 0.6		0.59 ± 0.05
Fraction of fine pores	f_{fp}	-	1 - f_{lp}		0.41 ± 0.05
Air capacity of soil	θ_{ac}	-	θ_{eff} ・ f_{lp}		0.13 ± 0.03
Plant available field capacity of soil	θ_{ufc}	-	θ_{eff} ・ f_{fp}		0.09 ± 0.02
Permanent wilting point of soil	θ_{pwp}	-	0.15 - 0.25	0.1 - 0.25	0.2 ± 0.03
Saturated hydraulic conductivity of soil	k_s	mm h^{-1}	5 - 150		83.3 ± 43.6
Hydraulic conductivity of bedrock	k_f	mm h^{-1}	2500		2500

[1]describes the total volume of mobile soil water storage

- **Surface runoff:** Surface runoff is generated either by Hortonian (HOF; i.e. infiltration excess) or saturation overland flow (SOF; i.e. saturation of soil storage).
- **Capillary rise / Percolation:** Vertical drainage and upward water movement is described by the approach of Salvucci (1993). For this study, we implemented a free drainage for the lower boundary condition by setting the hydraulic conductivity of bedrock (k_f) to a constant value of 2500 mm/h (Table 1).

For detailed process and parameter descriptions including all model equations, we refer to the supporting information or to Schwemmle (2023) for most current information.

We run Monte Carlo simulations with 30 000 samples in predefined boundaries (see Table 1). Initial soil water content was set to field capacity. A multi-objective metric E_{multi} serves to identify the best performing parameter set.

$$E_{multi} = 0.4\,KGE_{ET} + 0.2\,KGE_{\Delta S} + 0.4\,KGE_{PERC} \quad (1)$$

where KGE_{ET} is the Kling-Gupta efficiency of evapotranspiration fluxes, $KGE_{\Delta S}$ is the Kling-Gupta efficiency of total storage change and KGE_{PERC} is the Kling-Gupta efficiency of percolation fluxes. E_{multi} ranges between 1 and ∞ in which $E_{multi} = 1$ indicates a perfect agreement between observations and simulations. KGE_{ET} and KGE_{PERC} are assigned with greater weights due to longer coverage of observed values. The best 100 hydrological simulations are coupled with SAS functions by an offline-scheme (i.e. hydrologic response and hydrologic transport are not simulated simultaneously).

3.2 Representation of transport processes using StorAge Seclection (SAS) functions

We use the fractional SAS function type (fSAS; van der Velde et al., 2012) and solve the SAS functions for each hydrologic flux Q:

$$\overleftarrow{p}_Q(\mathrm{T},\mathrm{t}) = \frac{\partial}{\partial T}\Omega_Q(P_S(T,t),t) \quad (2)$$

with

$$P_S(T,t) = \frac{S_T(T,t)}{\mathrm{S(t)}} \quad (3)$$

where T is the water age, t is the time step, $\overleftarrow{p}_Q(\mathrm{T},\mathrm{t})$ is the backward travel time distribution of a specific hydrologic flux, ω_Q(T,t) is the probability distribution function of the hydrologic flux (where Ω_Q(T,t) is the cumulative probability distribution function), S_T(T,t) is the cumulative age-ranked storage (mm), S(t) is the soil water content (mm) and P_S (T,t) is the cumulative probability distribution of the storage (where p_S (T,t) is the probability distribution). The hydrologic processes sequentially update S_T(T,t) at time step t by looping over internal substeps n (n=6):

$$\mathrm{S(T,i+1)} = \mathrm{S(T,i)} \pm \overleftarrow{p}_Q(T,i)\cdot Q(t)\cdot h \quad (4)$$

where i is the substep, h is the time increment of the substep (day) and Q(t) (mm day^{-1}) is the flux from the corresponding hydrologic process. The hydrologic processes update S_T(T,t) in the following sequence: infiltration (1; *inf*), soil evaporation (2; $evap_{soil}$), transpiration (3; *transp*), root zone percolation (4; $perc_{rz}$), subsoil percolation (5; $perc_{ss}$) and capillary rise from subsoil into root zone (6; cpr_{rz}). When the soil surface is covered by snow, we fully mix δ^{18}O in precipitation with δ^{18}O in the snow cover (Seeger and Weiler, 2014). The δ^{18}O in the snow cover might infiltrate while snow melt.

Tracer concentrations (‰ for δ^{18}O; mg l^{-1} for bromide) are for each hydrologic flux Q are calculated as:

$$C_Q = \int_{T=0}^{\infty} C_S(T,t)\cdot\alpha_p\cdot\overleftarrow{p}_Q(T,t)dT \quad (5)$$

where C_S(T,t) is the age-ranked tracer storage and α_p is the partition coefficient which ranges from 0 (not dissolved) to 1 (fully dissolved). For δ^{18}O transport α_p is set to 1. For bromide transport, we

set α_p to a value of 0.8 since Menzel and Demuth (1993) found a bromide recovery rate of 80 %, which could be related to uptake by vegetation or sorption processes. Isotopic fractionation is not considered owing to the small difference between the average of $\delta^{18}O$ in precipitation and $\delta^{18}O$ in lysimeter seepage (see Figure 1).

The age preference of SAS functions and thus the shape of the travel time distribution (TTD) is controlled by the choice of the probability distribution function. By assigning a probability distribution function as a SAS function to each hydrologic process, we can conceptualize the underlying transport process. For example, faster transport may be represented by right-skewed ω_Q and slower transport by left-skewed ω_Q.

In order to test different hypotheses about the tracer transport processes at the Rietholzbach lysimeter, we group combinations of ω_Q according to four transport model structures. Within these transport model structures, we represent potential transport processes by specific parameters for ω_Q (Figure 3):

- **Complete-mixing model (CM):** All processes have no age preference (i.e. are well mixed). Each process uses a uniform SAS function:

$$\Omega_Q(T,t) = P_s(T,t) \quad (6)$$

- **Advection-Dispersion model (AD):** Transport processes of transpiration and percolation are implemented by an advective-dispersive scheme using a power law distribution function:

$$\Omega_Q(T,t) = P_s(T,t)^{k_Q} \quad (7)$$

  Soil evaporation and capillary rise prefer youngest water and are described by advective transport using a constant parameter k_Q (k_Q=0.1; see equation (7)).

- **Advection-Dispersion model with time-variant parameters (AD-TV):**

Soil evaporation and capillary rise are described as in AD. But transpiration has time-variant preference implemented by a power law distribution function with a time-variant parameter k_Q:

$$\Omega_Q(T,t) = P_s(T,t)^{k_Q},\ k_Q = c_{1-Q} + c_{2-Q}\frac{S(t) - S_{pwp}}{S_{sat} - S_{pwp}} \quad (8)$$

where S_{sat} is the soil storage volume at saturation (mm) and S_{pwp} is the soil storage volume at permanent wilting point (mm). In equation (8), preference for younger water increases for wet conditions and decreases for dry conditions.

The time-variant preference of percolation is formulated as:

$$\Omega_Q(T,t) = P_s(T,t)^{k_Q},\ k_Q = c_{1-Q} + c_{2-Q}\left(1 - \frac{S(t) - S_{pwp}}{S_{sat} - S_{pwp}}\right) \quad (9)$$

As a result, preference for older water increases for dry conditions and decreases for wet conditions.

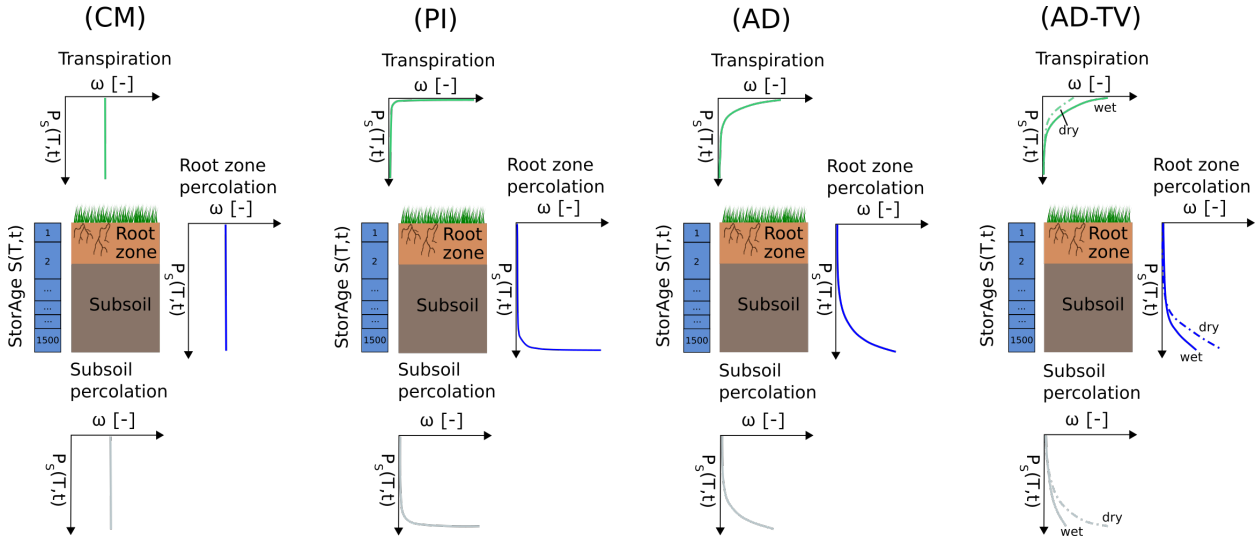

Figure 2. Transport model structures coupled with hydrologic simulations: Complete-mixing transport model (CM), Piston transport model (PI), Advection-dispersion transport model (AD) and Advection-dispersion transport model with time-variant SAS parameters (AD-TV). Soil evaporation and capillary rise (not shown) prefer in all transport model structures the youngest water (see equations (7) with constant k_Q=0.1).

Piston-flow model (PI): Transport processes are purely advective. The power law distribution function serves as a SAS function. Processes characterized by flux leaving the storage at the top have a strong preference for younger (equation (7) with constant k_Q=0.1). Processes dominated by bottom fluxes have a strong preference for older water (equation (7) with constant k_Q=100).

Table 2 Transport model parameters and their lower and upper parameter boundaries for the Monte-Carlo (MC) sampling and Saltelli (SA) sampling. Transp indicates parameters of transpiration process and perc indicates parameters of percolation processes. There are no MC and SA simulations for parameter-free CM and constant-parameter PI.

Transport model parameter	Unit	Transport model structure	Parameter boundaries		Best parameter
			MC	SA	
No parameters		CM	-	-	-
Constant parameters		PI	-	-	-
k_{transp}	-	AD	0.2 - 1	0.1 - 5	0.18
$k_{perc\text{-}rz}$	-	AD	1 - 5	0.1 - 5	2.54
$k_{perc\text{-}ss}$	-	AD	1 - 5	0.1 - 5	2.08
$c_{1\text{-}transp}$	-	AD-TV	0.1 - 0.5	0.1 - 5	-
$c_{2\text{-}transp}$	-	AD-TV	0.1 - 2	0.1 - 5	-
$k_{1\text{-}transp}$	-	AD-TV	$c_{1\text{-}transp}$		0.17
$k_{2\text{-}transp}$	-	AD-TV	$c_{1\text{-}transp} + c_{2\text{-}transp}$		0.97
$c_{1\text{-}perc\text{-}rz}$	-	AD-TV	1 - 2	0.1 - 5	-
$c_{2\text{-}perc\text{-}rz}$	-	AD-TV	0.1 - 3	0.1 - 5	-
$k_{1\text{-}perc\text{-}rz}$	-	AD-TV	$c_{1\text{-}perc\text{-}rz}$		1.83
$k_{2\text{-}perc\text{-}rz}$	-	AD-TV	$c_{1\text{-}perc\text{-}rz} + c_{2\text{-}perc\text{-}rz}$		4.16
$c_{1\text{-}perc\text{-}ss}$	-	AD-TV	1 - 2	0.1 - 5	-
$c_{2\text{-}perc\text{-}ss}$	-	AD-TV	0.1 - 5	0.1 - 5	-
$k_{1\text{-}perc\text{-}ss}$	-	AD-TV	$c_{1\text{-}perc\text{-}ss}$		1.66
$k_{2\text{-}perc\text{-}ss}$	-	AD-TV	$c_{1\text{-}perc\text{-}ss} + c_{2\text{-}perc\text{-}ss}$		1.98

3.3 Monte Carlo analysis and sensitivity analysis with the Sobol method

We run Monte Carlo simulations with 10 000 samples. The main purpose of the Monte Carlo Analysis is the parameter estimation, an additional uncertainty analysis goes beyond this study. Monte Carlo simulations are computed with the transport model structures AD and AD-TV, but not with parameter-free CM (see equation (6)) and constant-parameters PI (see equation (7) with

278 k_Q=0.1 and k_Q=100). Each simulation uses a 5-year simulation period (1997-2001) as a warmup
279 run (see Figure 1) to derive C_S(T,t=0). After warmup, we rescale S_T(T,t) with S_{init}/S_T(T,t), since we
280 have knowledge about initial soil water content but do not know initial $\delta^{18}O$ in soil water. Param-
281 eter ranges are provided in Table 2. We calculated KGE to evaluate simulations of $\delta^{18}O$ in perco-
282 lation. Since $\delta^{18}O$ in percolation are analyzed from bi-weekly bulk samples, we aggregate simula-
283 tions to bi-weekly bulk-samples by flux-weighted average.
284 We additionally conduct a sensitivity analysis using the Sobol method (Saltelli et al., 2008). Pa-
285 rameter sets are generated using Saltelli's extension of the Sobol sequence (Campolongo et al.,
286 2011; see Table 1 and Table 2) with a sample size of 1024. We calculate first order and total Sobol
287 indices for evaluation metrics and age statistics.

288 **3.4 Benchmark comparison to HYDRUS-1D and bromide experiment**

289 Simulations with HYDRUS-1D (Šimůnek et al., 2016, Collenteur et al., 2022) are performed with
290 a dual-porosity domain. A detailed description of the HYDRUS-1D setup is provided in the sup-
291 porting information (section S4). We run 30 000 Monte Carlo simulations and select the best per-
292 forming parameter set based on the multi-objective KGE_{multi} (Sprenger et al., 2016):

293 $$KGE_{multi} = \frac{1}{2}\left(\frac{1}{2}KGE_{\theta} + \frac{1}{2}\left(\frac{1}{2}KGE_{aet} + \frac{1}{2}KGE_{perc}\right)\right) + \frac{1}{2}KGE_{\delta^{18}O} \quad (10)$$

294 where the KGE_{θ} is the average KGE of soil water content at different soil depths z (5 cm, 15 cm,
295 25 cm 35 cm, 55 cm, 80 cm and 110 cm), KGE_{aet} compares simulated and observed actual evapo-
296 transpiration, KGE_{perc} compares simulated and observed actual evapotranspiration and $KGE_{\delta 18O}$
297 compares simulated and observed $\delta^{18}O$ in percolation.

Based on KGE_{multi} (see equation (10)), we select the best performing parameter set and perform three benchmark comparisons between HYDRUS-1D modeling results and RoGeR modeling results:

1. We compare our results to $\delta^{18}O$ transport simulations with HYDRUS-1D.
2. We compare our results to travel time distributions calculated with HYDRUS-1D.
3. For the virtual bromide experiments, we selected the best performing parameter set (i.e. best $KGE_{\delta 18_O}$) for each transport model structure to simulate $\delta^{18}O$ transport. We, then, transfer the $\delta^{18}O$ model parameters to the bromide model. Bromide breakthrough is simulated with each transport model structure and compared to the results of Menzel and Demuth (1993) and bromide transport simulations with HYDRUS-1D. Since the bromide experiment was conducted on 12th November 1991 prior to the time period of our study and the available meteorological input data, we repeat virtual experiments for each year between 1997 and 2006 and inject a bromide mass of 79.9 g (i.e. one mole potassium bromide dissolved in one liter water) at 12th November. Additionally, we used meteorologic data from the nearby station MeteoSwiss station St. Gallen (775 m above sea level; 9°24'W 47°26'N) to simulate the period of the bromide experiment. We adjusted the precpitation data by rescaling with the average annual precipitation at the Rietholzbach lysimeter and air temperature data to the altitude difference between St. Gallen and Rietholzbach lysimeter.

4 Results

4.1 Simulated hydrologic fluxes and storages

The best 100 hydrologic parameters according to E_{multi} (see equation (1)) are summarized in Table 1. The corresponding values of E_{multi} and its metric terms are displayed in Table 3. Values for E_{multi} are larger for simulations with RoGeR than for simulations with HYDRUS-1D. E_{multi} of simulations with RoGeR show an increasing tendency from drier to wetter antecedent conditions. The cumulated values of the best 100 simulations according to E_{multi} are compared with observed values and the best HYDRUS-1D simulation. The comparison for two time periods with highest consistent coverage of observations is shown in Figure 5. Despite a low variance of E_{multi} (see Table 3), simulations reveal differences in the cumulated flux volumes. In particular, absolute differences are greatest for percolation (Figure 5c and 5f).

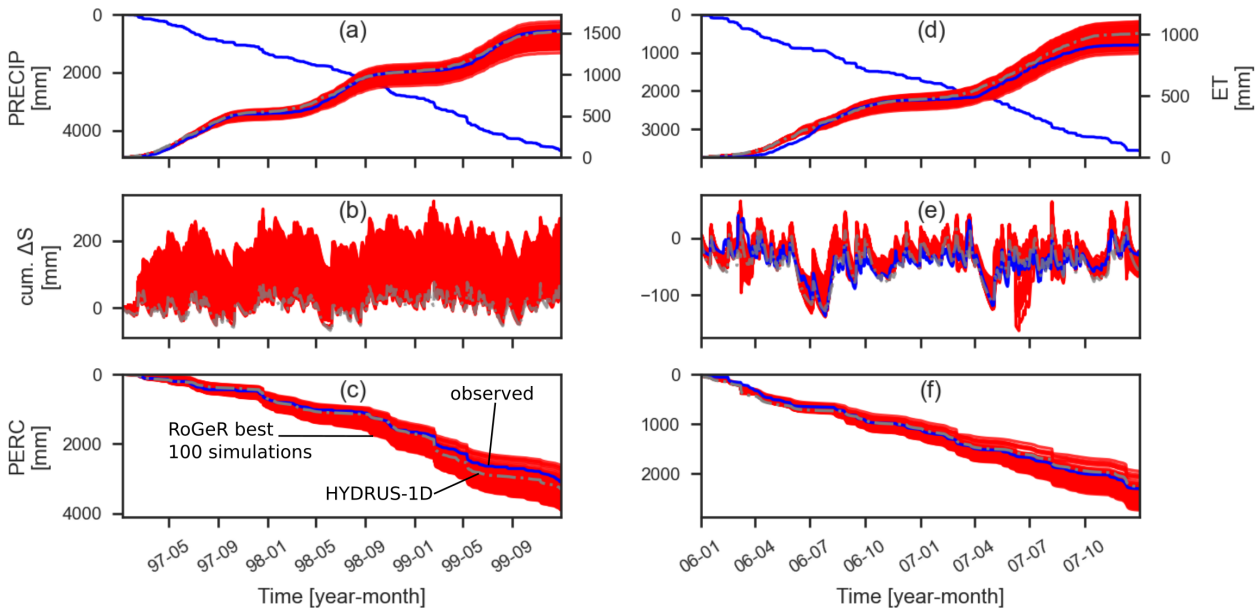

Figure 3. Cumulative precipitation, cumulative simulated and observed evapotranspiration (a,d), cumulative simulated and observed storage change (b,e), and cumulative simulated and observed percolation (c,f). Data for observed storage change from 1997 to 1999 is not available.

Table 3. Evaluation metrics of best 100 RoGeR simulations (average ± standard deviation) and best HYDRUS-1D simulation for different antecedent soil moisture conditions. Antecedent soil moisture conditions are defined by 10^{th} (θ_{a10}) and 90^{th} (θ_{a90}) percentiles of average observed soil moisture from previous 5 days (θ_a; dry: $\theta_a < \theta_{a10}$; normal: $\theta_{a10} \leq \theta_a \leq \theta_{a90}$; wet: $\theta_a > \theta_{a90}$)

	KGE_{aet}		$KGE_{\Delta S}$		KGE_{perc}		E_{multi}	
	RoGeR	HYDRUS-1D	RoGeR	HYDRUS-1D	RoGeR	HYDRUS-1D	RoGeR	HYDRUS-1D
total	0.78 ± 0.05	0.80	0.74 ± 0.1	-0.05	0.53 ± 0.06	0.58	0.67 ± 0.02	0.54
dry	0.55 ± 0.09	0.60	0.83 ± 0.05	0.59	0.16 ± 0.1	0.06	0.45 ± 0.03	0.39
normal	0.79 ± 0.05	0.81	0.69 ± 0.1	-0.1	0.43 ± 0.08	-0.74	0.63 ± 0.03	0.01
wet	0.81 ± 0.04	0.88	0.67 ± 0.13	0.52	0.65 ± 0.1	0.69	0.72 ± 0.06	0.73

4.2 Monte Carlo analysis

The best simulation for $\delta^{18}O$ in percolation of each transport model structure is shown in Figure 6. The AD and AD-TV model structure visually agrees with the general pattern of $\delta^{18}O$ observations in the percolation flux. The CM-model depicts lower agreement between simulations and observations, while the PI-model shows the lowest agreement among the four model structures. KGE values (Table 4) confirm the visual pattern of Figure 6. The AD-model structure scores highest KGE values and performs slightly better than HYDRUS-1D. We tested further transport model structures with RoGeR (e.g. preferential transport). For the results of the additional model structures, we refer to the supporting information (section S2). In contrast to the hydrologic simulations, the transport simulations from the CM, AD and AD-TV transport model structure picture a decrease of model performance from drier antecedent conditions to wetter antecedent conditions.

4.3 Sensitivity analysis with the Sobol' method

Figure 7 shows Sobol' indices of hydrologic model parameters for averaged median travel time of transpiration ($TT_{50\text{-}transp}$) and percolation ($TT_{50\text{-}perc}$) and for KGE of $\delta^{18}O$ in percolation ($KGE_{\delta 18_O}$). The four transport model structures share the same set of sensitive hydrologic model parameters. For the two travel time statistics, Sobol' indices are greatest for fraction of large pores (f_{lp}) except

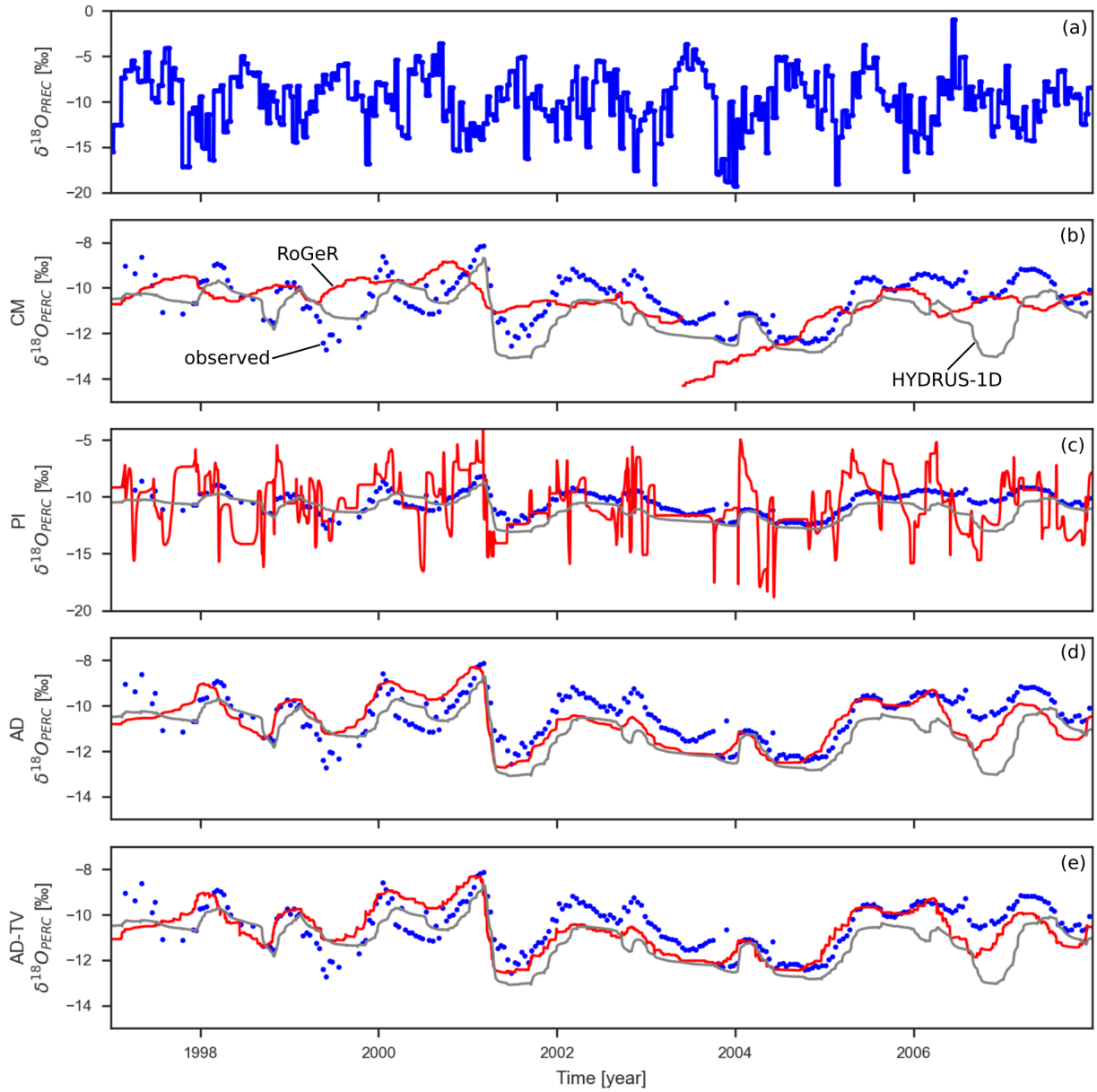

Figure 4. Observed $\delta^{18}O$ in precipitation (a) and observed and simulated $\delta^{18}O$ in percolation with RoGeR and HYDRUS-1D (b-e). Values are shown for different model structures (see Figure 2).

for $KGE_{\delta 18O}$ of AD and AD-TV for which Sobol' indices of permanent wilting point (θ_{pwp}) are greatest. In addition to that, averaged $TT_{50\text{-}perc}$ is sensitive for macropore parameters (ρ_{mpv} and l_{mpv}). In general, total Sobol' indices exceed values of first-order Sobol' indices. Total Sobol' indices describe the fraction of variance that is caused by the variability of the considered parameter. First-

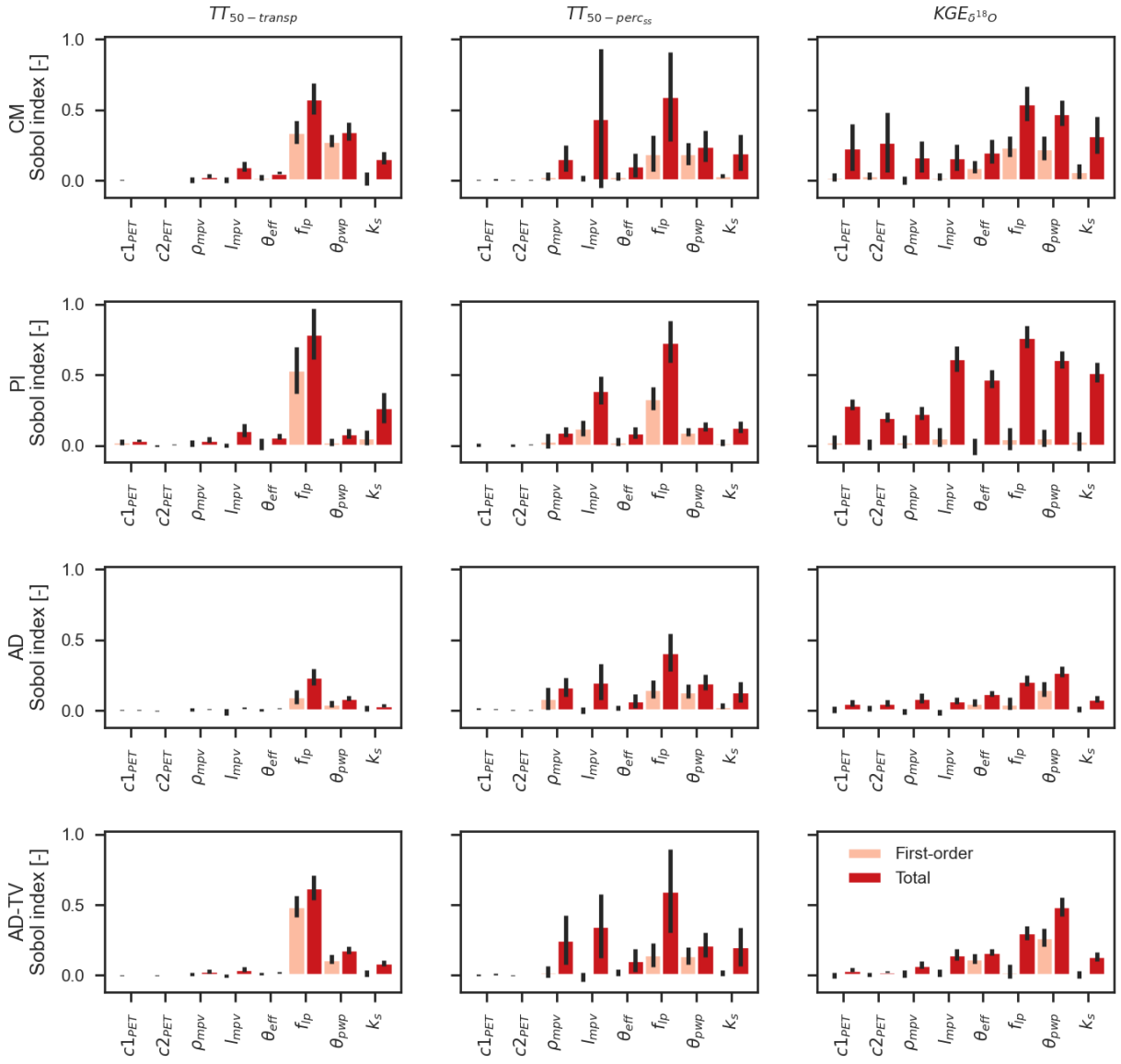

Figure 5. Sobol' indices with error bars (95% confidence interval) of hydrologic model parameters (see Table 1) calculated for averaged median travel time of transpiration ($TT_{50\text{-transp}}$), averaged median travel time of percolation ($TT_{50\text{-percss}}$) and KGE of $\delta^{18}O$ in percolation ($KGE_{\delta^{18}O}$). Values are shown for complete-mixing transport model structure (CM), piston-flow transport model structure (PI), advection-dispersion transport model structure (AD) and advection-dispersion transport model structure with time-variant SAS parameters (AD-TV).

order Sobol' indices represent direct contribution to the total Sobol' indices of the considered parameter. A difference between total Sobol' indices and first-order Sobol' indices might be ex-

plained by parameter interactions. These differences are more distinct for $TT_{50\text{-}perc}$. The gap between first-order Sobol' indices and total Sobol' indices suggests a strong interaction between parameters.

Sobol' indices of SAS parameters for $TT_{50\text{-}transp}$, $TT_{50\text{-}perc}$ and $KGE_{\delta^{18}O}$ are displayed in Figure 8. Comparing the Sobol indices between hydrologic model parameters and SAS parameters reveal two different results: (i) The AD model structure is more sensitive for SAS parameters than for hydrologic model parameters. (ii) The AD-TV model structure is more sensitive for hydrologic model parameters than for SAS parameters. Regarding travel times, we found greater Sobol' indices for $TT_{50\text{-}transp}$ than for $TT_{50\text{-}perc}$.

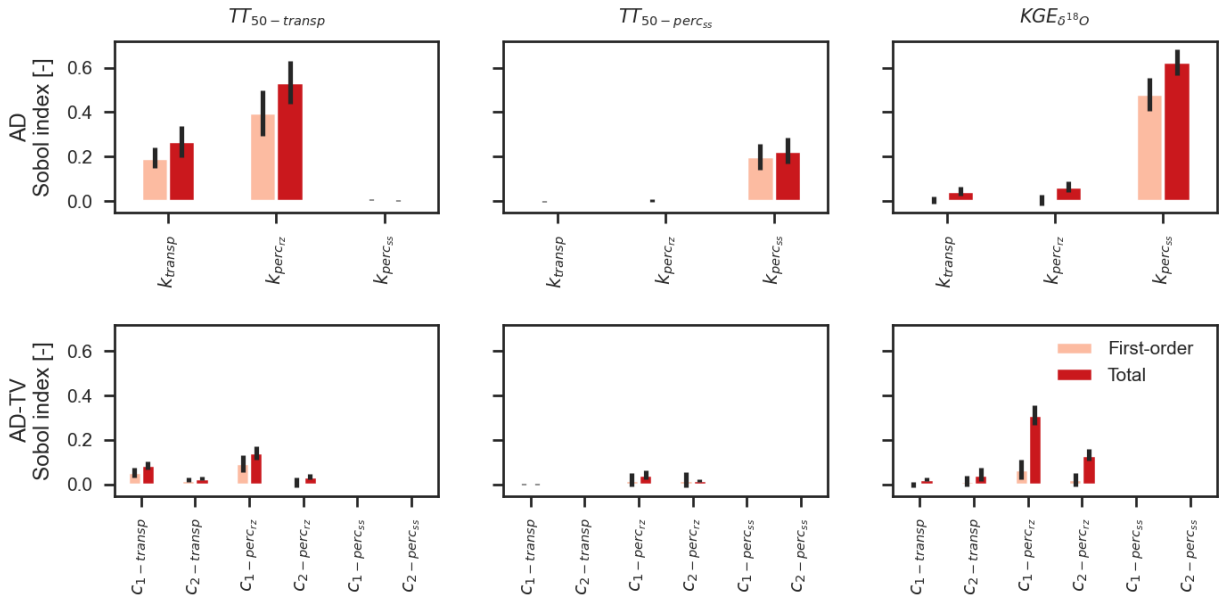

Figure 6. Sobol' indices with error bars (95% confidence interval) of SAS parameters (see Table 2) calculated for averaged median travel time of transpiration ($TT_{50\text{-transp}}$), averaged median travel time of percolation ($TT_{50\text{-percss}}$) and KGE of $\delta^{18}O$ in percolation ($KGE_{\delta^{18}O}$). Values are shown for advection-dispersion transport model structure (AD) and advection-dispersion transport model structure with time-variant SAS parameters (AD-TV).

Table 4. KGE of best $\delta^{18}O$ simulations for different antecedent soil moisture conditions. Antecedent soil moisture conditions are defined by 10^{th} (θ_{a10}) and 90^{th} (θ_{a90}) percentiles of average observed soil moisture from previous 5 days (θ_a; dry: $\theta_a < \theta_{a10}$; normal: $\theta_{a10} \leq \theta_a \leq \theta_{a90}$; wet: $\theta_a > \theta_{a90}$)

	CM	PI	AD	AD-TV	HYDRUS-1D
total	0.47	-0.37	0.74	0.74	0.68
dry	0.54	0.06	0.78	0.78	0.62
normal	0.47	-0.37	0.73	0.74	0.60
wet	0.31	0.21	0.71	0.71	0.69

4.4 Benchmark comparison to virtual bromide experiments and water age statistics of HYDRUS-1D simulations

Results of virtual bromide experiments are presented in Figure 7. The four model structures predict different bromide breakthrough curves. We found that bromide breakthrough curves of single virtual experiments deviate from each other due to different meteorological conditions. Furthermore, single virtual experiments diverge from observed bromide breakthrough curves. For example, the drought in year 2003 causes a late arrival of the bromide pulse. However, the average breakthrough curves produced by AD and AD-TV are similar and the average breakthrough curves agree well in terms of timing and magnitude with the observed bromide breakthrough curve. The average bromide breakthrough curves derived from CM and PI are different. In particular, CM simulates bromide breakthrough too early. PI simulates bromide breakthrough too late and the magnitude of the breakthrough is strongly overestimated.

The comparison between the backward travel time distributions calculated with the four transport model structures and HYDRUS-1D is depicted in Figure 8. Again, backward travel time distributions calculated by CM and PI are different to the backward travel time distributions calculated by AD, AD-TV and HYDRUS-1D. Especially travel times computed with CM extend to a wider range of water ages than the other models. While backward travel time distributions of percolation

derived from AD, AD-TV and HYDRUS-1D are similar, backward travel time distributions of transpiration estimated by AD, AD-TV and HYDRUS-1D reveal differences. AD-TV estimates older travel times for transpiration than AD. Transpiration travel times from HYDRUS-1D cover a wider range of water ages and the tails are older.

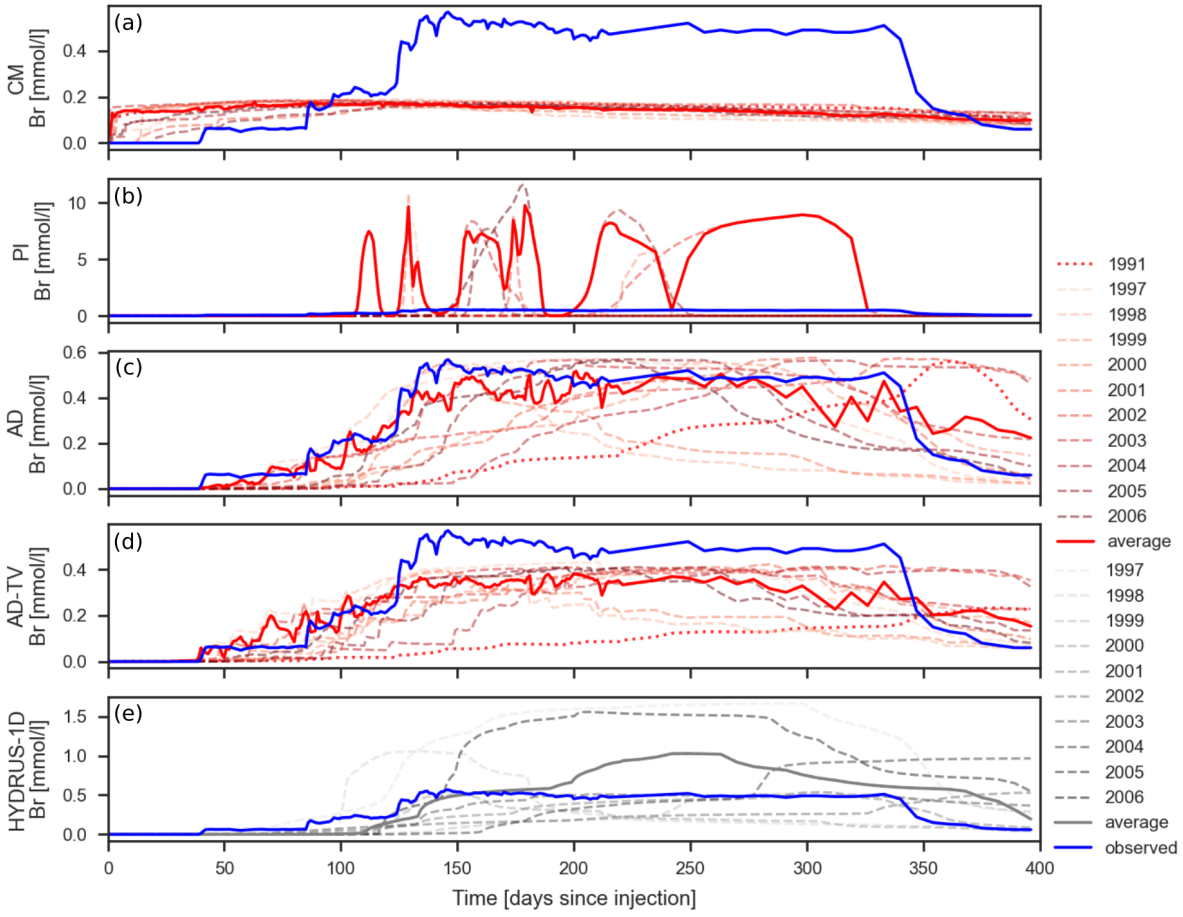

Figure 7. Bromide breakthrough curves from virtual bromide experiments and observed bromide breakthrough curve (modified from Menzel and Demuth (1993)). 79.9 g of bromide has been injected at 12th November of each year. Average values are weighted by bromide mass of percolation. Simulations are shown for complete-mixing transport model structure (a; CM), piston-flow transport model structure (b; PI), advection-dispersion transport model structure (c; AD), advection-dispersion transport model structure with time-variant SAS parameters (d; AD-TV) and HYDRUS-1D with dual-porosity domain (e; HYDRUS-1D).

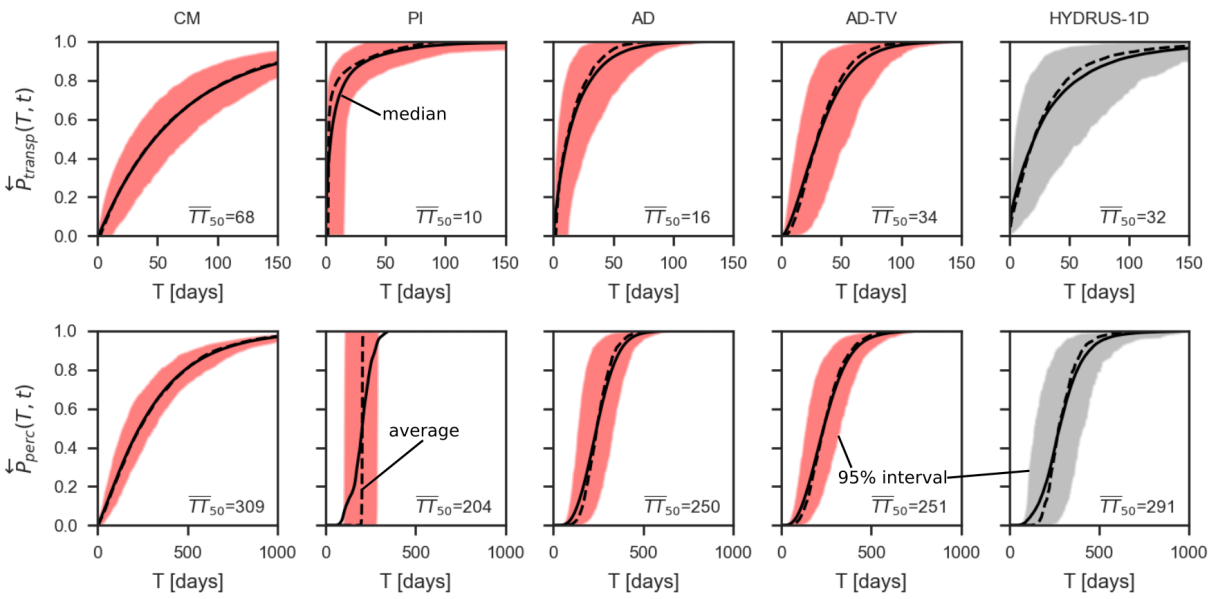

Figure 8. Simulated backward travel time distributions of transpiration and percolation. Averaged median travel times (in days) are displayed in the right bottom corner.

5 Discussion

5.1 Sensitive parameters for travel time statistics and model accuracy

The sensitivity analysis using the Sobol method for the coupled RoGeR model with SAS functions revealed different sensitivities for the RoGeR-AD and RoGeR-AD-TV model structure (Figures 6 and 7). The results for a static SAS parameterization imply that travel time estimates and predictive model accuracy are similarly affected by parameters of the hydrologic model and SAS functions. When using a time-variant SAS parameterization, hydrologic model parameters have a greater impact than SAS parameters on the results. One reason for this larger sensitivity might be the dependency from the soil water content (see equations (8) and (9)) on the transport simultations. Despite this difference, RoGeR-AD and RoGeR-AD-TV have in common that parameters related to soil water storage (f_{lp} and θ_{pwp}) have the greatest impact on travel times and model accuracy.

The two studies of Menzel and Demuth (1993) and Weiler and Naef (2003) at the Rietholzbach site provided experimental evidence that macropores play an important role for soil water fluxes and tracer transport. The macropore parameters estimated by the Monte Carlo analysis (Table 1) agree well with observations from Weiler and Naef (2003). They found a macropore density of 228 m^{-2} compared to the estimated 202 ± 70 m^{-2}. The sensitivity analysis shows that macropores influence the travel time estimation of percolation, while they have little impact on model accuracy and travel times of transpiration.

The closure of the lysimeter solute balance could only be partly constrained since solute (^{18}O) information has only been available at the bottom of the lysimeter. To fully constrain the model would require solute information from soil water and root water uptake (e.g. Asadollahi et al., 2022). As a consequence, age preference of transpiration and sensitive parameters for predictive accuracy of the transpiration process cannot be directly evaluated. For example, the model reproduces a similar signal of $\delta^{18}O$ in percolation with a younger age preference and an older age preference (Figures 2,4, S6 and S7). However, the best SAS parameter of transpiration (Table 2) are consistent with Asadollahi et al. (2020) who found k=0.2 for the evapotranspiration process (without constrains for evapotranspiration) at another grassland lysimeter.

5.2 Hypothesis-driven modelling of ^{18}O transport and bromide transport

The comparison between observed and simulated $\delta^{18}O$ in percolation and the virtual bromide experiments proved that SAS parameters which can be linked to an advective-dispersive transport process can explain ^{18}O transport and bromide transport to a large extent (Figures 4 and 7). However, uniform SAS functions could explain the dampening of the isotope signal well, but not the transport process of a individual tracer signal like the bromide application. The estimated model parameters of the AD models demonstrate a realistic pattern of the conceptualized processes. Since

447 the soil water dynamics are represented by equations which are governed capillary forces, RoGeR
448 enables a bypass flow in the root zone but mobile soil water is ultimately abstracted by the soil
449 matrix and thus leads to a slower transport (i.e. preference for older water with $k_Q > 1$). From
450 capillary-driven perspective, the older age preference ($k_Q > 1$) of percolation processes is physi-
451 cally consistent. However, RoGeR may reach its limits in case of a rapid response. We suppose,
452 that such a rapid response is more important for shallow soils with high connectivity of macropores
453 from the soil surface to the percolation depths. In such cases, it might be more consistent to imple-
454 ment preferential flow through gravity-driven theory (Germann and Prasuhn, 2018). The dye tracer
455 experiments of Weiler and Naef (2003) conducted within the Rietholzbach catchment proved the
456 occurrence of preferential flow at 1 m soil depth. Consequently, age preference of SAS might be
457 younger where macropores exist. In order to test the hypothesis of specific transport with a young
458 water preference, we would need a higher sampling frequency of ^{18}O during events from the ly-
459 simeter seepage and additional soil water samples at different soil depths.
460 The virtual bromide experiments revealed that SAS parameters of advective-dispersive transport
461 estimated with ^{18}O could be successfully transferred to predict bromide breakthrough (Figure 7).
462 The average bromide breakthrough simulated by RoGeR-AD exhibits visually a better agreement
463 than RoGeR-AD-TV or HYDRUS-1D, respectively. The lower agreement of RoGeR-AD-TV
464 might be due to parameter estimation with bi-weekly ^{18}O samples which causes a loss of infor-
465 mation and a better agreement might be feasible with higher sampling frequency of ^{18}O. HY-
466 DRUS-1D cannot predict the first arrival of the solute at the bottom very well, which could be
467 attributed to its caplillary-driven model framework. The comparison between individual bromide
468 breakthrough curves demonstrate nicely the impact of different meteorologic conditions on
469 transport velocities. For example, bromide pulse arrives later when injected in a drought year (e.g.

year 2003; see Figure S2) whereas bromide pulse arrives earlier when injected under wetter meteorologic conditions (e.g. year 1998; see Figure S2).

A key result of the virtual bromide experiments is that the tracer signals simulated by SAS with a uniform probability distribution function arrive substantially earlier than indicated by the observations (Figure 7). We found a similar pattern for the ^{18}O modelling experiments which support the findings from the virtual bromide experiments. These results clearly demonstrate the consequence of using the complete-mixing assumption for depth-implict solute transport model (e.g. soil is discretized by 2-3 soil layers). We can support the argumentation in Sternagel et al. (2022) and we suggest going beyond the commonly applied complete-mixing assumption (e.g. Heße et al., 2017; Kumar et al., 2020).

Finally, we want to stress several limitations of the hypothesis-driven modelling approach presented in this study. Since evaporative fractionation of ^{18}O has not been implemented into the model framwork, evaporative fractionation of ^{18}O should be neglible, which is the case at the Rietholzbach lysimeter due to the dense gras cover and site specific climate conditions. Although we account for non-conservative behavior of bromide by considering partitioning of either root water uptake or sorption processes (see equation (5)), the assumption of α_p=0.8 might not be transferable to other sites. The non-conservative behavior is important for longer time periods (i.e. longer than the event length; Sternagel et al., 2019) and sorption processes are controlled by clay content of soil and pH-conditions (Groh et al., 2018). We suppose that RoGeR-SAS is limited to deep soils and/or partly structured soils (e.g. macropore network of the soil column is partly connected) for which solute flushing at the event scale are less relevant. For a better representation of solute flushing, it might be worth to implement infiltration and percolation based on gravity-driven theory

(Germann and Prasuhn, 2018) and compare it to the approach presented in this study. Such a comparison should investigate how and when gravity-driven transport is induced. For example, the interplay between rainfall characteristics (e.g. rainfall intensity) or soil properties (e.g. macropore network) may play a decisive role (Demand and Weiler, 2021).

5.3 Coupling simulated hydrologic fluxes and storages with SAS functions

We estimated parameters of HYDRUS-1D with dual-porosity domains using the observed soil water content time series at different soil depth to maximize information for the spatially discrete HYDRUS model (see equation (10)). However, to allow for a fair comparison between RoGeR and HYDRUS-1D, we evaluated the model results with the same metrics (Tables 3 and 4). These results show that RoGeR predicts hydrologic variables in general better than HYDRUS-1D. $\delta^{18}O$ in percolation and bromide breakthrough are reproduced similarly well by RoGeR and HYDRUS-1D (Figures 4 and 7). RoGeR performs slightly better than HYDRUS-1D in terms of $KGE_{\delta 18O}$ and for predicting the bromide experiment. Furthermore, travel time statistics estimated by RoGeR with advective-dispersive transport and by HYDRUS-1D show similar distributions (Figure 8). The similarities between the two models and the good agreement between simualtions with RoGeR and observations confirm the usability of coupling SAS functions with a process-based hydrologic model.

Besides that the complete program code used for this study is publicly available and thus fosters reproducibility, another major advantage of RoGeR compared to HYDRUS-1D is that the computation of travel times is approximately 340 times faster. Travel time compuation with HYDRUS-1D took 340 hours whereas travel time compuation with RoGeR took 1 hour. Comparing the coupled-SAS model as presented here with a pure-SAS model (e.g. Benettin and Bertuzzo, 2018) in terms of applicability shows that only data of the upper condition is required rather than measured

fluxes of all outflows from the considered hydrologic system. In many cases, such measurements are not available. Another advantage is that RoGeR requires a lower number of parameters. Moreover, the model does not rely on complex calibration schemes. Instead, parameters of RoGeR can be derived from available environmental data (e.g. soil maps; Steinbrich et al., 2016) and may readily applied to sites with such datasets. Disadvantages of RoGeR compared to HYDRUS-1D are mainly attributed to the low vertical discretization with two soil layers. HYDRUS-1D provides more information in the vertical dimension (e.g. spatio-temporal tracer distributions in the soil). For example, research questions concerning highly dynamic processes (e.g. depth of root water uptake) can only be obtain with spatially detailed results of HYDRUS-1D.

Although data requirements of coupled-SAS models are less strict than for pure-SAS models, a major challenge for coupling SAS functions with simulated hydrologic variables consists of the realistic representation of the considered hydrologic system. We selected the best 100 hydrologic simulations according to a performance metric realized with different parameters and coupled the simulations with SAS functions. All 100 hydrologic model realization coupled with AD and AD-TV were capable to achieve $KGE_{\delta^{18}O} > 0.7$, hence a certain parameter equifinality could not be resolved (Figure S4). For example, values for k_s range from 11.6 to 149.6 mm/h.

As alredy been shown by Asadollahi et al. (2020), we could also confirm that using single-parameter SAS function is suitable to predict solute leaching within a soil column. Since a dual-parameter SAS function produced very similar results, the question about the shape of SAS functions (e.g. Heidbüchel et al., 2020) remains open. We suggest to perform a multi-site (e.g. lysimeters with different soil properties, vegetation cover and climatic conditions) comparison including different kind of tracer signals (e.g. seasonally varying isotopic signal vs injection of pollution tracers or nutrients at specific time) to further improve our knowledge about SAS-based solute transport.

6 Conclusions

The ^{18}O and bromide transport through a grass covered weighted lysimeter has been extensively investigated using simulations of RoGeR-SAS and HYDRUS-1D with a dual-porosity domain. The simulations with different transport model structures exhibited high sensitivities for parameters related to the soil water storages. The two advective-dispersive transport model structures of RoGeR showed particularly different sensitivities depending on the choice between a static or a time-variant SAS parameterization. We further found that the leaching of ^{18}O and bromide can be realistically explained to a large extent by SAS with power law distribution function linked to advective-dispersive transport. The two selected advective-dispersive transport model structures of RoGeR-SAS showed particularly different sensitivities depending on the choice between a static or a time-variant SAS parameterization. Although a uniform SAS resulting in complete-mixing reproduces well the dampening of the ^{18}O percolation signal, this transport assumption leads to a strong temporal mismatch of the tracer signal (i.e. early arriving of tracer signal), if used in transport models with coarse vertical discretization at sites with deep soils. The results of RoGeR-SAS with advective-dispersive transport model structures show very similar results than the more complex HYDRUS-1D model and agrees well with the lysimeter measurements. RoGeR-SAS substantially reduces computational time of travel times but at the cost of a simpler, but more parsimonious vertical discretization. Therefore, the combination of a hydrologic model with SAS function linked to individual fluxes and processes has a great potential to effectively simulate water balance components and the related solute transport at various temporal and spatial scales. The new RoGeR-SAS could also be extended to solutes with more complex transport processes to allow simulations of nutrient cycles or pollutants.

Acknowledgments

This research was supported by the Helmholtz Association of German Research Centres through grant no 42-2017. We are grateful to Jens Lange and Dominic Demand for their constructive comments on the first draft. Jürgen Strub provided the illustration of the lysimeter and the measured bromide breakthrough curve. We also acknowledge Martin Hirschi, Dominik Michel and Sonia I. Seneviratne from the Institute for Atmospheric and Climate Science at ETH Zürich for providing the measurements from the Rietholzbach site, including the stable water isotope measurements, lysimeter data, and meteorological data. The authors acknowledge support by the High Performance and Cloud Computing Group at the Zentrum für Datenverarbeitung of the University of Tübingen, the state of Baden-Württemberg through bwHPC and the German Research Foundation (DFG) through grant no INST 37/935-1 FUGG.

Open Research

The code and data used for this project are available at https://doi.org/10.5281/zenodo.7633362 (Schwemmle, 2023) and https://doi.org/10.5281/zenodo.763228. The observational data used in this project is available from the Land-Climate Dynamics group (Prof. Sonia Seneviratne) at ETH Zurich (isotope data will be available at https://doi.org/10.3929/ethz-b-000596572 (Michel et al., 2023); other Rietholzbach data will be available at https://doi.org/10.3929/ethz-b-000596657 (Seneviratne et al., 2012a)).

References

Asadollahi, M., C. Stumpp, A. Rinaldo, and P. Benettin (2020), Transport and Water Age Dynamics in Soils: A Comparative Study of Spatially Integrated and Spatially Explicit Models, *Water Resources Research*, *56*(3), e2019WR025539. https://doi.org/10.1029/2019wr025539

Asadollahi, M., M. F. Nehemy, J. J. McDonnell, A. Rinaldo, and P. Benettin (2022), Toward a Closure of Catchment Mass Balance: Insight on the Missing Link From a Vegetated Lysimeter, *Water Resources Research*, *58*(4), e2021WR030698. https://doi.org/10.1029/2021WR030698

Benettin, P., and E. Bertuzzo (2018), tran-SAS v1.0: a numerical model to compute catchment-scale hydrologic transport using StorAge Selection functions, *Geosci. Model Dev.*, *11*(4), 1627-1639. https://doi.org/10.5194/gmd-11-1627-2018

Benettin, P., J. W. Kirchner, A. Rinaldo, and G. Botter (2015a), Modeling chloride transport using travel time distributions at Plynlimon, Wales, *Water Resources Research*, *51*(5), 3259-3276. https://doi.org/10.1002/2014WR016600

Benettin, P., C. Soulsby, C. Birkel, D. Tetzlaff, G. Botter, and A. Rinaldo (2017), Using SAS functions and high-resolution isotope data to unravel travel time distributions in headwater catchments, *Water Resources Research*, *53*(3), 1864-1878. https://doi.org/10.1002/2016WR020117

Benettin, P., S. W. Bailey, J. L. Campbell, M. B. Green, A. Rinaldo, G. E. Likens, K. J. McGuire, and G. Botter (2015b), Linking water age and solute dynamics in streamflow at the Hubbard Brook Experimental Forest, NH, USA, *Water Resources Research*, *51*(11), 9256-9272. https://doi.org/10.1002/2015WR017552

Botter, G., E. Bertuzzo, and A. Rinaldo (2011), Catchment residence and travel time distributions: The master equation, *Geophysical Research Letters*, *38*(11). https://doi.org/10.1029/2011GL047666

Brinkmann, N., S. Seeger, M. Weiler, N. Buchmann, W. Eugster, and A. Kahmen (2018), Employing stable isotopes to determine the residence times of soil water and the temporal origin of water taken up by Fagus sylvatica and Picea abies in a temperate forest, *New Phytol*, *219*(4), 1300-1313. https://doi.org/10.1111/nph.15255

Brooks, R. H., and A. T. Corey (1966), Properties of porous media affecting fluid flow, *Journal of the Irrigation and Drainage Division*, *92*(2), 61-90.

Campolongo, F., A. Saltelli, and J. Cariboni (2011), From screening to quantitative sensitivity analysis. A unified approach, *Comput Phys Commun*, *182*(4), 978-988. https://doi.org/10.1016/j.cpc.2010.12.039

Collenteur, R. A., G. Brunetti, and M. Vremec, Phydrus: Python implementation of the HYDRUS-1D unsaturated zone model, Version 0.2.0, available at https://github.com/phydrus/phydrus (last access: 30 August 2022)

Demand, D., and M. Weiler (2021), Potential of a Gravity-Driven Film Flow Model to Predict Infiltration in a Catchment for Diverse Soil and Land Cover Combinations, *Water Resources Research*, *57*(5), e2019WR026988. https://doi.org/10.1029/2019WR026988

Germann, P. F., and V. Prasuhn (2018), Viscous Flow Approach to Rapid Infiltration and Drainage in a Weighing Lysimeter, *Vadose Zone Journal*, *17*(1), 170020. https://doi.org/10.2136/vzj2017.01.0020

GNIP, Global Network of Isotopes in Precipitation available at https://www.iaea.org/services/networks/gnip (last access: 12.02.2023)

Green, W. H., and G. A. Ampt (1911), Studies in soil physics. 1 The flow of air and water through soils, *J Agric Sci*, *4*, 1–24.

Groh, J., C. Stumpp, A. Lücke, T. Pütz, J. Vanderborght, and H. Vereecken (2018), Inverse Estimation of Soil Hydraulic and Transport Parameters of Layered Soils from Water Stable Isotope and Lysimeter Data, *Vadose Zone Journal*, *17*(1). https://doi.org/10.2136/vzj2017.09.0168

Hansen, S., P. Abrahamsen, C. T. Petersen, and M. Styczen (2012), Daisy: Model Use, Calibration, and Validation, *Transactions of the ASABE*, *55*(4), 1317. https://doi.org/10.13031/2013.42244

Harman, C. J. (2015), Time-variable transit time distributions and transport: Theory and application to storage-dependent transport of chloride in a watershed, *Water Resources Research*, *51*(1), 1-30. https://doi.org/10.1002/2014WR015707

Heidbüchel, I., J. Yang, A. Musolff, P. Troch, T. Ferré, and J. H. Fleckenstein (2020), On the shape of forward transit time distributions in low-order catchments, *Hydrol. Earth Syst. Sci.*, *24*(6), 2895-2920. https://doi.org/10.5194/hess-24-2895-2020

Heße, F., M. Zink, R. Kumar, L. Samaniego, and S. Attinger (2017), Spatially distributed characterization of soil-moisture dynamics using travel-time distributions, *Hydrol. Earth Syst. Sci.*, *21*(1), 549-570. https://doi.org/10.5194/hess-21-549-2017

Hirschi, M., D. Michel, I. Lehner, and S. I. Seneviratne (2017), A site-level comparison of lysimeter and eddy covariance flux measurements of evapotranspiration, *Hydrol. Earth Syst. Sci.*, *21*(3), 1809-1825. https://doi.org/10.5194/hess-21-1809-2017

Hrachowitz, M., H. Savenije, T. A. Bogaard, D. Tetzlaff, and C. Soulsby (2013), What can flux tracking teach us about water age distribution patterns and their temporal dynamics?, *Hydrol. Earth Syst. Sci.*, *17*(2), 533-564. https://doi.org/10.5194/hess-17-533-2013

Hrachowitz, M., P. Benettin, B. M. van Breukelen, O. Fovet, N. J. K. Howden, L. Ruiz, Y. van der Velde, and A. J. Wade (2016), Transit times—the link between hydrology and water quality at the catchment scale, *Wiley Interdisciplinary Reviews: Water*, *3*(5), 629-657. https://doi.org/10.1002/wat2.1155

Jing, M., R. Kumar, F. Heße, S. Thober, O. Rakovec, L. Samaniego, and S. Attinger (2020), Assessing the response of groundwater quantity and travel time distribution to 1.5, 2, and 3 °C global warming in a mesoscale central German basin, *Hydrol. Earth Syst. Sci.*, *24*(3), 1511-1526. https://doi.org/10.5194/hess-24-1511-2020

Köhne, J. M., S. Köhne, B. P. Mohanty, and J. Šimůnek (2004), Inverse Mobile–Immobile Modeling of Transport During Transient Flow: Effects of Between-Domain Transfer and Initial Water Content, *Vadose Zone Journal*, *3*(4), 1309-1321. https://doi.org/10.2113/3.4.1309

Kumar, R., et al. (2020), Strong hydroclimatic controls on vulnerability to subsurface nitrate contamination across Europe, *Nature Communications*, *11*(1), 6302. https://doi.org/10.1038/s41467-020-19955-8

Kumaraswamy, P. (1980), A generalized probability density function for double-bounded random processes, *Journal of Hydrology*, *46*(1), 79-88. https://doi.org/10.1016/0022-1694(80)90036-0

Larsbo, M., and N. Jarvis (2005), Simulating Solute Transport in a Structured Field Soil, *J Environ Qual*, *34*(2), 621-634. https://doi.org/10.2134/jeq2005.0621

Makkink, G. F. (1957), Testing the Penman formula by means of lysimeters, *Journal of the Institution of Water Engineers*, *11*(3), 277-288.

Menzel, L., and N. Demuth (1993), Tracerhydrologische Untersuchungen am Lysimeter Rietholzbach, 24 pp, Geographisches Institut ETH Zürich, Zurich, Switzerland.

Michel, D., M. Hirschi, and S. I. Seneviratne, Stable water isotopes at Rietholbach lysimeter, Switzerland, available at https://doi.org/10.3929/ethz-b- (last access: 3 February 2023)

Nelson, D. B., D. Basler, and A. Kahmen (2021), Precipitation isotope time series predictions from machine learning applied in Europe, *Proceedings of the National Academy of Sciences*, *118*(26), e2024107118. doi:10.1073/pnas.2024107118

Nguyen, T. V., R. Kumar, A. Musolff, S. R. Lutz, F. Sarrazin, S. Attinger, and J. H. Fleckenstein (2022), Disparate Seasonal Nitrate Export From Nested Heterogeneous Subcatchments Revealed With StorAge Selection Functions, *Water Resources Research*, *58*(3), e2021WR030797. https://doi.org/10.1029/2021WR030797

Or, D., P. Lehmann, E. Shahraeeni, and N. Shokri (2013), Advances in Soil Evaporation Physics—A Review, *Vadose Zone Journal*, *12*(4), vzj2012.0163. https://doi.org/10.2136/vzj2012.0163

Peschke, G. (1985), Zur Bildung und Berechnung von Regenabfluß, *Wissenschaftliche Zeitschrift der Technischen Universität Dresden*, *34*(4).

Queloz, P., L. Carraro, P. Benettin, G. Botter, A. Rinaldo, and E. Bertuzzo (2015), Transport of fluorobenzoate tracers in a vegetated hydrologic control volume: 2. Theoretical inferences and modeling, *Water Resources Research*, *51*(4), 2793-2806. https://doi.org/10.1002/2014WR016508

Richter, D. (1995), Ergebnisse methodischer Untersuchungen zur Korrektur des systematischen Meßfehlers des Hellmann-Niederschlagsmessers, Selbstverlag des Deutschen Wetterdienstes, Offenbach am Main.

Rigon, R., and M. Bancheri (2021), On the relations between the hydrological dynamical systems of water budget, travel time, response time and tracer concentrations, *Hydrological Processes*, *35*(1), e14007. https://doi.org/10.1002/hyp.14007

Rinaldo, A., P. Benettin, C. J. Harman, M. Hrachowitz, K. J. McGuire, Y. van der Velde, E. Bertuzzo, and G. Botter (2015), Storage selection functions: A coherent framework for quantifying how catchments store and release water and solutes, *Water Resources Research*, *51*(6), 4840-4847. https://doi.org/10.1002/2015WR017273

Saltelli, A., M. Ratto, T. Andres, F. Campolongo, J. Cariboni, D. Gatelli, M. Saisana, and S. Tarantola (2008), *Global Sensitivity Analysis. The Primer*, John Wiley & Sons, Ltd, Chichester, England.

Salvucci, G. D. (1993), An approximate solution for steady vertical flux of moisture through an unsaturated homogeneous soil, *Water Resources Research*, *29*(11), 3749-3753. https://doi.org/10.1029/93wr02068

Schwemmle, R., Roger - a process-based hydrologic toolbox in Python, available at https://github.com/Hydrology-IFH/roger (last access: 20 January 2023)

Seeger, S., and M. Weiler (2014), Reevaluation of transit time distributions, mean transit times and their relation to catchment topography, *Hydrol. Earth Syst. Sci.*, *18*(12), 4751-4771. https://doi.org/10.5194/hess-18-4751-2014

Seneviratne, S. I., et al., Swiss prealpine Rietholzbach research catchment and lysimeter: 32 year time series and 2003 drought event, available at https://doi.org/10.3929/ethz-b- (last access: 3 February 2023)

Seneviratne, S. I., et al. (2012b), Swiss prealpine Rietholzbach research catchment and lysimeter: 32 year time series and 2003 drought event, *Water Resources Research*, *48*(6). https://doi.org/10.1029/2011wr011749

Šimůnek, J., M. T. van Genuchten, and M. Šejna (2016), Recent Developments and Applications of the HYDRUS Computer Software Packages, *Vadose Zone Journal*, *15*(7), vzj2016.2004.0033. https://doi.org/10.2136/vzj2016.04.0033

Sprenger, M., S. Seeger, T. Blume, and M. Weiler (2016), Travel times in the vadose zone: Variability in space and time, *Water Resources Research*, *52*(8), 5727-5754. https://doi.org/10.1002/2015WR018077

Sprenger, M., et al. (2019), The Demographics of Water: A Review of Water Ages in the Critical Zone, *Reviews of Geophysics*, *57*(3), 800-834. https://doi.org/10.1029/2018rg000633

Steinbrich, A., H. Leistert, and M. Weiler (2016), Model-based quantification of runoff generation processes at high spatial and temporal resolution, *Environmental Earth Sciences*, *75*(21), 1423. https://doi.org/10.1007/s12665-016-6234-9

Sternagel, A., R. Loritz, W. Wilcke, and E. Zehe (2019), Simulating preferential soil water flow and tracer transport using the Lagrangian Soil Water and Solute Transport Model, *Hydrol. Earth Syst. Sci.*, *23*(10), 4249-4267. https://doi.org/10.5194/hess-23-4249-2019

Sternagel, A., R. Loritz, B. Berkowitz, and E. Zehe (2022), Stepping beyond perfectly mixed conditions in soil hydrological modelling using a Lagrangian approach, *Hydrol. Earth Syst. Sci.*, *26*(6), 1615-1629. https://doi.org/10.5194/hess-26-1615-2022

van der Velde, Y., P. J. J. F. Torfs, S. E. A. T. M. van der Zee, and R. Uijlenhoet (2012), Quantifying catchment-scale mixing and its effect on time-varying travel time distributions, *Water Resources Research*, *48*(6). https://doi.org/10.1029/2011WR011310

Weiler, M. (2005), An infiltration model based on flow variability in macropores: development, sensitivity analysis and applications, *Journal of Hydrology*, *310*(1), 294-315. https://doi.org/10.1016/j.jhydrol.2005.01.010

Weiler, M., and F. Naef (2003), An experimental tracer study of the role of macropores in infiltration in grassland soils, *Hydrological Processes*, *17*(2), 477-493. https://doi.org/10.1002/hyp.1136

Wilusz, D. C., C. J. Harman, W. P. Ball, R. M. Maxwell, and A. R. Buda (2020), Using Particle Tracking to Understand Flow Paths, Age Distributions, and the Paradoxical Origins of the Inverse Storage Effect in an Experimental Catchment, *Water Resources Research*, *56*(4), e2019WR025140. https://doi.org/10.1029/2019WR025140

Yang, X., S. Jomaa, and M. Rode (2019), Sensitivity Analysis of Fully Distributed Parameterization Reveals Insights Into Heterogeneous Catchment Responses for Water Quality Modeling, *Water Resources Research*, *55*(12), 10935-10953. https://doi.org/10.1029/2019wr025575

Consistent modelling of transport processes and travel times – coupling soil hydrologic processes with StorAge Selection functions

Robin Schwemmle[1] and Markus Weiler[1]

[1]Hydrology, Faculty of Environment and Natural Resources, University of Freiburg, Freiburg, Germany

Corresponding author: Robin Schwemmle (robin.schwemmle@hydrology.uni-freiburg.de)

Key Points:

- Transport processes and the selection of appropriate StorAge Selection (SAS) functions depend on the considered soil hydrological processes
- Using a coupled-SAS approach representing advection-dispersion tranport by power law distribution function explains the transport of ^{18}O and bromide in a grassland lysimeter better than other transport representations
- The complete-mixing transport based on uniform SAS functions and a coarse vertical discretization may lead to errors in tracer arrival
- Choice between static or time-variant StorAge Selection differently affects parameter sensitivity of hydrologic model and transport model

Abstract

Understanding the transport processes and travel times of pollutants in the subsurface is crucial for an effective management of drinking water resources. Transport processes and soil hydrologic

processes are inherently linked to each other. In order to account for this link, we couple the process-based hydrologic model RoGeR with StorAge Selection (SAS) functions. We assign to each hydrological process a specific SAS function (e.g. power law distribution function). To represent different transport mechanisms, we combined a specific set of SAS functions into four transport model structures: complete-mixing, piston flow, advection-dispersion and advection-dispersion with time-variant parameters. In this study, we conduct modelling experiments at the Rietholzbach lysimeter, Switzerland. All modelling experiments are benchmarked with HYDRUS-1D. We compare our simulations to the measured hydrologic variables (percolation and evapotranspiration fluxes and soil water storage dynamics) and the measured water stable isotope signal (^{18}O) in the lysimeter seepage for a period of ten years (1997-2007). An additional virtual bromide tracer experiment was used to benchmark the models. Additionally, we carried out a sensitivity analysis and provide Sobol indices for hydrologic model parameters and SAS parameters. Our results show that the advection-dispersion transport model produces the best results. And thus, advective-dispersive transport processes play a dominant role at Rietholzbach lysimeter. Our modelling approach provides the capability to test hypotheses of different transport mechanisms and to improve process understanding and predictions of transport processes. Overall, the combined model allows a very effective simulation of combined flux and transport processes at various temporal and spatial scales.

Plain Language Summary

Knowledge about transport velocities of solutes through the soil is fundamental for an effective protection of drinking water resources from different pollution sources. We subsume transport velocities by the concept of travel times which is time from entering to leaving the soil. The calculation of travel times is based on the combination of a model representing the soil-vegetation-

atmosphere continuum and model representing the dynamics of solute ages based on probability distributions. The predictive accuracy of our calculations are satisfactory and travel times can be effectively estimated in space and time.

1 Introduction

Understanding the underlying transport processes of solutes, such as nitrate or pesticides, in soils is crucial for an effective management of drinking water resources. Thereby, solute transport and soil hydrologic processes, including percolation of soil water, root water uptake or runoff generation processes, are inherently linked to each other (e.g. Hrachowitz et al., 2016, Sprenger et al., 2019). The quantification of solute transport is still challenging and a unified approach considering flow and transport processes is still missing. Travel times are a widely used concept to enable the quantification of transport processes. They describe the time period of water parcels from entering (e.g. by infiltration) to leaving (e.g. by evapotranspiration, groundwater recharge) a system (e.g soil). Travel time distributions can inter alia be used to disentangle slow (e.g. transport through soil matrix) from fast transport (e.g. transport through macropores) (Benettin et al., 2015b; Sprenger et al., 2019).

In order to simulate water-bound transport of solutes in soil, two types of models can be discerned. On the one hand, physically-based transport models (e.g. Hansen et al., 2012; Köhne et al., 2004; Larsbo and Jarvis, 2005; Sternagel et al., 2019) provide information at high spatial and temporal resolution and important insights into process understanding of solute transport, once they are realistically parameterized. However, realistic parameterization requires detailed information on the modelled system (e.g. soil properties), which are usually not available in adequate spatial resolution. Moreover, estimation of solute breakthroughs or travel times requires the application of particle tracking which is computational expensive (e.g Brinkmann et al., 2018). On the other hand,

66 travel-time-based transport models try to include the calculation of travel times in their modelling
67 procedure and the empirical linkage between travel times and solute transport provide useful in-
68 formation about the soil transport patterns. However, they also simplify the transient processes of
69 solute transport in soils. In recent years, travel-time-based transport models using StorAge selec-
70 tion (SAS) functions (Rinaldo et al., 2015) have particularly emerged in solute transport studies
71 (e.g. Asadollahi et al., 2020; Asadollahi et al., 2022; Kumar et al., 2020; Nguyen et al., 2022;
72 Rigon and Bancheri, 2021). They can be distinguished into pure-SAS (e.g. Benettin and Bertuzzo,
73 2018) and coupled-SAS approaches (e.g. Heße et al., 2017). Pure-SAS models rely on measured
74 storage states (e.g. soil water content) and input/output fluxes (e.g. streamflow) and represent un-
75 derlying hydrologic processes in a lumped way, whereas coupled-SAS models link simulated
76 fluxes and storages from hydrologic models with SAS functions. A prerequisite for coupled-SAS
77 models is an appropriate model structure, i.e. a model structure that contains all relevant hydro-
78 logical processes of the considered hydrological system. Unlike pure-SAS models, coupled-SAS
79 models only require a upper boundary condition (e.g. precipitation, potential evapotranspiration)
80 and can be applied as lumped (e.g. Hrachowitz et al., 2013) or spatially-distributed predictions
81 (e.g. Jing et al., 2020).
82 Since Botter et al. (2011) has introduced the master equation, pure-SAS models have widely been
83 applied at the plot scale (e.g. Asadollahi et al., 2020; Asadollahi et al., 2022; Queloz et al., 2015)
84 and catchment scales (e.g. Benettin et al., 2015a; Benettin et al., 2017; Harman, 2015; Wilusz et
85 al., 2020). Thereby, pure-SAS models successfully reproduced measured solute or stable isotope
86 concentrations in lysimeter seepage or streamflow. Due to spatial heterogeneity, travel times at
87 plot scale derived by pure-SAS models differed from those at catchment scale (Queloz et al., 2015).
88 At the plot-scale, pure-SAS modelling experiments with isotope and flourobenzol tracers modeled

found that tracer transport is realistically explained if soil water percolation was dominated by old water (Asadollahi et al., 2020; Asadollahi et al., 2022; Queloz et al., 2015).

In contrast to pure-SAS models, coupled-SAS models were applied mainly applied at the catchment scale (e.g. Benettin et al., 2017; Jing et al., 2020; Kumar et al., 2020; Nguyen et al., 2022; Yang et al., 2019) to predict conservative (e.g. deuterium) and non-conservative solute transport (e.g. nitrate). In these studies, simulations were compared to measured concentrations at the catchment outlet. Those integrate all processes and hence only allow for a non-direct, spatially-implicit analysis of internal transport processes (e.g. groundwater recharge). Furthermore, using a non-conservative instead of a conservative tracer blurs the analysis of underlying transport processes due to inherent interaction between transport and biogeochemical processes. To date, coupled-SAS models have neither been applied at the plot scale nor evaluated with plot-scale observations.

In this study, we couple the soil hydrologic model RoGeR (Runoff Generation Research; Steinbrich et al., 2016) with SAS functions. We assign SAS functions to each implemented hydrologic process and test different transport hypotheses (e.g. piston, advection-dispersion) represented by different model structures, each evaluated by a sensitivity analysis using the Sobol method. We use bromide and isotope data from the Rietholzbach lysimeter in Switzerland (Menzel and Demuth, 1993; Seneviratne et al., 2012b). Similar to other studies investigating travel times at the plot scale (e.g. Asadollahi et al., 2020; Sprenger et al., 2016), we provide a benchmark comparison with HYDRUS-1D.

We will address three main research questions: (i) What are the sensitivities of hydrologic model parameters and SAS parameters for the different transport model structures using a coupled-SAS

approach? (ii) Which transport model structure explains isotope and bromide transport at the Rietholzbach lysimeter most realistically? (iii) What are the advantages of a coupled-SAS transport model compared to a physically-based transport model?

2 Study site

The Rietholzbach lysimeter is situated within the pre-alpine Rietholzbach research catchment, Switzerland (Hirschi et al., 2017; Seneviratne et al., 2012b). The lysimeter is located at an elevation of 755 m above sea level and climatic characteristics can be summarized by an average air temperature of 7.1 °C, average annual precipitation of 1459 mm and annual actual evapotranspiration of 560 mm. The weightable lysimeter container is filled with the local gleyic cambisol and has an entire depth of 2.5 m (Figure 1). A 0.5 m thick layer of sand and gravel at the bottom of the lysimeter enables free drainage. The 3.14 m^2 lysimeter surface is covered by grass, which is cut at similar times as the surrounding grassland. We use hydrometeorological data and bi-weekly bulk samples of the stable water isotope oxygen-18 ($\delta^{18}O$) in precipitation and lysimeter seepage from Seneviratne et al. (2012b). Data gaps in $\delta^{18}O$ of precipitation have been filled with data from nearby GNIP station St. Gallen (GNIP, 2023) and using Piso.AI (Nelson et al., 2021). Additional model evaluation was possible by including data from a bromide tracer experiment (Menzel and Demuth, 1993) carried out from November 1991 to February 1993. Due to data availability, our study investigates bromide transport the period from November 1991 to February 1993 (see Sect. 3.4) and bromide and ^{18}O transport for the period from January 1997 to December 2007 (see Figure 1).

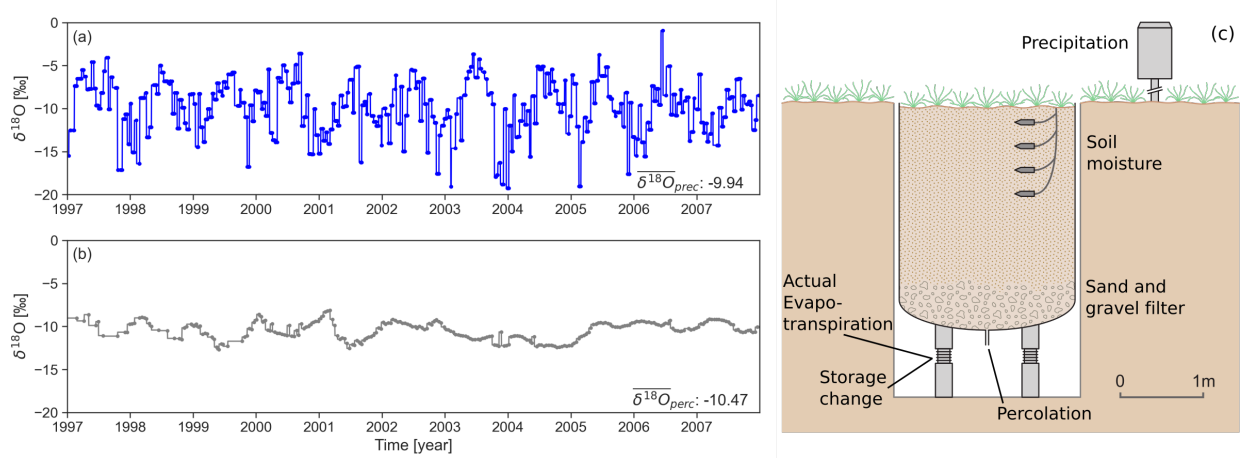

Figure 1. (a) Bi-weekly measured $\delta^{18}O$ in precipitation and (b) measured $\delta^{18}O$ in lysimeter seepage at Rietholzbach lysimeter. (c) Cross-section of Rietholzbach lysimeter with measured variables (modified from Seneviratne et al. (2012b)). Storage change and actual evapotranspiration are derived from measured lysimeter weight change. Air temperature and global radiation were measured at the nearby are measured at the nearby weather station (not shown).

3 Methods

3.1 Representation of soil hydrologic processes using the hydrologic model RoGeR

As stated above, realistic process-oriented hydrological modelling should be the prerequisite for successful coupled-SAS approaches. Here, we use the RoGeR model (Steinbrich et al., 2016), which was developed from the soil hydrological model IN^{3}M (Weiler, 2005) to calculate hydrologic fluxes and storage volumes. These fluxes and storage volumes were then coupled with the SAS functions. In RoGeR, hydrologic fluxes and storage dynamics are simulated with an adapted temporal resolution (time steps of 10 minutes for high rainfall intensities, hourly time steps for low rainfall intensities or snow melt, and daily time steps for dry periods). The model requires precipitation (mm/10 minutes), daily air temperature (°C) and daily potential evapotranspiration (mm/day) data as input. We corrected the original precipitation data according to Richter (1995) to account for systematic errors due to wind uncercatch in the measurement of precipitation. Po-

147 tential evapotranspiration is calculated after Makkink (Makkink, 1957) with daily average air tem-
148 perature (°C) and daily average global radiation (MJ/m^2). Model parameters are listed in Table 1.
149 The hydrologic processes considered in this study are summarizes as:

150 - **Surface water storage:** Surface water storage comprises an interception storage. Storage pa-
151 rameters are land cover specific and seasonally time-variant.
152 - **Soil water storage:** Soil water storage is divided into an upper (i.e. root zone) and lower
153 storage (i.e. subsoil). Soil hydraulic parameters are derived using a Brooks-Corey scheme
154 (Brooks and Corey, 1966). The two soil storage layers have the same soil hydraulic param-
155 terization.
156 - **Evapotranspiration:** Evapotranspiration is limited by energy (i.e. potential evapotranspira-
157 tion) and water availability (i.e. soil water content). Evapotranspiration occurs sequentially
158 from top to bottom (interception evaporation, soil evaporation and transpiration). Soil evapo-
159 ration is represented by the Stage I – Stage II scheme (Or et al., 2013). Transpiration (i.e. flux
160 by root water uptake) is limited to vegetation/land cover specific root depth. The seasonal
161 variation of ground cover (e.g. deciduous trees) are quantified by a transpiration coefficient.
162 - **Interception:** Interception storage is represented by a single bucket. Liquid and solid precip-
163 itation fill the storage and the interception storage spills over if storage exceeds total storage
164 capacity. Evaporation empties the interception storage.
165 - **Snow accumulation/Snow melt**: Solid precipitation (air temperature below 0 °C) accumu-
166 lates in the interception storage or at the ground surface. Snow melt is calculated by a degree-
167 day approach and by a delayed release of melt water.
168 - **Infiltration:** Water infiltrates into the soil matrix, into macropores or shrinkage cracks. Matrix
169 infiltration is implementend by a modified Green-Ampt approach (Green and Ampt, 1911;

Peschke, 1985). Infiltration through macropores is represented by the approach from Weiler (2005) and requires excess of soil matrix infiltration. Macropore infiltration depends on density, length of vertical macropores and saturated hydraulic conductivity. Depending on the parameterization, macropore infiltration can attain shares up to 70 % of total infiltration. Infiltration through shrinkage cracks is adopted from Steinbrich et al. (2016) and depends on clay and soil water content. Water exchange from macropores/cracks is realized with a geometriy-dependend solution of horizontal infiltration by a Green-Ampt approach (Steinbrich et al., 2016)

Table 1. Hydrologic model parameters, their lower and upper parameter boundaries for the Monte-Carlo (MC) sampling and Saltelli (SA) sampling, and the final parameter sets of the best 100 simulations (average ± standard deviation). Usable porosity, fraction of large pores and fraction of fine pores are auxillary parameters used to set meaningful parameters for air capacity of soil and and plant available field capacity.

Hydrologic model parameter		**Unit**	**Parameter boundaries**		**Best parameter(s)**
			MC	**SA**	
Land use/Land cover	lu_id	-	8		8
Makkink coefficient	$c1_{PET}$	-	0.55 - 0.65	0.5 - 0.7	0.61 ± 0.03
Makkink coefficient	$c2_{PET}$	mm day^{-1}	-0.2 - 0.0	-0.4 - 0.2	-0.09 ± 0.05
Density of vertical macropores	ρ_{mpv}	m^{-2}	10 - 300	1 - 400	202 ± 70
Length of vertical macropores	l_{mpv}	mm	50 - 1500	1 - 2000	879 ± 165
Soil depth	z_{soil}	mm	2200		2200
Effective porosity[1]	θ_{eff}	-	0.15 - 0.35		0.21 ± 0.04
Fraction of large pores	f_{lp}	-	0.1 - 0.6		0.59 ± 0.05
Fraction of fine pores	f_{fp}	-	1 - f_{lp}		0.41 ± 0.05
Air capacity of soil	θ_{ac}	-	θ_{eff} ・ f_{lp}		0.13 ± 0.03
Plant available field capacity of soil	θ_{ufc}	-	θ_{eff} ・ f_{fp}		0.09 ± 0.02
Permanent wilting point of soil	θ_{pwp}	-	0.15 - 0.25	0.1 - 0.25	0.2 ± 0.03
Saturated hydraulic conductivity of soil	k_s	mm h^{-1}	5 - 150		83.3 ± 43.6
Hydraulic conductivity of bedrock	k_f	mm h^{-1}	2500		2500

[1]describes the total volume of mobile soil water storage

- **Surface runoff:** Surface runoff is generated either by Hortonian (HOF; i.e. infiltration excess) or saturation overland flow (SOF; i.e. saturation of soil storage).
- **Capillary rise / Percolation:** Vertical drainage and upward water movement is described by the approach of Salvucci (1993). For this study, we implemented a free drainage for the lower boundary condition by setting the hydraulic conductivity of bedrock (k_f) to a constant value of 2500 mm/h (Table 1).

For detailed process and parameter descriptions including all model equations, we refer to the supporting information or to Schwemmle (2023) for most current information.

We run Monte Carlo simulations with 30 000 samples in predefined boundaries (see Table 1). Initial soil water content was set to field capacity. A multi-objective metric E_{multi} serves to identify the best performing parameter set.

$$E_{multi} = 0.4\,KGE_{ET} + 0.2\,KGE_{\Delta S} + 0.4\,KGE_{PERC} \quad (1)$$

where KGE_{ET} is the Kling-Gupta efficiency of evapotranspiration fluxes, $KGE_{\Delta S}$ is the Kling-Gupta efficiency of total storage change and KGE_{PERC} is the Kling-Gupta efficiency of percolation fluxes. E_{multi} ranges between 1 and ∞ in which $E_{multi} = 1$ indicates a perfect agreement between observations and simulations. KGE_{ET} and KGE_{PERC} are assigned with greater weights due to longer coverage of observed values. The best 100 hydrological simulations are coupled with SAS functions by an offline-scheme (i.e. hydrologic response and hydrologic transport are not simulated simultaneously).

3.2 Representation of transport processes using StorAge Seclection (SAS) functions

We use the fractional SAS function type (fSAS; van der Velde et al., 2012) and solve the SAS functions for each hydrologic flux Q:

$$\overleftarrow{p}_Q(\mathrm{T},\mathrm{t}) = \frac{\partial}{\partial T}\Omega_Q(P_S(T,t),t) \quad (2)$$

with

$$P_S(T,t) = \frac{S_T(T,t)}{\mathrm{S(t)}} \quad (3)$$

where T is the water age, t is the time step, $\overleftarrow{p}_Q(\mathrm{T},\mathrm{t})$ is the backward travel time distribution of a specific hydrologic flux, ω_Q(T,t) is the probability distribution function of the hydrologic flux (where Ω_Q(T,t) is the cumulative probability distribution function), S_T(T,t) is the cumulative age-ranked storage (mm), S(t) is the soil water content (mm) and P_S (T,t) is the cumulative probability distribution of the storage (where p_S (T,t) is the probability distribution). The hydrologic processes sequentially update S_T(T,t) at time step t by looping over internal substeps n (n=6):

$$\mathrm{S(T,i+1)} = \mathrm{S(T,i)} \pm \overleftarrow{p}_Q(T,i)\cdot Q(t)\cdot h \quad (4)$$

where i is the substep, h is the time increment of the substep (day) and Q(t) (mm day^{-1}) is the flux from the corresponding hydrologic process. The hydrologic processes update S_T(T,t) in the following sequence: infiltration (1; *inf*), soil evaporation (2; $evap_{soil}$), transpiration (3; *transp*), root zone percolation (4; $perc_{rz}$), subsoil percolation (5; $perc_{ss}$) and capillary rise from subsoil into root zone (6; cpr_{rz}). When the soil surface is covered by snow, we fully mix δ^{18}O in precipitation with δ^{18}O in the snow cover (Seeger and Weiler, 2014). The δ^{18}O in the snow cover might infiltrate while snow melt.

Tracer concentrations (‰ for δ^{18}O; mg l^{-1} for bromide) are for each hydrologic flux Q are calculated as:

$$C_Q = \int_{T=0}^{\infty} C_S(T,t)\cdot\alpha_p\cdot\overleftarrow{p}_Q(T,t)dT \quad (5)$$

where C_S(T,t) is the age-ranked tracer storage and α_p is the partition coefficient which ranges from 0 (not dissolved) to 1 (fully dissolved). For δ^{18}O transport α_p is set to 1. For bromide transport, we

set α_p to a value of 0.8 since Menzel and Demuth (1993) found a bromide recovery rate of 80 %, which could be related to uptake by vegetation or sorption processes. Isotopic fractionation is not considered owing to the small difference between the average of $\delta^{18}O$ in precipitation and $\delta^{18}O$ in lysimeter seepage (see Figure 1).

The age preference of SAS functions and thus the shape of the travel time distribution (TTD) is controlled by the choice of the probability distribution function. By assigning a probability distribution function as a SAS function to each hydrologic process, we can conceptualize the underlying transport process. For example, faster transport may be represented by right-skewed ω_Q and slower transport by left-skewed ω_Q.

In order to test different hypotheses about the tracer transport processes at the Rietholzbach lysimeter, we group combinations of ω_Q according to four transport model structures. Within these transport model structures, we represent potential transport processes by specific parameters for ω_Q (Figure 3):

- **Complete-mixing model (CM):** All processes have no age preference (i.e. are well mixed). Each process uses a uniform SAS function:

$$\Omega_Q(T,t) = P_s(T,t) \quad (6)$$

- **Advection-Dispersion model (AD):** Transport processes of transpiration and percolation are implemented by an advective-dispersive scheme using a power law distribution function:

$$\Omega_Q(T,t) = P_s(T,t)^{k_Q} \quad (7)$$

  Soil evaporation and capillary rise prefer youngest water and are described by advective transport using a constant parameter k_Q (k_Q=0.1; see equation (7)).

- **Advection-Dispersion model with time-variant parameters (AD-TV):**

Soil evaporation and capillary rise are described as in AD. But transpiration has time-variant preference implemented by a power law distribution function with a time-variant parameter k_Q:

$$\Omega_Q(T,t) = P_s(T,t)^{k_Q},\ k_Q = c_{1-Q} + c_{2-Q}\frac{S(t) - S_{pwp}}{S_{sat} - S_{pwp}} \quad (8)$$

where S_{sat} is the soil storage volume at saturation (mm) and S_{pwp} is the soil storage volume at permanent wilting point (mm). In equation (8), preference for younger water increases for wet conditions and decreases for dry conditions.

The time-variant preference of percolation is formulated as:

$$\Omega_Q(T,t) = P_s(T,t)^{k_Q},\ k_Q = c_{1-Q} + c_{2-Q}\left(1 - \frac{S(t) - S_{pwp}}{S_{sat} - S_{pwp}}\right) \quad (9)$$

As a result, preference for older water increases for dry conditions and decreases for wet conditions.

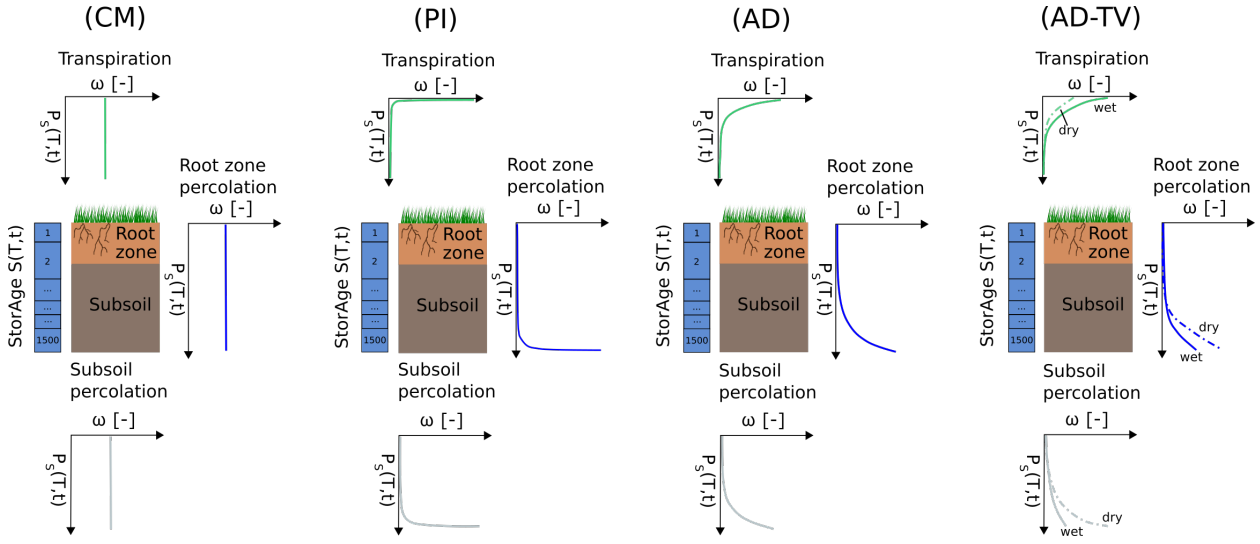

Figure 2. Transport model structures coupled with hydrologic simulations: Complete-mixing transport model (CM), Piston transport model (PI), Advection-dispersion transport model (AD) and Advection-dispersion transport model with time-variant SAS parameters (AD-TV). Soil evaporation and capillary rise (not shown) prefer in all transport model structures the youngest water (see equations (7) with constant k_Q=0.1).

Piston-flow model (PI): Transport processes are purely advective. The power law distribution function serves as a SAS function. Processes characterized by flux leaving the storage at the top have a strong preference for younger (equation (7) with constant k_Q=0.1). Processes dominated by bottom fluxes have a strong preference for older water (equation (7) with constant k_Q=100).

Table 2 Transport model parameters and their lower and upper parameter boundaries for the Monte-Carlo (MC) sampling and Saltelli (SA) sampling. Transp indicates parameters of transpiration process and perc indicates parameters of percolation processes. There are no MC and SA simulations for parameter-free CM and constant-parameter PI.

Transport model parameter	Unit	Transport model structure	Parameter boundaries		Best parameter
			MC	SA	
No parameters		CM	-	-	-
Constant parameters		PI	-	-	-
k_{transp}	-	AD	0.2 - 1	0.1 - 5	0.18
$k_{perc\text{-}rz}$	-	AD	1 - 5	0.1 - 5	2.54
$k_{perc\text{-}ss}$	-	AD	1 - 5	0.1 - 5	2.08
$c_{1\text{-}transp}$	-	AD-TV	0.1 - 0.5	0.1 - 5	-
$c_{2\text{-}transp}$	-	AD-TV	0.1 - 2	0.1 - 5	-
$k_{1\text{-}transp}$	-	AD-TV	$c_{1\text{-}transp}$		0.17
$k_{2\text{-}transp}$	-	AD-TV	$c_{1\text{-}transp} + c_{2\text{-}transp}$		0.97
$c_{1\text{-}perc\text{-}rz}$	-	AD-TV	1 - 2	0.1 - 5	-
$c_{2\text{-}perc\text{-}rz}$	-	AD-TV	0.1 - 3	0.1 - 5	-
$k_{1\text{-}perc\text{-}rz}$	-	AD-TV	$c_{1\text{-}perc\text{-}rz}$		1.83
$k_{2\text{-}perc\text{-}rz}$	-	AD-TV	$c_{1\text{-}perc\text{-}rz} + c_{2\text{-}perc\text{-}rz}$		4.16
$c_{1\text{-}perc\text{-}ss}$	-	AD-TV	1 - 2	0.1 - 5	-
$c_{2\text{-}perc\text{-}ss}$	-	AD-TV	0.1 - 5	0.1 - 5	-
$k_{1\text{-}perc\text{-}ss}$	-	AD-TV	$c_{1\text{-}perc\text{-}ss}$		1.66
$k_{2\text{-}perc\text{-}ss}$	-	AD-TV	$c_{1\text{-}perc\text{-}ss} + c_{2\text{-}perc\text{-}ss}$		1.98

3.3 Monte Carlo analysis and sensitivity analysis with the Sobol method

We run Monte Carlo simulations with 10 000 samples. The main purpose of the Monte Carlo Analysis is the parameter estimation, an additional uncertainty analysis goes beyond this study. Monte Carlo simulations are computed with the transport model structures AD and AD-TV, but not with parameter-free CM (see equation (6)) and constant-parameters PI (see equation (7) with

278 k_Q=0.1 and k_Q=100). Each simulation uses a 5-year simulation period (1997-2001) as a warmup
279 run (see Figure 1) to derive C_S(T,t=0). After warmup, we rescale S_T(T,t) with S_{init}/S_T(T,t), since we
280 have knowledge about initial soil water content but do not know initial $\delta^{18}O$ in soil water. Param-
281 eter ranges are provided in Table 2. We calculated KGE to evaluate simulations of $\delta^{18}O$ in perco-
282 lation. Since $\delta^{18}O$ in percolation are analyzed from bi-weekly bulk samples, we aggregate simula-
283 tions to bi-weekly bulk-samples by flux-weighted average.
284 We additionally conduct a sensitivity analysis using the Sobol method (Saltelli et al., 2008). Pa-
285 rameter sets are generated using Saltelli's extension of the Sobol sequence (Campolongo et al.,
286 2011; see Table 1 and Table 2) with a sample size of 1024. We calculate first order and total Sobol
287 indices for evaluation metrics and age statistics.

288 **3.4 Benchmark comparison to HYDRUS-1D and bromide experiment**

289 Simulations with HYDRUS-1D (Šimůnek et al., 2016, Collenteur et al., 2022) are performed with
290 a dual-porosity domain. A detailed description of the HYDRUS-1D setup is provided in the sup-
291 porting information (section S4). We run 30 000 Monte Carlo simulations and select the best per-
292 forming parameter set based on the multi-objective KGE_{multi} (Sprenger et al., 2016):

293 $$KGE_{multi} = \frac{1}{2}\left(\frac{1}{2}KGE_{\theta} + \frac{1}{2}\left(\frac{1}{2}KGE_{aet} + \frac{1}{2}KGE_{perc}\right)\right) + \frac{1}{2}KGE_{\delta^{18}O} \quad (10)$$

294 where the KGE_{θ} is the average KGE of soil water content at different soil depths z (5 cm, 15 cm,
295 25 cm 35 cm, 55 cm, 80 cm and 110 cm), KGE_{aet} compares simulated and observed actual evapo-
296 transpiration, KGE_{perc} compares simulated and observed actual evapotranspiration and $KGE_{\delta 18O}$
297 compares simulated and observed $\delta^{18}O$ in percolation.

Based on KGE_{multi} (see equation (10)), we select the best performing parameter set and perform three benchmark comparisons between HYDRUS-1D modeling results and RoGeR modeling results:

1. We compare our results to $\delta^{18}O$ transport simulations with HYDRUS-1D.
2. We compare our results to travel time distributions calculated with HYDRUS-1D.
3. For the virtual bromide experiments, we selected the best performing parameter set (i.e. best $KGE_{\delta 18_O}$) for each transport model structure to simulate $\delta^{18}O$ transport. We, then, transfer the $\delta^{18}O$ model parameters to the bromide model. Bromide breakthrough is simulated with each transport model structure and compared to the results of Menzel and Demuth (1993) and bromide transport simulations with HYDRUS-1D. Since the bromide experiment was conducted on 12th November 1991 prior to the time period of our study and the available meteorological input data, we repeat virtual experiments for each year between 1997 and 2006 and inject a bromide mass of 79.9 g (i.e. one mole potassium bromide dissolved in one liter water) at 12th November. Additionally, we used meteorologic data from the nearby station MeteoSwiss station St. Gallen (775 m above sea level; 9°24'W 47°26'N) to simulate the period of the bromide experiment. We adjusted the precpitation data by rescaling with the average annual precipitation at the Rietholzbach lysimeter and air temperature data to the altitude difference between St. Gallen and Rietholzbach lysimeter.

4 Results

4.1 Simulated hydrologic fluxes and storages

The best 100 hydrologic parameters according to E_{multi} (see equation (1)) are summarized in Table 1. The corresponding values of E_{multi} and its metric terms are displayed in Table 3. Values for E_{multi} are larger for simulations with RoGeR than for simulations with HYDRUS-1D. E_{multi} of simulations with RoGeR show an increasing tendency from drier to wetter antecedent conditions. The cumulated values of the best 100 simulations according to E_{multi} are compared with observed values and the best HYDRUS-1D simulation. The comparison for two time periods with highest consistent coverage of observations is shown in Figure 5. Despite a low variance of E_{multi} (see Table 3), simulations reveal differences in the cumulated flux volumes. In particular, absolute differences are greatest for percolation (Figure 5c and 5f).

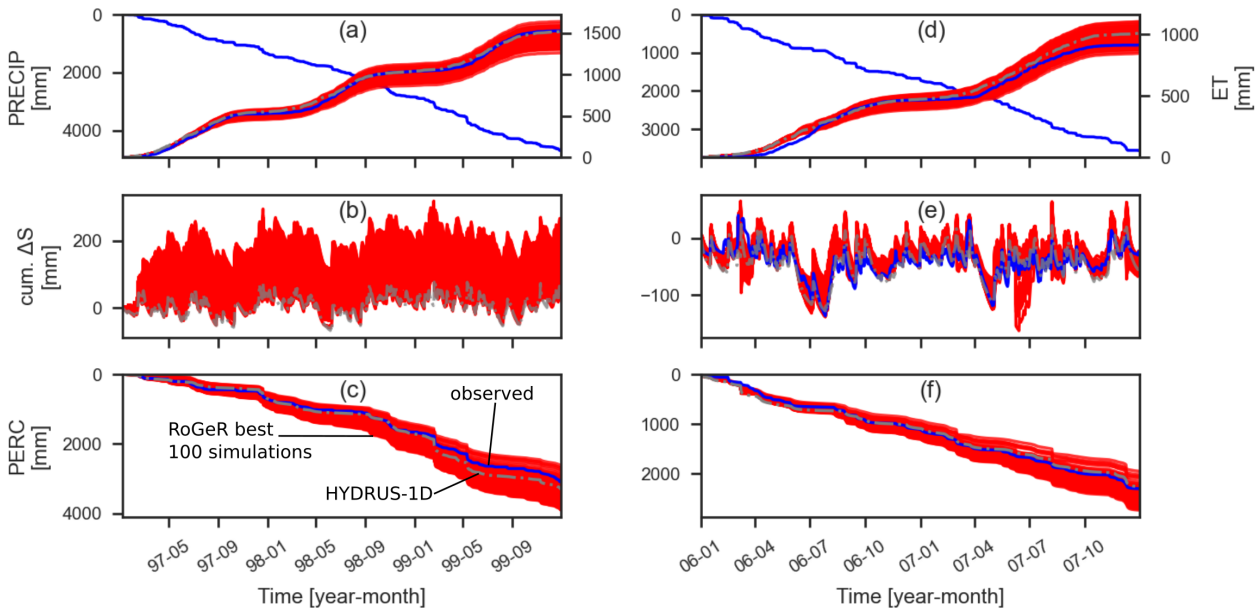

Figure 3. Cumulative precipitation, cumulative simulated and observed evapotranspiration (a,d), cumulative simulated and observed storage change (b,e), and cumulative simulated and observed percolation (c,f). Data for observed storage change from 1997 to 1999 is not available.

Table 3. Evaluation metrics of best 100 RoGeR simulations (average ± standard deviation) and best HYDRUS-1D simulation for different antecedent soil moisture conditions. Antecedent soil moisture conditions are defined by 10^{th} (θ_{a10}) and 90^{th} (θ_{a90}) percentiles of average observed soil moisture from previous 5 days (θ_a; dry: $\theta_a < \theta_{a10}$; normal: $\theta_{a10} \leq \theta_a \leq \theta_{a90}$; wet: $\theta_a > \theta_{a90}$)

	KGE_{aet}		$KGE_{\Delta S}$		KGE_{perc}		E_{multi}	
	RoGeR	HYDRUS-1D	RoGeR	HYDRUS-1D	RoGeR	HYDRUS-1D	RoGeR	HYDRUS-1D
total	0.78 ± 0.05	0.80	0.74 ± 0.1	-0.05	0.53 ± 0.06	0.58	0.67 ± 0.02	0.54
dry	0.55 ± 0.09	0.60	0.83 ± 0.05	0.59	0.16 ± 0.1	0.06	0.45 ± 0.03	0.39
normal	0.79 ± 0.05	0.81	0.69 ± 0.1	-0.1	0.43 ± 0.08	-0.74	0.63 ± 0.03	0.01
wet	0.81 ± 0.04	0.88	0.67 ± 0.13	0.52	0.65 ± 0.1	0.69	0.72 ± 0.06	0.73

4.2 Monte Carlo analysis

The best simulation for $\delta^{18}O$ in percolation of each transport model structure is shown in Figure 6. The AD and AD-TV model structure visually agrees with the general pattern of $\delta^{18}O$ observations in the percolation flux. The CM-model depicts lower agreement between simulations and observations, while the PI-model shows the lowest agreement among the four model structures. KGE values (Table 4) confirm the visual pattern of Figure 6. The AD-model structure scores highest KGE values and performs slightly better than HYDRUS-1D. We tested further transport model structures with RoGeR (e.g. preferential transport). For the results of the additional model structures, we refer to the supporting information (section S2). In contrast to the hydrologic simulations, the transport simulations from the CM, AD and AD-TV transport model structure picture a decrease of model performance from drier antecedent conditions to wetter antecedent conditions.

4.3 Sensitivity analysis with the Sobol' method

Figure 7 shows Sobol' indices of hydrologic model parameters for averaged median travel time of transpiration ($TT_{50\text{-}transp}$) and percolation ($TT_{50\text{-}perc}$) and for KGE of $\delta^{18}O$ in percolation ($KGE_{\delta 18_O}$). The four transport model structures share the same set of sensitive hydrologic model parameters. For the two travel time statistics, Sobol' indices are greatest for fraction of large pores (f_{lp}) except

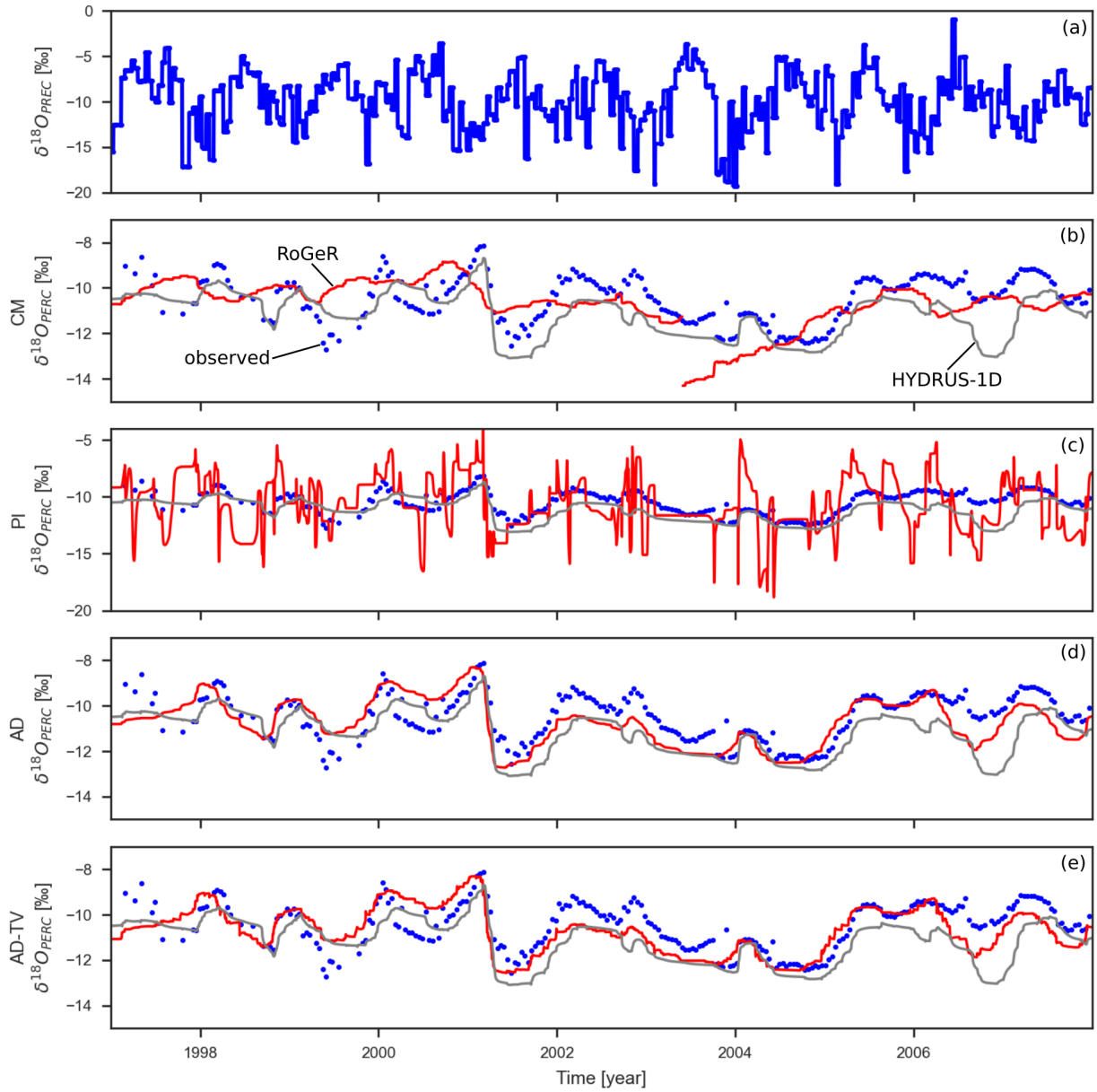

Figure 4. Observed $\delta^{18}O$ in precipitation (a) and observed and simulated $\delta^{18}O$ in percolation with RoGeR and HYDRUS-1D (b-e). Values are shown for different model structures (see Figure 2).

for $KGE_{\delta 18O}$ of AD and AD-TV for which Sobol' indices of permanent wilting point (θ_{pwp}) are greatest. In addition to that, averaged $TT_{50\text{-}perc}$ is sensitive for macropore parameters (ρ_{mpv} and l_{mpv}). In general, total Sobol' indices exceed values of first-order Sobol' indices. Total Sobol' indices describe the fraction of variance that is caused by the variability of the considered parameter. First-

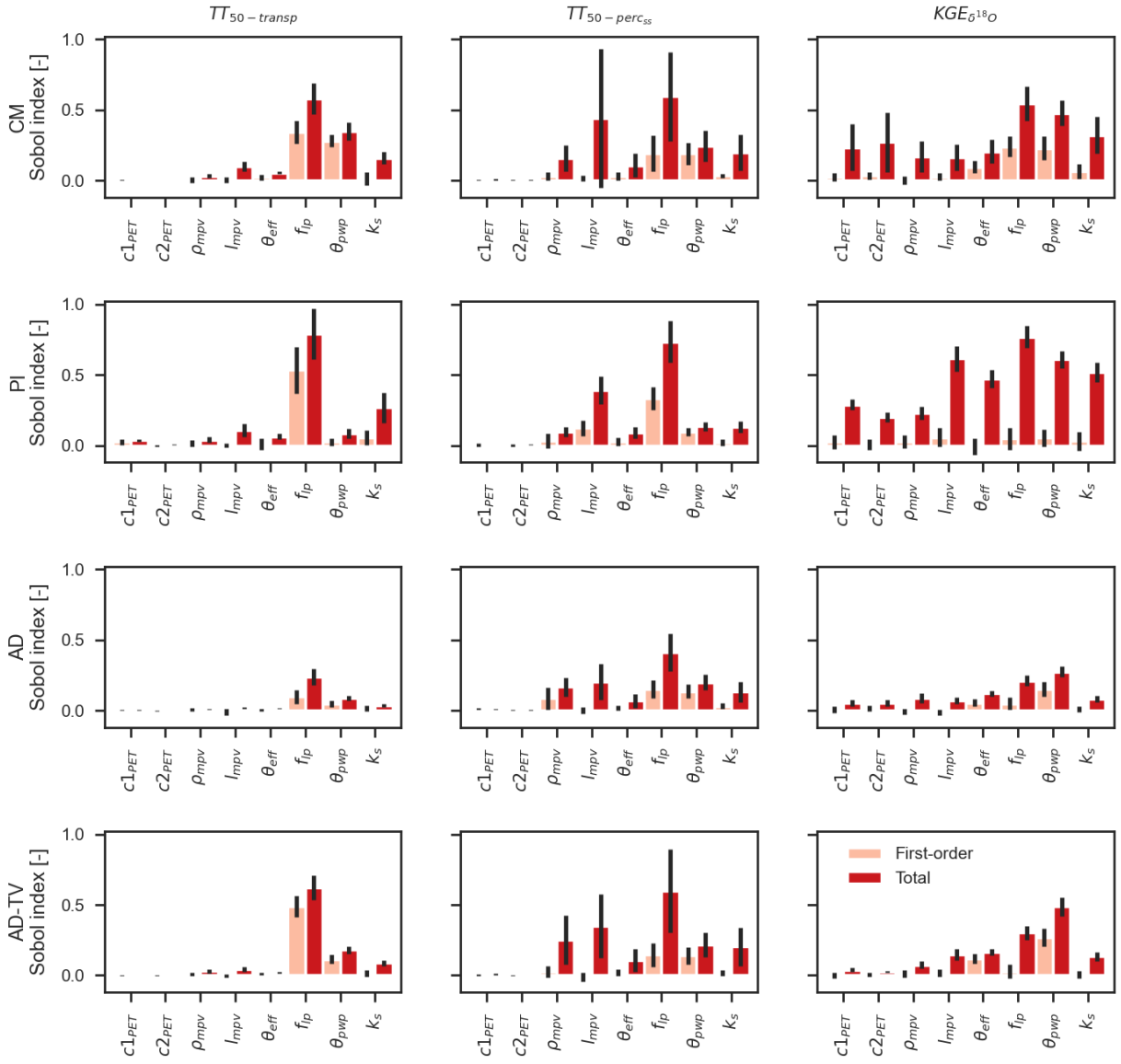

Figure 5. Sobol' indices with error bars (95% confidence interval) of hydrologic model parameters (see Table 1) calculated for averaged median travel time of transpiration ($TT_{50\text{-transp}}$), averaged median travel time of percolation ($TT_{50\text{-percss}}$) and KGE of $\delta^{18}O$ in percolation ($KGE_{\delta^{18}O}$). Values are shown for complete-mixing transport model structure (CM), piston-flow transport model structure (PI), advection-dispersion transport model structure (AD) and advection-dispersion transport model structure with time-variant SAS parameters (AD-TV).

order Sobol' indices represent direct contribution to the total Sobol' indices of the considered parameter. A difference between total Sobol' indices and first-order Sobol' indices might be ex-

plained by parameter interactions. These differences are more distinct for $TT_{50\text{-}perc}$. The gap between first-order Sobol' indices and total Sobol' indices suggests a strong interaction between parameters.

Sobol' indices of SAS parameters for $TT_{50\text{-}transp}$, $TT_{50\text{-}perc}$ and $KGE_{\delta^{18}O}$ are displayed in Figure 8. Comparing the Sobol indices between hydrologic model parameters and SAS parameters reveal two different results: (i) The AD model structure is more sensitive for SAS parameters than for hydrologic model parameters. (ii) The AD-TV model structure is more sensitive for hydrologic model parameters than for SAS parameters. Regarding travel times, we found greater Sobol' indices for $TT_{50\text{-}transp}$ than for $TT_{50\text{-}perc}$.

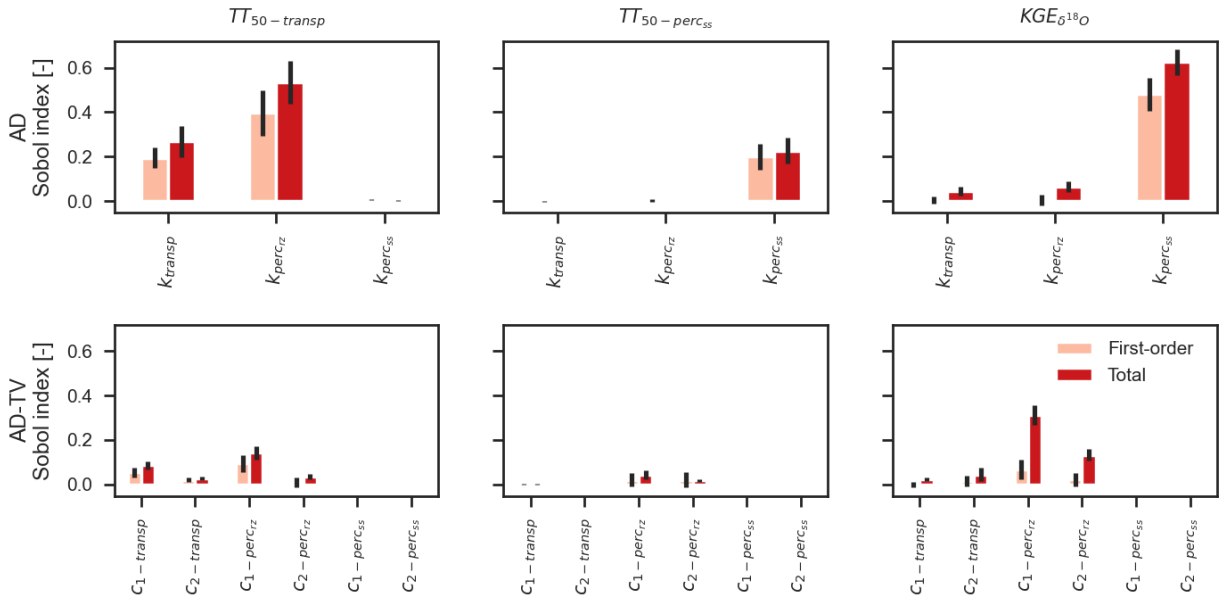

Figure 6. Sobol' indices with error bars (95% confidence interval) of SAS parameters (see Table 2) calculated for averaged median travel time of transpiration ($TT_{50\text{-transp}}$), averaged median travel time of percolation ($TT_{50\text{-percss}}$) and KGE of $\delta^{18}O$ in percolation ($KGE_{\delta^{18}O}$). Values are shown for advection-dispersion transport model structure (AD) and advection-dispersion transport model structure with time-variant SAS parameters (AD-TV).

Table 4. KGE of best $\delta^{18}O$ simulations for different antecedent soil moisture conditions. Antecedent soil moisture conditions are defined by 10^{th} (θ_{a10}) and 90^{th} (θ_{a90}) percentiles of average observed soil moisture from previous 5 days (θ_a; dry: $\theta_a < \theta_{a10}$; normal: $\theta_{a10} \leq \theta_a \leq \theta_{a90}$; wet: $\theta_a > \theta_{a90}$)

	CM	PI	AD	AD-TV	HYDRUS-1D
total	0.47	-0.37	0.74	0.74	0.68
dry	0.54	0.06	0.78	0.78	0.62
normal	0.47	-0.37	0.73	0.74	0.60
wet	0.31	0.21	0.71	0.71	0.69

4.4 Benchmark comparison to virtual bromide experiments and water age statistics of HYDRUS-1D simulations

Results of virtual bromide experiments are presented in Figure 7. The four model structures predict different bromide breakthrough curves. We found that bromide breakthrough curves of single virtual experiments deviate from each other due to different meteorological conditions. Furthermore, single virtual experiments diverge from observed bromide breakthrough curves. For example, the drought in year 2003 causes a late arrival of the bromide pulse. However, the average breakthrough curves produced by AD and AD-TV are similar and the average breakthrough curves agree well in terms of timing and magnitude with the observed bromide breakthrough curve. The average bromide breakthrough curves derived from CM and PI are different. In particular, CM simulates bromide breakthrough too early. PI simulates bromide breakthrough too late and the magnitude of the breakthrough is strongly overestimated.

The comparison between the backward travel time distributions calculated with the four transport model structures and HYDRUS-1D is depicted in Figure 8. Again, backward travel time distributions calculated by CM and PI are different to the backward travel time distributions calculated by AD, AD-TV and HYDRUS-1D. Especially travel times computed with CM extend to a wider range of water ages than the other models. While backward travel time distributions of percolation

derived from AD, AD-TV and HYDRUS-1D are similar, backward travel time distributions of transpiration estimated by AD, AD-TV and HYDRUS-1D reveal differences. AD-TV estimates older travel times for transpiration than AD. Transpiration travel times from HYDRUS-1D cover a wider range of water ages and the tails are older.

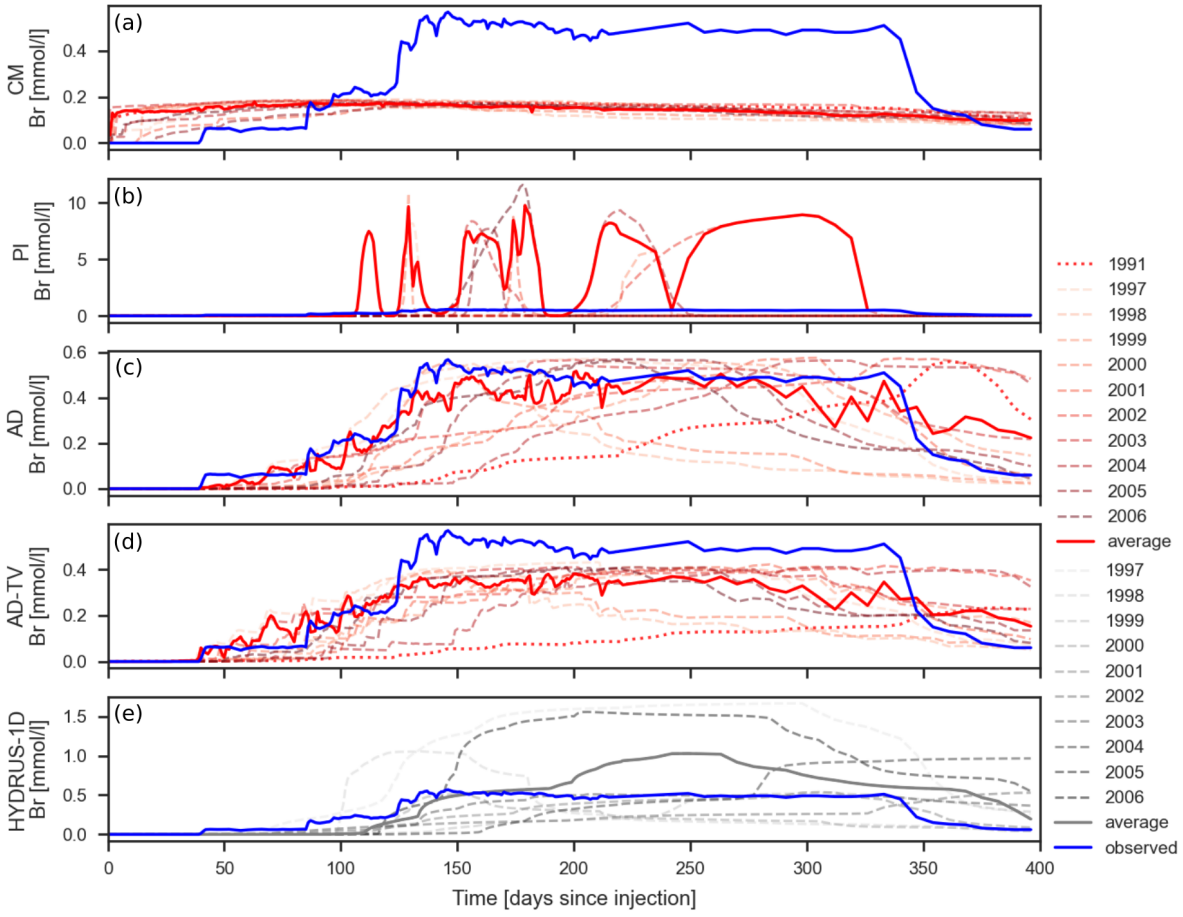

Figure 7. Bromide breakthrough curves from virtual bromide experiments and observed bromide breakthrough curve (modified from Menzel and Demuth (1993)). 79.9 g of bromide has been injected at 12th November of each year. Average values are weighted by bromide mass of percolation. Simulations are shown for complete-mixing transport model structure (a; CM), piston-flow transport model structure (b; PI), advection-dispersion transport model structure (c; AD), advection-dispersion transport model structure with time-variant SAS parameters (d; AD-TV) and HYDRUS-1D with dual-porosity domain (e; HYDRUS-1D).

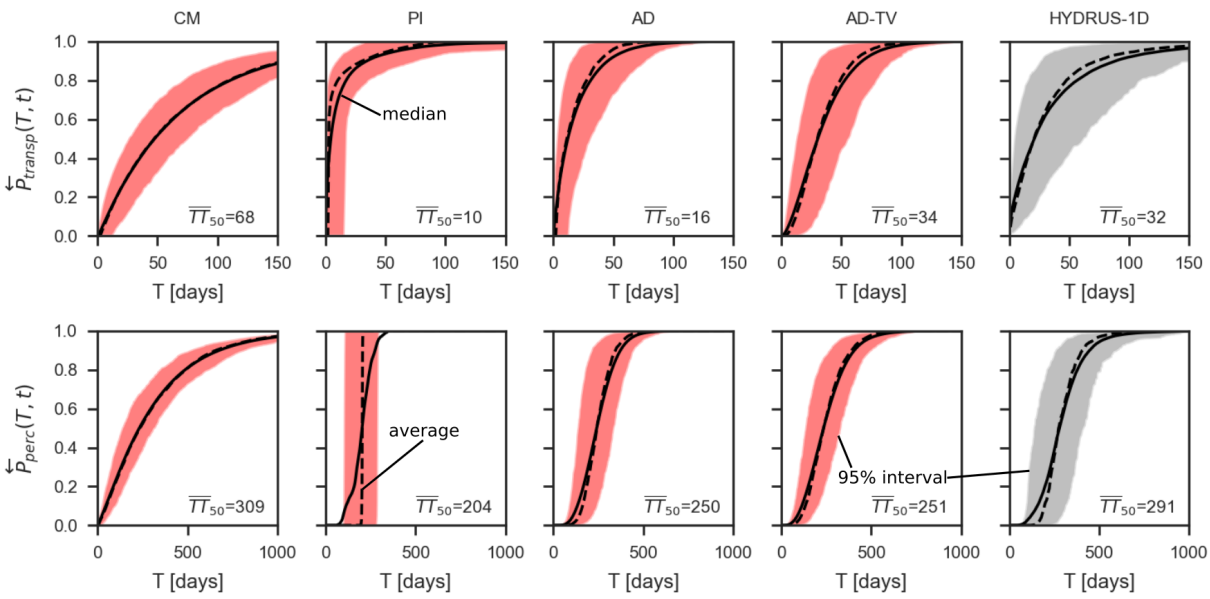

Figure 8. Simulated backward travel time distributions of transpiration and percolation. Averaged median travel times (in days) are displayed in the right bottom corner.

5 Discussion

5.1 Sensitive parameters for travel time statistics and model accuracy

The sensitivity analysis using the Sobol method for the coupled RoGeR model with SAS functions revealed different sensitivities for the RoGeR-AD and RoGeR-AD-TV model structure (Figures 6 and 7). The results for a static SAS parameterization imply that travel time estimates and predictive model accuracy are similarly affected by parameters of the hydrologic model and SAS functions. When using a time-variant SAS parameterization, hydrologic model parameters have a greater impact than SAS parameters on the results. One reason for this larger sensitivity might be the dependency from the soil water content (see equations (8) and (9)) on the transport simultations. Despite this difference, RoGeR-AD and RoGeR-AD-TV have in common that parameters related to soil water storage (f_{lp} and θ_{pwp}) have the greatest impact on travel times and model accuracy.

The two studies of Menzel and Demuth (1993) and Weiler and Naef (2003) at the Rietholzbach site provided experimental evidence that macropores play an important role for soil water fluxes and tracer transport. The macropore parameters estimated by the Monte Carlo analysis (Table 1) agree well with observations from Weiler and Naef (2003). They found a macropore density of 228 m^{-2} compared to the estimated 202 ± 70 m^{-2}. The sensitivity analysis shows that macropores influence the travel time estimation of percolation, while they have little impact on model accuracy and travel times of transpiration.

The closure of the lysimeter solute balance could only be partly constrained since solute (^{18}O) information has only been available at the bottom of the lysimeter. To fully constrain the model would require solute information from soil water and root water uptake (e.g. Asadollahi et al., 2022). As a consequence, age preference of transpiration and sensitive parameters for predictive accuracy of the transpiration process cannot be directly evaluated. For example, the model reproduces a similar signal of $\delta^{18}O$ in percolation with a younger age preference and an older age preference (Figures 2,4, S6 and S7). However, the best SAS parameter of transpiration (Table 2) are consistent with Asadollahi et al. (2020) who found k=0.2 for the evapotranspiration process (without constrains for evapotranspiration) at another grassland lysimeter.

5.2 Hypothesis-driven modelling of ^{18}O transport and bromide transport

The comparison between observed and simulated $\delta^{18}O$ in percolation and the virtual bromide experiments proved that SAS parameters which can be linked to an advective-dispersive transport process can explain ^{18}O transport and bromide transport to a large extent (Figures 4 and 7). However, uniform SAS functions could explain the dampening of the isotope signal well, but not the transport process of a individual tracer signal like the bromide application. The estimated model parameters of the AD models demonstrate a realistic pattern of the conceptualized processes. Since

447 the soil water dynamics are represented by equations which are governed capillary forces, RoGeR
448 enables a bypass flow in the root zone but mobile soil water is ultimately abstracted by the soil
449 matrix and thus leads to a slower transport (i.e. preference for older water with $k_Q > 1$). From
450 capillary-driven perspective, the older age preference ($k_Q > 1$) of percolation processes is physi-
451 cally consistent. However, RoGeR may reach its limits in case of a rapid response. We suppose,
452 that such a rapid response is more important for shallow soils with high connectivity of macropores
453 from the soil surface to the percolation depths. In such cases, it might be more consistent to imple-
454 ment preferential flow through gravity-driven theory (Germann and Prasuhn, 2018). The dye tracer
455 experiments of Weiler and Naef (2003) conducted within the Rietholzbach catchment proved the
456 occurrence of preferential flow at 1 m soil depth. Consequently, age preference of SAS might be
457 younger where macropores exist. In order to test the hypothesis of specific transport with a young
458 water preference, we would need a higher sampling frequency of ^{18}O during events from the ly-
459 simeter seepage and additional soil water samples at different soil depths.
460 The virtual bromide experiments revealed that SAS parameters of advective-dispersive transport
461 estimated with ^{18}O could be successfully transferred to predict bromide breakthrough (Figure 7).
462 The average bromide breakthrough simulated by RoGeR-AD exhibits visually a better agreement
463 than RoGeR-AD-TV or HYDRUS-1D, respectively. The lower agreement of RoGeR-AD-TV
464 might be due to parameter estimation with bi-weekly ^{18}O samples which causes a loss of infor-
465 mation and a better agreement might be feasible with higher sampling frequency of ^{18}O. HY-
466 DRUS-1D cannot predict the first arrival of the solute at the bottom very well, which could be
467 attributed to its caplillary-driven model framework. The comparison between individual bromide
468 breakthrough curves demonstrate nicely the impact of different meteorologic conditions on
469 transport velocities. For example, bromide pulse arrives later when injected in a drought year (e.g.

year 2003; see Figure S2) whereas bromide pulse arrives earlier when injected under wetter meteorologic conditions (e.g. year 1998; see Figure S2).

A key result of the virtual bromide experiments is that the tracer signals simulated by SAS with a uniform probability distribution function arrive substantially earlier than indicated by the observations (Figure 7). We found a similar pattern for the ^{18}O modelling experiments which support the findings from the virtual bromide experiments. These results clearly demonstrate the consequence of using the complete-mixing assumption for depth-implict solute transport model (e.g. soil is discretized by 2-3 soil layers). We can support the argumentation in Sternagel et al. (2022) and we suggest going beyond the commonly applied complete-mixing assumption (e.g. Heße et al., 2017; Kumar et al., 2020).

Finally, we want to stress several limitations of the hypothesis-driven modelling approach presented in this study. Since evaporative fractionation of ^{18}O has not been implemented into the model framwork, evaporative fractionation of ^{18}O should be neglible, which is the case at the Rietholzbach lysimeter due to the dense gras cover and site specific climate conditions. Although we account for non-conservative behavior of bromide by considering partitioning of either root water uptake or sorption processes (see equation (5)), the assumption of α_p=0.8 might not be transferable to other sites. The non-conservative behavior is important for longer time periods (i.e. longer than the event length; Sternagel et al., 2019) and sorption processes are controlled by clay content of soil and pH-conditions (Groh et al., 2018). We suppose that RoGeR-SAS is limited to deep soils and/or partly structured soils (e.g. macropore network of the soil column is partly connected) for which solute flushing at the event scale are less relevant. For a better representation of solute flushing, it might be worth to implement infiltration and percolation based on gravity-driven theory

(Germann and Prasuhn, 2018) and compare it to the approach presented in this study. Such a comparison should investigate how and when gravity-driven transport is induced. For example, the interplay between rainfall characteristics (e.g. rainfall intensity) or soil properties (e.g. macropore network) may play a decisive role (Demand and Weiler, 2021).

5.3 Coupling simulated hydrologic fluxes and storages with SAS functions

We estimated parameters of HYDRUS-1D with dual-porosity domains using the observed soil water content time series at different soil depth to maximize information for the spatially discrete HYDRUS model (see equation (10)). However, to allow for a fair comparison between RoGeR and HYDRUS-1D, we evaluated the model results with the same metrics (Tables 3 and 4). These results show that RoGeR predicts hydrologic variables in general better than HYDRUS-1D. $\delta^{18}O$ in percolation and bromide breakthrough are reproduced similarly well by RoGeR and HYDRUS-1D (Figures 4 and 7). RoGeR performs slightly better than HYDRUS-1D in terms of $KGE_{\delta 18O}$ and for predicting the bromide experiment. Furthermore, travel time statistics estimated by RoGeR with advective-dispersive transport and by HYDRUS-1D show similar distributions (Figure 8). The similarities between the two models and the good agreement between simualtions with RoGeR and observations confirm the usability of coupling SAS functions with a process-based hydrologic model.

Besides that the complete program code used for this study is publicly available and thus fosters reproducibility, another major advantage of RoGeR compared to HYDRUS-1D is that the computation of travel times is approximately 340 times faster. Travel time compuation with HYDRUS-1D took 340 hours whereas travel time compuation with RoGeR took 1 hour. Comparing the coupled-SAS model as presented here with a pure-SAS model (e.g. Benettin and Bertuzzo, 2018) in terms of applicability shows that only data of the upper condition is required rather than measured

fluxes of all outflows from the considered hydrologic system. In many cases, such measurements are not available. Another advantage is that RoGeR requires a lower number of parameters. Moreover, the model does not rely on complex calibration schemes. Instead, parameters of RoGeR can be derived from available environmental data (e.g. soil maps; Steinbrich et al., 2016) and may readily applied to sites with such datasets. Disadvantages of RoGeR compared to HYDRUS-1D are mainly attributed to the low vertical discretization with two soil layers. HYDRUS-1D provides more information in the vertical dimension (e.g. spatio-temporal tracer distributions in the soil). For example, research questions concerning highly dynamic processes (e.g. depth of root water uptake) can only be obtain with spatially detailed results of HYDRUS-1D.

Although data requirements of coupled-SAS models are less strict than for pure-SAS models, a major challenge for coupling SAS functions with simulated hydrologic variables consists of the realistic representation of the considered hydrologic system. We selected the best 100 hydrologic simulations according to a performance metric realized with different parameters and coupled the simulations with SAS functions. All 100 hydrologic model realization coupled with AD and AD-TV were capable to achieve $KGE_{\delta^{18}O} > 0.7$, hence a certain parameter equifinality could not be resolved (Figure S4). For example, values for k_s range from 11.6 to 149.6 mm/h.

As alredy been shown by Asadollahi et al. (2020), we could also confirm that using single-parameter SAS function is suitable to predict solute leaching within a soil column. Since a dual-parameter SAS function produced very similar results, the question about the shape of SAS functions (e.g. Heidbüchel et al., 2020) remains open. We suggest to perform a multi-site (e.g. lysimeters with different soil properties, vegetation cover and climatic conditions) comparison including different kind of tracer signals (e.g. seasonally varying isotopic signal vs injection of pollution tracers or nutrients at specific time) to further improve our knowledge about SAS-based solute transport.

6 Conclusions

The ^{18}O and bromide transport through a grass covered weighted lysimeter has been extensively investigated using simulations of RoGeR-SAS and HYDRUS-1D with a dual-porosity domain. The simulations with different transport model structures exhibited high sensitivities for parameters related to the soil water storages. The two advective-dispersive transport model structures of RoGeR showed particularly different sensitivities depending on the choice between a static or a time-variant SAS parameterization. We further found that the leaching of ^{18}O and bromide can be realistically explained to a large extent by SAS with power law distribution function linked to advective-dispersive transport. The two selected advective-dispersive transport model structures of RoGeR-SAS showed particularly different sensitivities depending on the choice between a static or a time-variant SAS parameterization. Although a uniform SAS resulting in complete-mixing reproduces well the dampening of the ^{18}O percolation signal, this transport assumption leads to a strong temporal mismatch of the tracer signal (i.e. early arriving of tracer signal), if used in transport models with coarse vertical discretization at sites with deep soils. The results of RoGeR-SAS with advective-dispersive transport model structures show very similar results than the more complex HYDRUS-1D model and agrees well with the lysimeter measurements. RoGeR-SAS substantially reduces computational time of travel times but at the cost of a simpler, but more parsimonious vertical discretization. Therefore, the combination of a hydrologic model with SAS function linked to individual fluxes and processes has a great potential to effectively simulate water balance components and the related solute transport at various temporal and spatial scales. The new RoGeR-SAS could also be extended to solutes with more complex transport processes to allow simulations of nutrient cycles or pollutants.

Acknowledgments

This research was supported by the Helmholtz Association of German Research Centres through grant no 42-2017. We are grateful to Jens Lange and Dominic Demand for their constructive comments on the first draft. Jürgen Strub provided the illustration of the lysimeter and the measured bromide breakthrough curve. We also acknowledge Martin Hirschi, Dominik Michel and Sonia I. Seneviratne from the Institute for Atmospheric and Climate Science at ETH Zürich for providing the measurements from the Rietholzbach site, including the stable water isotope measurements, lysimeter data, and meteorological data. The authors acknowledge support by the High Performance and Cloud Computing Group at the Zentrum für Datenverarbeitung of the University of Tübingen, the state of Baden-Württemberg through bwHPC and the German Research Foundation (DFG) through grant no INST 37/935-1 FUGG.

Open Research

The code and data used for this project are available at https://doi.org/10.5281/zenodo.7633362 (Schwemmle, 2023) and https://doi.org/10.5281/zenodo.763228. The observational data used in this project is available from the Land-Climate Dynamics group (Prof. Sonia Seneviratne) at ETH Zurich (isotope data will be available at https://doi.org/10.3929/ethz-b-000596572 (Michel et al., 2023); other Rietholzbach data will be available at https://doi.org/10.3929/ethz-b-000596657 (Seneviratne et al., 2012a)).

References

Asadollahi, M., C. Stumpp, A. Rinaldo, and P. Benettin (2020), Transport and Water Age Dynamics in Soils: A Comparative Study of Spatially Integrated and Spatially Explicit Models, *Water Resources Research*, *56*(3), e2019WR025539. https://doi.org/10.1029/2019wr025539

Asadollahi, M., M. F. Nehemy, J. J. McDonnell, A. Rinaldo, and P. Benettin (2022), Toward a Closure of Catchment Mass Balance: Insight on the Missing Link From a Vegetated Lysimeter, *Water Resources Research*, *58*(4), e2021WR030698. https://doi.org/10.1029/2021WR030698

Benettin, P., and E. Bertuzzo (2018), tran-SAS v1.0: a numerical model to compute catchment-scale hydrologic transport using StorAge Selection functions, *Geosci. Model Dev.*, *11*(4), 1627-1639. https://doi.org/10.5194/gmd-11-1627-2018

Benettin, P., J. W. Kirchner, A. Rinaldo, and G. Botter (2015a), Modeling chloride transport using travel time distributions at Plynlimon, Wales, *Water Resources Research*, *51*(5), 3259-3276. https://doi.org/10.1002/2014WR016600

Benettin, P., C. Soulsby, C. Birkel, D. Tetzlaff, G. Botter, and A. Rinaldo (2017), Using SAS functions and high-resolution isotope data to unravel travel time distributions in headwater catchments, *Water Resources Research*, *53*(3), 1864-1878. https://doi.org/10.1002/2016WR020117

Benettin, P., S. W. Bailey, J. L. Campbell, M. B. Green, A. Rinaldo, G. E. Likens, K. J. McGuire, and G. Botter (2015b), Linking water age and solute dynamics in streamflow at the Hubbard Brook Experimental Forest, NH, USA, *Water Resources Research*, *51*(11), 9256-9272. https://doi.org/10.1002/2015WR017552

Botter, G., E. Bertuzzo, and A. Rinaldo (2011), Catchment residence and travel time distributions: The master equation, *Geophysical Research Letters*, *38*(11). https://doi.org/10.1029/2011GL047666

Brinkmann, N., S. Seeger, M. Weiler, N. Buchmann, W. Eugster, and A. Kahmen (2018), Employing stable isotopes to determine the residence times of soil water and the temporal origin of water taken up by Fagus sylvatica and Picea abies in a temperate forest, *New Phytol*, *219*(4), 1300-1313. https://doi.org/10.1111/nph.15255

Brooks, R. H., and A. T. Corey (1966), Properties of porous media affecting fluid flow, *Journal of the Irrigation and Drainage Division*, *92*(2), 61-90.

Campolongo, F., A. Saltelli, and J. Cariboni (2011), From screening to quantitative sensitivity analysis. A unified approach, *Comput Phys Commun*, *182*(4), 978-988. https://doi.org/10.1016/j.cpc.2010.12.039

Collenteur, R. A., G. Brunetti, and M. Vremec, Phydrus: Python implementation of the HYDRUS-1D unsaturated zone model, Version 0.2.0, available at https://github.com/phydrus/phydrus (last access: 30 August 2022)

Demand, D., and M. Weiler (2021), Potential of a Gravity-Driven Film Flow Model to Predict Infiltration in a Catchment for Diverse Soil and Land Cover Combinations, *Water Resources Research*, *57*(5), e2019WR026988. https://doi.org/10.1029/2019WR026988

Germann, P. F., and V. Prasuhn (2018), Viscous Flow Approach to Rapid Infiltration and Drainage in a Weighing Lysimeter, *Vadose Zone Journal*, *17*(1), 170020. https://doi.org/10.2136/vzj2017.01.0020

GNIP, Global Network of Isotopes in Precipitation available at https://www.iaea.org/services/networks/gnip (last access: 12.02.2023)

Green, W. H., and G. A. Ampt (1911), Studies in soil physics. 1 The flow of air and water through soils, *J Agric Sci*, *4*, 1–24.

Groh, J., C. Stumpp, A. Lücke, T. Pütz, J. Vanderborght, and H. Vereecken (2018), Inverse Estimation of Soil Hydraulic and Transport Parameters of Layered Soils from Water Stable Isotope and Lysimeter Data, *Vadose Zone Journal*, *17*(1). https://doi.org/10.2136/vzj2017.09.0168

Hansen, S., P. Abrahamsen, C. T. Petersen, and M. Styczen (2012), Daisy: Model Use, Calibration, and Validation, *Transactions of the ASABE*, *55*(4), 1317. https://doi.org/10.13031/2013.42244

Harman, C. J. (2015), Time-variable transit time distributions and transport: Theory and application to storage-dependent transport of chloride in a watershed, *Water Resources Research*, *51*(1), 1-30. https://doi.org/10.1002/2014WR015707

Heidbüchel, I., J. Yang, A. Musolff, P. Troch, T. Ferré, and J. H. Fleckenstein (2020), On the shape of forward transit time distributions in low-order catchments, *Hydrol. Earth Syst. Sci.*, *24*(6), 2895-2920. https://doi.org/10.5194/hess-24-2895-2020

Heße, F., M. Zink, R. Kumar, L. Samaniego, and S. Attinger (2017), Spatially distributed characterization of soil-moisture dynamics using travel-time distributions, *Hydrol. Earth Syst. Sci.*, *21*(1), 549-570. https://doi.org/10.5194/hess-21-549-2017

Hirschi, M., D. Michel, I. Lehner, and S. I. Seneviratne (2017), A site-level comparison of lysimeter and eddy covariance flux measurements of evapotranspiration, *Hydrol. Earth Syst. Sci.*, *21*(3), 1809-1825. https://doi.org/10.5194/hess-21-1809-2017

Hrachowitz, M., H. Savenije, T. A. Bogaard, D. Tetzlaff, and C. Soulsby (2013), What can flux tracking teach us about water age distribution patterns and their temporal dynamics?, *Hydrol. Earth Syst. Sci.*, *17*(2), 533-564. https://doi.org/10.5194/hess-17-533-2013

Hrachowitz, M., P. Benettin, B. M. van Breukelen, O. Fovet, N. J. K. Howden, L. Ruiz, Y. van der Velde, and A. J. Wade (2016), Transit times—the link between hydrology and water quality at the catchment scale, *Wiley Interdisciplinary Reviews: Water*, *3*(5), 629-657. https://doi.org/10.1002/wat2.1155

Jing, M., R. Kumar, F. Heße, S. Thober, O. Rakovec, L. Samaniego, and S. Attinger (2020), Assessing the response of groundwater quantity and travel time distribution to 1.5, 2, and 3 °C global warming in a mesoscale central German basin, *Hydrol. Earth Syst. Sci.*, *24*(3), 1511-1526. https://doi.org/10.5194/hess-24-1511-2020

Köhne, J. M., S. Köhne, B. P. Mohanty, and J. Šimůnek (2004), Inverse Mobile–Immobile Modeling of Transport During Transient Flow: Effects of Between-Domain Transfer and Initial Water Content, *Vadose Zone Journal*, *3*(4), 1309-1321. https://doi.org/10.2113/3.4.1309

Kumar, R., et al. (2020), Strong hydroclimatic controls on vulnerability to subsurface nitrate contamination across Europe, *Nature Communications*, *11*(1), 6302. https://doi.org/10.1038/s41467-020-19955-8

Kumaraswamy, P. (1980), A generalized probability density function for double-bounded random processes, *Journal of Hydrology*, *46*(1), 79-88. https://doi.org/10.1016/0022-1694(80)90036-0

Larsbo, M., and N. Jarvis (2005), Simulating Solute Transport in a Structured Field Soil, *J Environ Qual*, *34*(2), 621-634. https://doi.org/10.2134/jeq2005.0621

Makkink, G. F. (1957), Testing the Penman formula by means of lysimeters, *Journal of the Institution of Water Engineers*, *11*(3), 277-288.

Menzel, L., and N. Demuth (1993), Tracerhydrologische Untersuchungen am Lysimeter Rietholzbach, 24 pp, Geographisches Institut ETH Zürich, Zurich, Switzerland.

Michel, D., M. Hirschi, and S. I. Seneviratne, Stable water isotopes at Rietholbach lysimeter, Switzerland, available at https://doi.org/10.3929/ethz-b- (last access: 3 February 2023)

Nelson, D. B., D. Basler, and A. Kahmen (2021), Precipitation isotope time series predictions from machine learning applied in Europe, *Proceedings of the National Academy of Sciences*, *118*(26), e2024107118. doi:10.1073/pnas.2024107118

Nguyen, T. V., R. Kumar, A. Musolff, S. R. Lutz, F. Sarrazin, S. Attinger, and J. H. Fleckenstein (2022), Disparate Seasonal Nitrate Export From Nested Heterogeneous Subcatchments Revealed With StorAge Selection Functions, *Water Resources Research*, *58*(3), e2021WR030797. https://doi.org/10.1029/2021WR030797

Or, D., P. Lehmann, E. Shahraeeni, and N. Shokri (2013), Advances in Soil Evaporation Physics—A Review, *Vadose Zone Journal*, *12*(4), vzj2012.0163. https://doi.org/10.2136/vzj2012.0163

Peschke, G. (1985), Zur Bildung und Berechnung von Regenabfluß, *Wissenschaftliche Zeitschrift der Technischen Universität Dresden*, *34*(4).

Queloz, P., L. Carraro, P. Benettin, G. Botter, A. Rinaldo, and E. Bertuzzo (2015), Transport of fluorobenzoate tracers in a vegetated hydrologic control volume: 2. Theoretical inferences and modeling, *Water Resources Research*, *51*(4), 2793-2806. https://doi.org/10.1002/2014WR016508

Richter, D. (1995), Ergebnisse methodischer Untersuchungen zur Korrektur des systematischen Meßfehlers des Hellmann-Niederschlagsmessers, Selbstverlag des Deutschen Wetterdienstes, Offenbach am Main.

Rigon, R., and M. Bancheri (2021), On the relations between the hydrological dynamical systems of water budget, travel time, response time and tracer concentrations, *Hydrological Processes*, *35*(1), e14007. https://doi.org/10.1002/hyp.14007

Rinaldo, A., P. Benettin, C. J. Harman, M. Hrachowitz, K. J. McGuire, Y. van der Velde, E. Bertuzzo, and G. Botter (2015), Storage selection functions: A coherent framework for quantifying how catchments store and release water and solutes, *Water Resources Research*, *51*(6), 4840-4847. https://doi.org/10.1002/2015WR017273

Saltelli, A., M. Ratto, T. Andres, F. Campolongo, J. Cariboni, D. Gatelli, M. Saisana, and S. Tarantola (2008), *Global Sensitivity Analysis. The Primer*, John Wiley & Sons, Ltd, Chichester, England.

Salvucci, G. D. (1993), An approximate solution for steady vertical flux of moisture through an unsaturated homogeneous soil, *Water Resources Research*, *29*(11), 3749-3753. https://doi.org/10.1029/93wr02068

Schwemmle, R., Roger - a process-based hydrologic toolbox in Python, available at https://github.com/Hydrology-IFH/roger (last access: 20 January 2023)

Seeger, S., and M. Weiler (2014), Reevaluation of transit time distributions, mean transit times and their relation to catchment topography, *Hydrol. Earth Syst. Sci.*, *18*(12), 4751-4771. https://doi.org/10.5194/hess-18-4751-2014

Seneviratne, S. I., et al., Swiss prealpine Rietholzbach research catchment and lysimeter: 32 year time series and 2003 drought event, available at https://doi.org/10.3929/ethz-b- (last access: 3 February 2023)

Seneviratne, S. I., et al. (2012b), Swiss prealpine Rietholzbach research catchment and lysimeter: 32 year time series and 2003 drought event, *Water Resources Research*, *48*(6). https://doi.org/10.1029/2011wr011749

Šimůnek, J., M. T. van Genuchten, and M. Šejna (2016), Recent Developments and Applications of the HYDRUS Computer Software Packages, *Vadose Zone Journal*, *15*(7), vzj2016.2004.0033. https://doi.org/10.2136/vzj2016.04.0033

Sprenger, M., S. Seeger, T. Blume, and M. Weiler (2016), Travel times in the vadose zone: Variability in space and time, *Water Resources Research*, *52*(8), 5727-5754. https://doi.org/10.1002/2015WR018077

Sprenger, M., et al. (2019), The Demographics of Water: A Review of Water Ages in the Critical Zone, *Reviews of Geophysics*, *57*(3), 800-834. https://doi.org/10.1029/2018rg000633

Steinbrich, A., H. Leistert, and M. Weiler (2016), Model-based quantification of runoff generation processes at high spatial and temporal resolution, *Environmental Earth Sciences*, *75*(21), 1423. https://doi.org/10.1007/s12665-016-6234-9

Sternagel, A., R. Loritz, W. Wilcke, and E. Zehe (2019), Simulating preferential soil water flow and tracer transport using the Lagrangian Soil Water and Solute Transport Model, *Hydrol. Earth Syst. Sci.*, *23*(10), 4249-4267. https://doi.org/10.5194/hess-23-4249-2019

Sternagel, A., R. Loritz, B. Berkowitz, and E. Zehe (2022), Stepping beyond perfectly mixed conditions in soil hydrological modelling using a Lagrangian approach, *Hydrol. Earth Syst. Sci.*, *26*(6), 1615-1629. https://doi.org/10.5194/hess-26-1615-2022

van der Velde, Y., P. J. J. F. Torfs, S. E. A. T. M. van der Zee, and R. Uijlenhoet (2012), Quantifying catchment-scale mixing and its effect on time-varying travel time distributions, *Water Resources Research*, *48*(6). https://doi.org/10.1029/2011WR011310

Weiler, M. (2005), An infiltration model based on flow variability in macropores: development, sensitivity analysis and applications, *Journal of Hydrology*, *310*(1), 294-315. https://doi.org/10.1016/j.jhydrol.2005.01.010

Weiler, M., and F. Naef (2003), An experimental tracer study of the role of macropores in infiltration in grassland soils, *Hydrological Processes*, *17*(2), 477-493. https://doi.org/10.1002/hyp.1136

Wilusz, D. C., C. J. Harman, W. P. Ball, R. M. Maxwell, and A. R. Buda (2020), Using Particle Tracking to Understand Flow Paths, Age Distributions, and the Paradoxical Origins of the Inverse Storage Effect in an Experimental Catchment, *Water Resources Research*, *56*(4), e2019WR025140. https://doi.org/10.1029/2019WR025140

Yang, X., S. Jomaa, and M. Rode (2019), Sensitivity Analysis of Fully Distributed Parameterization Reveals Insights Into Heterogeneous Catchment Responses for Water Quality Modeling, *Water Resources Research*, *55*(12), 10935-10953. https://doi.org/10.1029/2019wr025575

Supporting Information for "Consistent modelling of transport processes and travel times – coupling hydrologic processes with StorAge Selection functions "

Robin Schwemmle[1], Markus Weiler[1]

[1]Hydrology, Faculty of Environment and Natural Resources, University of Freiburg, Freiburg, Germany

Table of Contents

February 22, 2023, 4:12pm

1. Hydrologic processes and storages

Here, we provide the equations which were used to implement the hydrologic processes. Constant model parameters are listed in Table S2.

1.1. Surface storage

Storage capacity (i.e. available storage volume) of lower interception storage $S_{int-lower-tot}$ (mm) is land use dependent. Parameters used for grassland are shown in Table S1.

Leaf area index LAI (-):

$$LAI = \frac{S_{int-lower-tot}}{0.2} \tag{S1}$$

Fraction of ground cover $f_{ground-cover}$ (-):

$$f_{ground-cover} = 1 - 0.7^{LAI} \tag{S2}$$

1.2. Soil storage

Soil storage divides into a root zone layer rz (i.e. upper soil) and a subsoil layer ss (i.e. lower soil). The two soil layers share the same soil hydraulic parameters. However, absolute storage values are different due to different thickness of the layers. Root depth (z_{root}; mm) is shown in Table S1.

Soil hydraulic parameters are calculated with the Brooks-Corey scheme (Brooks & Corey, 1966). Pore size distribution parameter λ is calculated as:

$$\lambda = \frac{1}{\frac{\log\left(\frac{h_{fc}}{h_{pwp}}\right)}{\log\left(\frac{\omega_{fc}}{\omega_{pwp}}\right)}} \tag{S3}$$

where h_{fc} is soil water potential at field capacity (hPa; h_{fc}=63) and h_{pwp} is the soil water potential at permanent wilting point (hPa; h_{pwp}=15850)

Pore size disconnectedness index m:

$$m = b + \frac{a}{\lambda} \tag{S4}$$

where a and b are parameters with a fixed value of 2.

Salvucci exponent n (Salvucci, 1993):

$$n = \lambda \cdot a + b \tag{S5}$$

Effective soil water content at field capacity ω_{fc} (-):

$$\omega_{fc} = \frac{\theta_{fc}}{\theta_{sat}} \tag{S6}$$

where θ_{fc} is soil water content at field capacity (-) and θ_{sat} is soil water content at saturation (-).

Effective soil water content at permanent wilting point ω_{pwp} (-):

$$\omega_{pwp} = \frac{\theta_{pwp}}{\theta_{sat}} \tag{S7}$$

where θ_{pwp} is soil water content at permanent wilting point (-).

Effective soil water content ω (-):

$$\omega = \frac{\theta}{\theta_{sat}} \tag{S8}$$

Air entry value h_a (i.e. bubbling pressure, hPa):

$$h_a = \omega_{pwp}^{\frac{1}{\lambda}} \cdot (-1) \cdot h_{pwp} \tag{S9}$$

Soil water potential h (hPa):

$$h = \frac{h_a}{\omega^{\frac{1}{\lambda}}} \tag{S10}$$

Wetting front suction ψ_f (mm):

$$\psi_f = \frac{2 + 3\lambda}{(1 + 3\lambda) \cdot \frac{h_a}{2} \cdot (-10)} \tag{S11}$$

Hydraulic conductivity k (mm h-1):

$$k = \frac{k_s}{1 + \omega^m} \tag{S12}$$

Soil water content at $10^{2.7}$ hPa θ_{27} (-):

$$theta_{27} = \frac{h_a}{-10^{2.7}}^{\lambda_{bc} \cdot \theta_{sat}} \tag{S13}$$

Soil water content at 10^4 hPa θ_6 (-):

$$theta_4 = \frac{h_a}{-10^4}^{\lambda_{bc} \cdot \theta_{sat}} \tag{S14}$$

Soil water content at 10^6 hPa θ_6 (-):

$$theta_6 = \frac{h_a}{-10^6}^{\lambda_{bc} \cdot \theta_{sat}} \tag{S15}$$

Soil moisture deficit $\Delta\theta$ (-):

$$\Delta\theta = \theta_{sat} - \theta_{rz} \tag{S16}$$

1.3. Interception

Interception storage is represented by a bucket. The storage is filled by liquid and solid precipitation and spills if the storage is full. Interception at lower interception Storage $S_{int-lower}$ (mm Δt^{-1}):

Interception at lower interception Storage $S_{int-lower}$ (mm Δt^{-1}):

$$\frac{\Delta S_{int-lower}}{\Delta t} = \begin{cases} PREC(i) & PREC(i) \leq S_{tot-int-lower} - S_{int-lower} \\ S_{tot-int-lower} - S_{int-lower} & PREC(i) > S_{tot-int-lower} - S_{int-lower} \end{cases} \tag{S17}$$

1.4. Snow

Solid precipitation accumulates in the interception storage and at the land surface if air temperatures are below 0 °C. Snow melt occurs for air temperatures above 0 °C and is based on degree-day approach. Snow melt runoff is initiated if liquid storage of the snow cover (S_{snow-l}) exceeds the retention capacity of the snow cover. Retention capacity $S_{snow-ret}$ (mm):

$$S_{snow-ret} = \frac{10000}{\frac{100-r_{max}}{100}} \cdot swe \tag{S18}$$

where r_{max} is the retention factor of the snow cover (%) and swe is the snow water equivalent of the snow cover (mm).

Snow melt q_{snow} (mm):

$$q_{snow} = s_f \cdot (TA - TA_m) \cdot \Delta t \tag{S19}$$

where s_f is the degree-day factor (mm $°C^{-1}$ h^{-1}), TA is the air temperature (°C), TA_m is equal to 0 °C and Δt is time step (h).

1.5. Evapotranspiration

The calculation of evapotranspiration requires daily potential evapotranspiration, which is calculated with the Makkink formula (Makkink, 1957):

$$\text{PET} = \frac{\Delta}{\Delta + \gamma} \cdot (c_1 \cdot \frac{r_s}{L(TA)} + c_2) \tag{S20}$$

with

$$L(TA) = c_L \cdot (28.4 - 0.028 \cdot TA) \tag{S21}$$

where Δ is the saturation slope vapour pressure curve ($kPa\ ^{\circ}C^{-1}$) at TA, γ is the psychometric constant ($kPa\ ^{\circ}C^{-1}$), r_s is the measured or calculated solar radiation ($MJ\ m^{-2}\ day^{-1}$), L is the special heat of evaporation ($MJ\ m^{-2}\ mm^{-1}$), c_L is a conversion factor ($c_L = 0.0864$), $c1_{PET}$ is the Makkink coefficient (-) and $c2_{PET}$ is the Makkink coefficient (mm day^{-1}).

Actual evapotranspiration is energy-limited or water-limited, respectively. The evapotranspiration processes sequentially subtract from PET.

Evaporation from interception storage $EVAP_{int-lower}$ (mm Δt^{-1}):

$$EVAP_{int-lower} = \begin{cases} S_{int-lower} & PET_{res} > S_{int-lower} \\ PET_{res} & PET_{res} \leq S_{int-lower} \end{cases} \tag{S22}$$

Soil evaporation $EVAP_{soil}$ (mm Δt^{-1}) implemented with Stage I-Stage II approach (Or et al., 2013). Threshold between Stage I and Stage II is defined by readily evaporable water S_{rew}. Within Stage I capillary flow connects to soil surface (i.e. constant evaporation rate) whereas within Stage II capillary flow collapses (i.e. vapour diffusion rate).

$$EVAP = PET_{res} \cdot c_{evap} \tag{S23}$$

with

$$c_{evap} = \begin{cases} 1 - \frac{f_{ground-cover}}{max(f_{ground-cover})} & EVAP_d \leq S_{rew} \\ 1 - \frac{f_{ground-cover}}{max(f_{ground-cover})} \cdot \frac{S_{tew} - EVAP_d}{S_{tew} - S_{rew}} & S_{rew} < EVAP_d \leq S_{tew} \\ 0 & EVAP_d > S_{tew} \end{cases} \tag{S24}$$

where $EVAP_d$ is the cumulated soil evaporation since last rainfall (mm) and S_{tew} is the total evaporable water (mm)

$$S_{tew} = (\theta_{fc} - 0.5 \cdot \theta_{pwp}) \cdot z_{evap} \tag{S25}$$

$$S_{rew} = \begin{cases} 0.02 & \theta_{pwp} < 0.02 \\ \frac{\theta_{pwp}}{0.24} & \theta_{pwp} \geq 0.02 \& \theta_{pwp} \leq 0.24 \\ 0.24 & \theta_{pwp} > 0.24 \end{cases} \tag{S26}$$

$$z_{evap} = \frac{S_{rew}}{0.24} \cdot z_{evap-max} \tag{S27}$$

where $z_{evap-max}$ is the maximum length of soil capillaries connected to the soil surface (mm; $z_{evap-max}$=150)

Transpiration $TRANSP$ (mm Δt^{-1}) with seasonally-variant transpiration coefficients c_{transp} and water stress coeffcient of transpiration $c_{transp-stress}$:

$$TRANSP = PET_{res} \cdot c_{transp} \tag{S28}$$

with

$$c_{transp} = \begin{cases} \frac{f_{ground-cover}}{max(f_{ground-cover})} & c_{transp-stress} \geq 1 \\ \frac{f_{ground-cover}}{max(f_{ground-cover})} \cdot c_{transp-stress} & c_{transp-stress} < 1 \end{cases} \tag{S29}$$

$$c_{transp-stress} = \frac{\theta - \theta_{pwp}}{f_{pwt} \cdot \theta_{fc} - \theta_{pwp}} \tag{S30}$$

where f_{pwt} is the fraction of plant water stress (-; f_{pwt}=0.75)

1.6. Infiltration

At the onset of rainfall or snow melt, we calculate event-specific parameters (e.g. soil moisture deficit $\Delta\theta$). For each event, we use two wetting fronts ($wf1$ and $wf2$). The second wetting front is active after a rainfall pause (i.e. calculation of event-specific parameters of $wf2$). $wf2$ is active while wetting front depth of $wf2$ is less than wetting front depth of $wf1$. In the following are the equations applied for dual-wetting front approach.

Total infiltration INF at time step t (mm Δt^{-1}):

$$INF = INF_{mat} + INF_{mp} + INF_{sc} \tag{S31}$$

Determining interval (i_s) when rainfall exceeds infiltrability within the current event:

$$i_s = \begin{cases} novalue & (PREC(i) - k_s \cdot \Delta t) \cdot \sum_{i=1}^{i} PREC(i) \leq k_s \cdot \Delta t \cdot \Delta\theta \cdot \psi_f \\ i & (PREC(i) - k_s \cdot \Delta t \cdot \sum_{i=1}^{i} PREC(i) > k_s \cdot \Delta t \cdot \Delta\theta \cdot \psi_f \end{cases} \tag{S32}$$

where $PREC$ is precipitation (mm Δt^{-1}), k_s is the saturated hydraulic conductivity of the soil matrix, $\Delta\theta$ is the soil moisture deficit (-) and ψ_f is the wetting front suction (mm)

Threshold rainfall intensity $PREC_{gr}$ (mm Δt^{-1}):

$$PREC_{gr} = k_s \cdot \Delta t \cdot \left(\frac{\Delta\theta \cdot \psi_f}{\sum_{i=1}^{i_s-1} PREC(i)} + 1 \right) \tag{S33}$$

$$i_s = \begin{cases} (i_s - 1) \cdot \Delta t & PREC(i_s) < PREC_{gr} \\ (i_s - 1) \cdot \Delta t + \frac{k_s \cdot \Delta t \cdot \Delta\theta \cdot \psi_f}{PREC(i_s) \cdot (PREC(i_s) - k_s \cdot \Delta t)} \frac{\Delta t}{PREC(i_s)} \sum_{v=1}^{i_s-1} PREC_v & PREC(i_s) \geq PREC_{gr} \end{cases} \tag{S34}$$

Infiltration at time step of saturation F_s (mm Δt^{-1}):

$$F_s = \frac{k_s \cdot \Delta t \cdot \theta_d \cdot \psi_f}{PREC(i_s) - k_s \cdot \Delta t} \tag{S35}$$

Matrix infiltration INF_{mat} at time step t (mm Δt^{-1}):

$$INF_{mat} = \begin{cases} z_0 \cdot & z_0 \leq INF_{mp-pot} \\ INF_{mat-pot} & z_0 > INF_{mp-pot} \end{cases} \tag{S36}$$

where z_0 is the surface ponding (mm; i.e. residual rainfall after interception or snow melt).

with potential matrix infiltration at time step t $INF_{mat-pot}$ (mm Δt^{-1}):

$$INF_{mat-pot} = \begin{cases} PREC(t) & t_s \geq t \\ PREC(t) \cdot (t_s - t - \Delta t) + \frac{k_s}{2}(1 + \frac{1+\frac{2B}{A}}{\sqrt{1+\frac{4B}{A}+\frac{4F_s^2}{A^2}}}) & t - \Delta t < t_S < t \\ \frac{k_s}{2}(1 + \frac{1+\frac{2B}{A}}{\sqrt{1+\frac{4B}{A}+\frac{4F_s^2}{A^2}}}) & t_s < t \end{cases} \tag{S37}$$

with auxiliary variables:

$$A = K_S \cdot (t - t_s) \tag{S38}$$

$$B = F_s + 2 \cdot \Delta\theta \cdot \psi_f \tag{S39}$$

Wetting front depth z_{wf} (mm):

$$z_{wf} = \frac{\sum_i^i INF_{mat}(i)}{\Delta\theta} \tag{S40}$$

where i_e is interval of the event start.

Macropore infiltration INF_{mp} at time step t (mm Δt^{-1}) following Weiler (2005):

$$INF_{mp} = \begin{cases} z_0 \cdot (1 - e^{-(\frac{\rho_{mpv}}{82})^{0.887}}) & 0 < z_0 \cdot (1 - e^{-(\frac{\rho_{mpv}}{82})^{0.887}}) \leq INF_{mp-pot} \\ INF_{mp-pot} & z_0 \cdot (1 - e^{-(\frac{\rho_{mpv}}{82})^{0.887}}) > INF_{mp-pot} \end{cases} \tag{S41}$$

where z_0 is the surface ponding (mm; i.e. matrix infiltration excess).

with potential macropore infiltration INF_{mp-pot} at time step t (mm Δt^{-1})

$$INF_{mp-pot} = \pi \cdot (y_{mp}(t)^2 - y_{mp}(t - \Delta t)^2) \cdot \rho_{mpv} \cdot \frac{\Delta z_{mp} \cdot \Delta\theta}{\Delta t} \tag{S42}$$

where ρ_{mpv} is density of vertical macropores (m^2) and Δz_{mp} depth of non-saturated macropore (mm)

Radial distance of the macropore wetting front y_{mp} (mm):

$$y_{mp} = \frac{1}{2} \cdot \frac{b^{(1/3)}}{\Delta\theta} + \frac{1}{2} \cdot \frac{a}{b^{(1/3)}} + \frac{1}{2} \cdot r_{mp} \tag{S43}$$

$$a = \Delta\theta \cdot r_{mp}^2 \tag{S44}$$

$$b = r \cdot \Delta\theta \cdot (12c - a + 2\sqrt{6} \cdot \sqrt{c \cdot (6c - a)} \tag{S45}$$

$$c = t_{mp} \cdot k_s \cdot \psi_s \tag{S46}$$

Duration of macropore infiltration t_{mp} (y_{mp}=r_{mp} at time t=0)

$$t_{mp} = \frac{\Delta\theta}{k_s \cdot \Psi_s \cdot r_{mp}} \cdot (\frac{y_{mp}^3}{3} - \frac{y_{mp}^2 r}{2} - \frac{r_{mp}^3}{6}) \tag{S47}$$

where r_{mp} is the radius of the macropore (mm; r_{mp}=2.5). Macropore infiltration stops if z_{wf} is greater than l_{mpv}.

Shrinkage crack infiltration INF_{cs} at time step t (mm Δt^{-1}) following Steinbrich, Leistert, and Weiler (2016):

$$INF_{sc} = \begin{cases} z_0 & z_0 \leq INF_{sc-pot} \\ INF_{sc-pot} & z_0 > INF_{sc-pot} \end{cases} \tag{S48}$$

where z_0 is the surface ponding (mm; i.e. macropore infiltration excess).

Potential shrinkage crack infiltration INF_{sc-pot} at time step t (mm Δt^{-1}):

$$INF_{sc-pot} = 2 \cdot l_{sc} \cdot (y_{sc}(t) - y_{sc}(t - \Delta t)) \cdot \frac{\Delta z_{sc} \cdot \Delta\theta}{\Delta t} \tag{S49}$$

where l_{sc} is the horizontal length of shrinkage cracks (mm m^{-2}) and Δz_{sc} is the depth of non-saturated shrinkage crack (mm)

Horizontal distance of the shrinkage crack wetting front y_{sc} (mm):

$$y_{sc}(t) = \sqrt{\frac{2 \cdot k_s \cdot \Psi_s \cdot t_{sc}}{\Delta\theta}} \tag{S50}$$

$$t_{sc} = \frac{y_{sc}(t - \Delta t)^2 \cdot \Delta\theta}{2 \cdot k_s \cdot \psi_s} \tag{S51}$$

Calculation of depth of shrinkage cracks z_{sc} at beginning of event:

$$z_{sc} = \begin{cases} 700 \cdot clay & \theta_{rz} < \theta_4 \\ 700 \cdot clay \cdot (1 - \frac{\theta_{rz}}{\theta_{27} - \theta_4}) & \theta_4 \leq \theta_{rz} \leq \theta_{27} \\ 0 & \theta_{rz} > \theta_{27} \end{cases} \tag{S52}$$

with clay content of soil $clay$ (-)

$$clay = \frac{clay_{max} \cdot (\theta_6 - clay_{min})}{0.3} \tag{S53}$$

where $clay_{min}$ is the lower limit of clay content (-; $clay_{min}$=0.01) and $clay_{max}$ is the upper limit of clay content (-; $clay_{max}$=0.71). INF_{sc} occurs only if shrinkage cracks are available and stops if z_{wf} is greater than z_{sc}.

1.7. Surface runoff

Hortonian surface runoff q_{HOF} at time step t (mm Δt^{-1}):

$$q_{HOF} = \begin{cases} PREC - INT - INF & PREC - INT - INF > 0 \\ 0 & PREC - INT - INF \leq 0 \end{cases} \tag{S54}$$

Saturation surface runoff q_{HOF} at time step t (mm Δt^{-1}):

$$q_{SOF} = \begin{cases} S_{soil} - S_{sat-soil} & S_{soil} - S_{sat-soil} > 0 \\ 0 & S_{soil} - S_{sat-soil} \leq 0 \end{cases} \tag{S55}$$

where $S_{sat-soil}$ is soil water content at saturation (mm) and S_{soil} and soil water content at time step t (mm).

1.8. Percolation/Capillary rise

Vertical flux q_v (mm Δt^{-1}):

$$q_v = \begin{cases} \frac{(z_{sat}/h_a)^{-n} - (h/h_a)^{-n}}{1+(h/h_a)^{-n}+(n-1)(z_{sat}/h_a)^{-n}} & z_{gw} \leq 10 \\ \frac{(z_{sat}/h_a)^{-n}}{1+(n-1)(z_{sat}/h_a)^{-n}} & z_{gw} > 10 \end{cases} \tag{S56}$$

where z_{gw} is the depth of groundwater table (m). For $q_v < 0$ soil water moves in downward direction and for with $q_v > 0$ soil water moves in upward direction.

Percolation q_{perc} (mm Δt^{-1}):

$$q_{perc} = \begin{cases} k_s & z_{sat} > 0 \\ q_v \cdot (-1) & q_v < 0 \& z_{sat} = 0 \\ 0 & q_v \geq 0 \& z_{sat} = 0 \end{cases} \tag{S57}$$

where z_{sat} is saturation water level at the soil-bedrock interface (mm).

Percolation might be limited by permeability of bedrock (k_f, mm Δt^{-1}), if q_{perc} exceeds k_f.

Saturation water level z_{sat} (mm) rises while saturation from top is connected to the bedrock interface:

$$z_{sat} = \begin{cases} \frac{S_{lp-ss}}{\theta_{ac}} & \frac{S_{lp-ss}}{\theta_{ac}} \geq z_{nomp} \\ z_{sat} & \frac{S_{lp-ss}}{\theta_{ac}} < z_{nomp} \end{cases} \tag{S58}$$

with thickness without macropores z_{nomp} (mm):

$$z_{nomp} = \begin{cases} 0 & z_{soil} - l_{mpv} - z_{sat} < 0 \\ z_{soil} - l_{mpv} - z_{sat} & z_{soil} - l_{mpv} - z_{sat} > 0 \end{cases} \tag{S59}$$

where S_{lp-ss} is soil water content in large pores of subsoil (mm). z_{sat} is reduced by percolation q_{perc}.

Capillary rise q_{cpr} (mm Δt^{-1}):

$$q_{cpr} = \begin{cases} 0 & q_v < 0 \\ q_v & q_v \geq 0 \& z_{sat} = 0 \end{cases} \tag{S60}$$

2. RoGeR - Monte Carlo analysis and Sensitivity analysis

Dotty plots of hydrologic Monte Carlo simulations are shown in Figure S3. Since best parameter values are not close to the parameter boundaries, the Monte Carlo approach provides a robust and hydrologically coherent estimation of the parameters. Sobol' indices of hydrologic Monte Carlo simulations are shown in Figure S8.

In addition to the single-parameter power law distribution function (see equation (7)), we implemented SAS with a dual-parameter distribution function (Figure S6) using the Kumaraswamy distribution function (Kumaraswamy, 1980):

$$\Omega_Q(T,t) = 1 - (1 - (P_s(T,t)^a)^b) \tag{S61}$$

with two parameters a and b, the Kumaraswamy distribution function provides a greater flexibility than a power law distribution function.

3. RoGeR - Model evaluation per hydrologic year

For further evaluation, we cumulated values for each year and compared hydrologic observations with best 100 hydrologic simulations. The results are shown in Figures S11, S12 and S13.

4. HYDRUS-1D - Model setup and dotty plots of Monte Carlo simulations

We use HYDRUS-1D with dual-porosity domain for which transfer is proportional to the effective saturation (Šimůnek et al., 2016). The model setup is summarized by Table S3. The soil is represented by a single layer. Input data comes with a daily temporal resolution. We modified precipitation input with the snow and interception routine of RoGeR. The partition of potential evapotranspiration in potential transpiration and potential soil evap-

oration is based on ground cover root depth (i.e. same values is for RoGeR). The potential root water uptake distribution is calculates as proposed by Hoffman and Van Genuchten (1983). Initial conditions for $\delta^{18}O$ of soil water are derived by a warmup period of 2 years (1997-1998). Initial soil water potentials are set to 100 hPa. Galerkin Finite Element method (Δz=2 cm) was used for the spatial discretization and Crank-Nicholson approach (Δt=0.01 day) was used for the temporal discretization. Convergence criteria is an absolute volumetric water tolerance of 0.001 for the unsaturated nodes and a pressure head tolerance of 1 cm for the saturated nodes.

In order to calculate forward travel time distributions and residence time distributions, we followed the approach described in Brinkmann et al. (2018). Since forward travel time distributions and backward travel time distributions relate to each other (Benettin et al., 2015), we calculate from forward travel time distributions the corresponding backward travel time distributions to enable a comparison with RoGeR. In order to avoid truncated travel time distributions, we skipped the first 1000 days to estimate backward travel time distributions.

We run 30 000 Monte Carlo simulations with HYDRUS-1D to derive a well performing parameter set which is used for benchmark simulations (see Table S3). Dotty plots of Monte Carlo simulations with HYDRUS-1D are exhibited in Figure S14. From the Monte Carlo simulations, we selected the best performing parameter set according to equation (10). This procedures provides robust and realistic parameter set (see Figure S14).

5. HYDRUS-1D - Soil water, $\delta^{18}O$ of soil water and mean residence time of soil water

The temporal evolution of soil water content (Figure S15) and $\delta^{18}O$ (Figure S16) in soil water simulated with HYDRUS-1D reveals that events with little precipitation stuck within the upper soil ($\leq$ 40 cm).

References

Benettin, P., Rinaldo, A., & Botter, G. (2015). Tracking residence times in hydrological systems: forward and backward formulations. *Hydrological Processes*, *29*(25), 5203-5213. Retrieved from `https://onlinelibrary.wiley.com/doi/abs/10.1002/hyp.10513` doi: https://doi.org/10.1002/hyp.10513

Brinkmann, N., Seeger, S., Weiler, M., Buchmann, N., Eugster, W., & Kahmen, A. (2018). Employing stable isotopes to determine the residence times of soil water and the temporal origin of water taken up by fagus sylvatica and picea abies in a temperate forest. *New Phytologist*, *219*(4), 1300-1313. Retrieved from `https://nph.onlinelibrary.wiley.com/doi/abs/10.1111/nph.15255` doi: https://doi.org/10.1111/nph.15255

Brooks, R. H., & Corey, A. T. (1966). Properties of porous media affecting fluid flow. *Journal of the Irrigation and Drainage Division*, *92*, 61-90.

Hoffman, G. J., & Van Genuchten, M. T. (1983). Soil properties and efficient water use: Water management for salinity control. *Limitations to Efficient Water Use in Crop Production*, 73-85.

Kumaraswamy, P. (1980). A generalized probability density function for double-bounded random processes. *Journal of Hydrology*, *46*(1), 79-88. Retrieved from `https://`

www.sciencedirect.com/science/article/pii/0022169480900360 doi: https://doi.org/10.1016/0022-1694(80)90036-0

Makkink, G. F. (1957). Testing the penman formula by means of lysimeters. *Journal of the Institution of Water Engineers*, *11*, 277-288.

Or, D., Lehmann, P., Shahraeeni, E., & Shokri, N. (2013). Advances in soil evaporation physics—a review. *Vadose Zone Journal*, *12*(4), vzj2012.0163. Retrieved from https://acsess.onlinelibrary.wiley.com/doi/abs/10.2136/vzj2012.0163 doi: https://doi.org/10.2136/vzj2012.0163

Salvucci, G. D. (1993). An approximate solution for steady vertical flux of moisture through an unsaturated homogeneous soil. *Water Resources Research*, *29*(11), 3749-3753. Retrieved from https://agupubs.onlinelibrary.wiley.com/doi/abs/10.1029/93WR02068 doi: https://doi.org/10.1029/93WR02068

Steinbrich, A., Leistert, H., & Weiler, M. (2016, Nov 02). Model-based quantification of runoff generation processes at high spatial and temporal resolution. *Environmental Earth Sciences*, *75*(21), 1423. Retrieved from https://doi.org/10.1007/s12665-016-6234-9 doi: https://doi.org/10.1007/s12665-016-6234-9

Weiler, M. (2005). An infiltration model based on flow variability in macropores: development, sensitivity analysis and applications. *Journal of Hydrology*, *310*(1), 294-315. Retrieved from https://www.sciencedirect.com/science/article/pii/S0022169405000132 doi: https://doi.org/10.1016/j.jhydrol.2005.01.010

Šimůnek, J., van Genuchten, M. T., & Šejna, M. (2016). Recent developments and applications of the hydrus computer software packages. *Vadose Zone Journal*, *15*(7), vzj2016.04.0033. Retrieved from https://acsess.onlinelibrary.wiley.com/doi/

abs/10.2136/vzj2016.04.0033 doi: https://doi.org/10.2136/vzj2016.04.0033

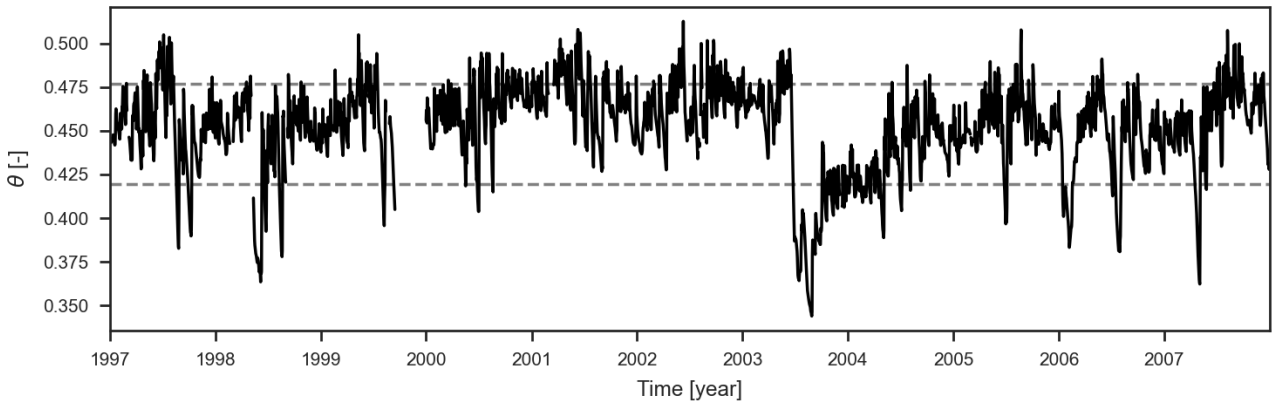

Figure S1. Moving average (5 days) of observed soil water content to define antecedent soil moisture conditions.

Table S1. Surface parameters and root depth of RoGeR for land use class grass (`lu_id`=8)

	Jan	Feb	Mar	Apr	May	Jun	Jul	Aug	Sep	Oct	Nov	Dec
$f_{ground-cover}$ [-]	0.51	0.51	0.66	0.76	0.83	0.83	0.83	0.83	0.83	0.66	0.59	0.51
LAI [-]	2	2	3	4	5	5	5	5	5	3	2.5	2
$S_{int-lower-tot}$ [mm]	0.4	0.4	0.6	0.8	1	1	1	1	1	0.6	0.5	0.4
z_{root} [mm]	400	400	400	400	400	400	400	400	400	400	400	400

Table S2. Constant model parameters of RoGeR

Constant parameters		**Unit**	**Value**
Degree-day factor	s_f	-	3
Threshold air temperature of freeze/melt	ta_{fm}	degC	0
Retention capacity of liquid water in snow cover	r_{max}	%	30
Threshold duration of no rainfall/snow melt	$t_{end-event}$	h	5
Threshold for classification of heavy rainfall event	hpi	mm 10 min^{-1}	5
Radius of macropores	r_{mp}	mm	2.5
Maximum length of shrinkage cracks	l_{sc}	mm m^{-2}	10000
Parameter for Brooks-Corey	a_{bc}	-	2
Parameter for Brooks-Corey	b_{bc}	-	2
Fraction for plant water stress	f_{pwt}	-	0.75

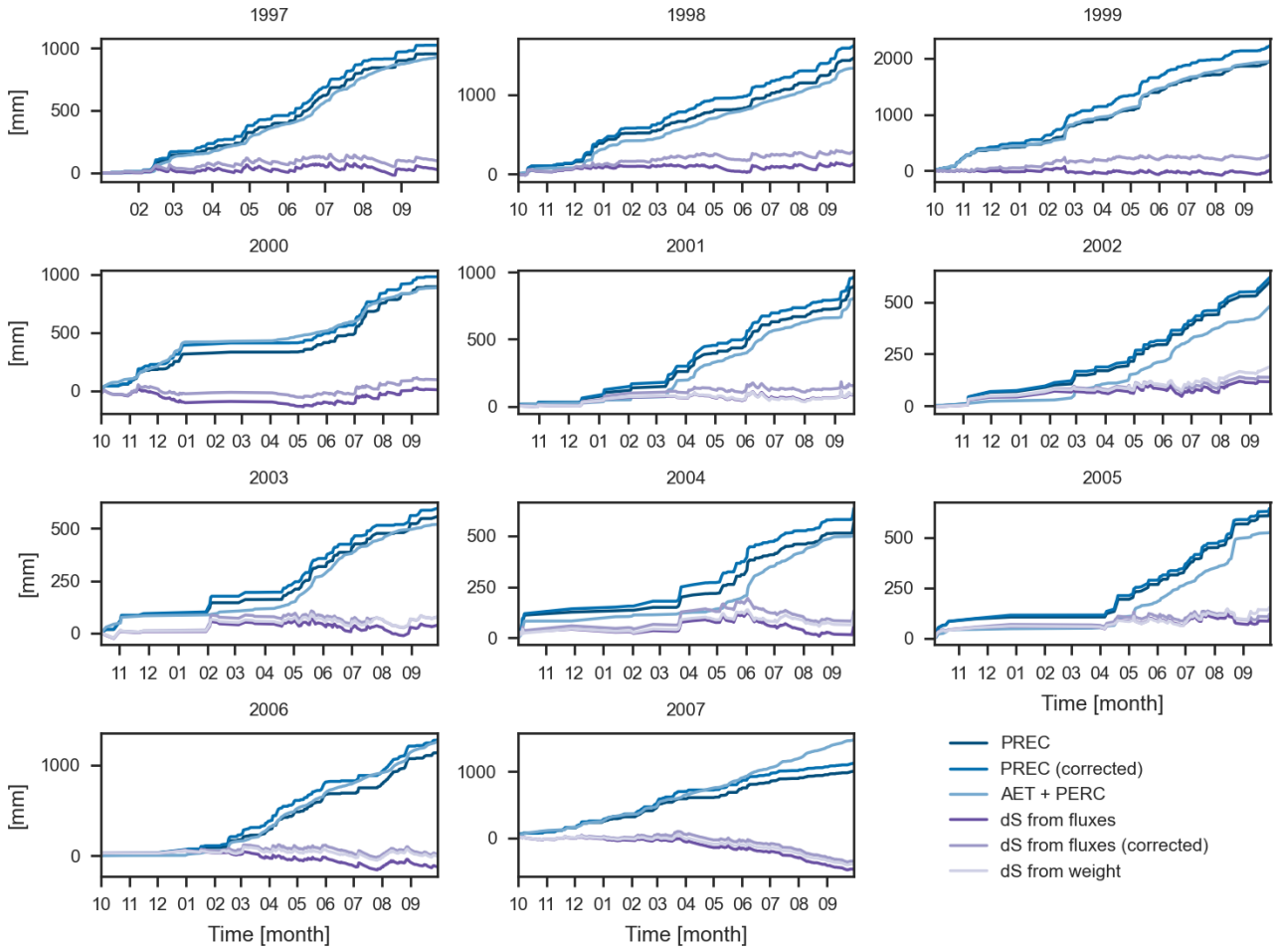

Figure S2. Cumulated values per hydrologic year of measured precipitation, evapotranspiration, storage change and lysimeter seepage at Rietholzbach lysimeter from 1997 to 2007.

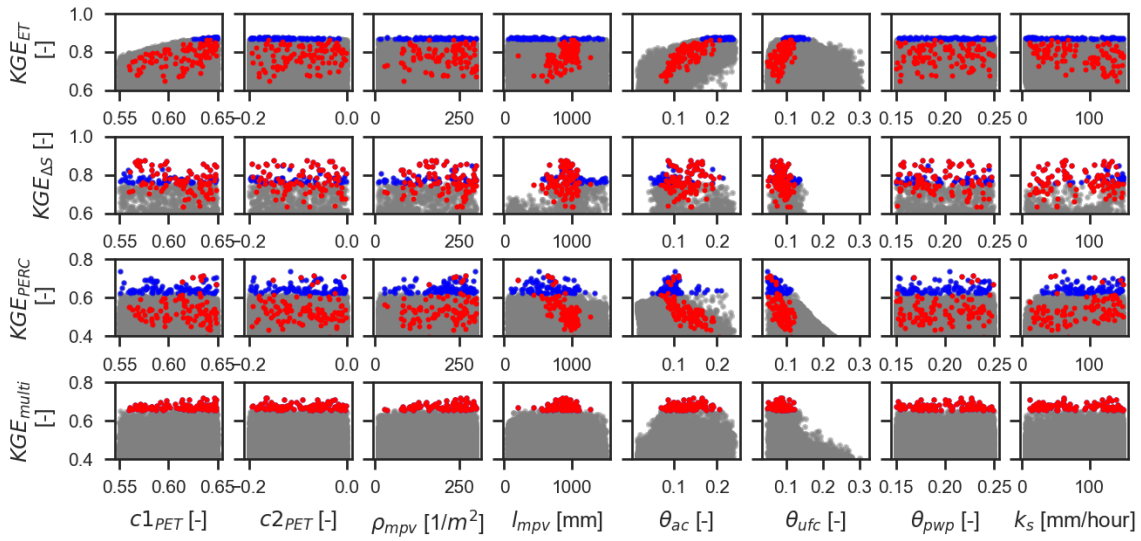

Figure S3. Dotty plots of Monte Carlo simulations with RoGeR. Red dots indicate best 100 simulations according to E_{multi} and blue dots show best 100 simulations for the corresponding metric.

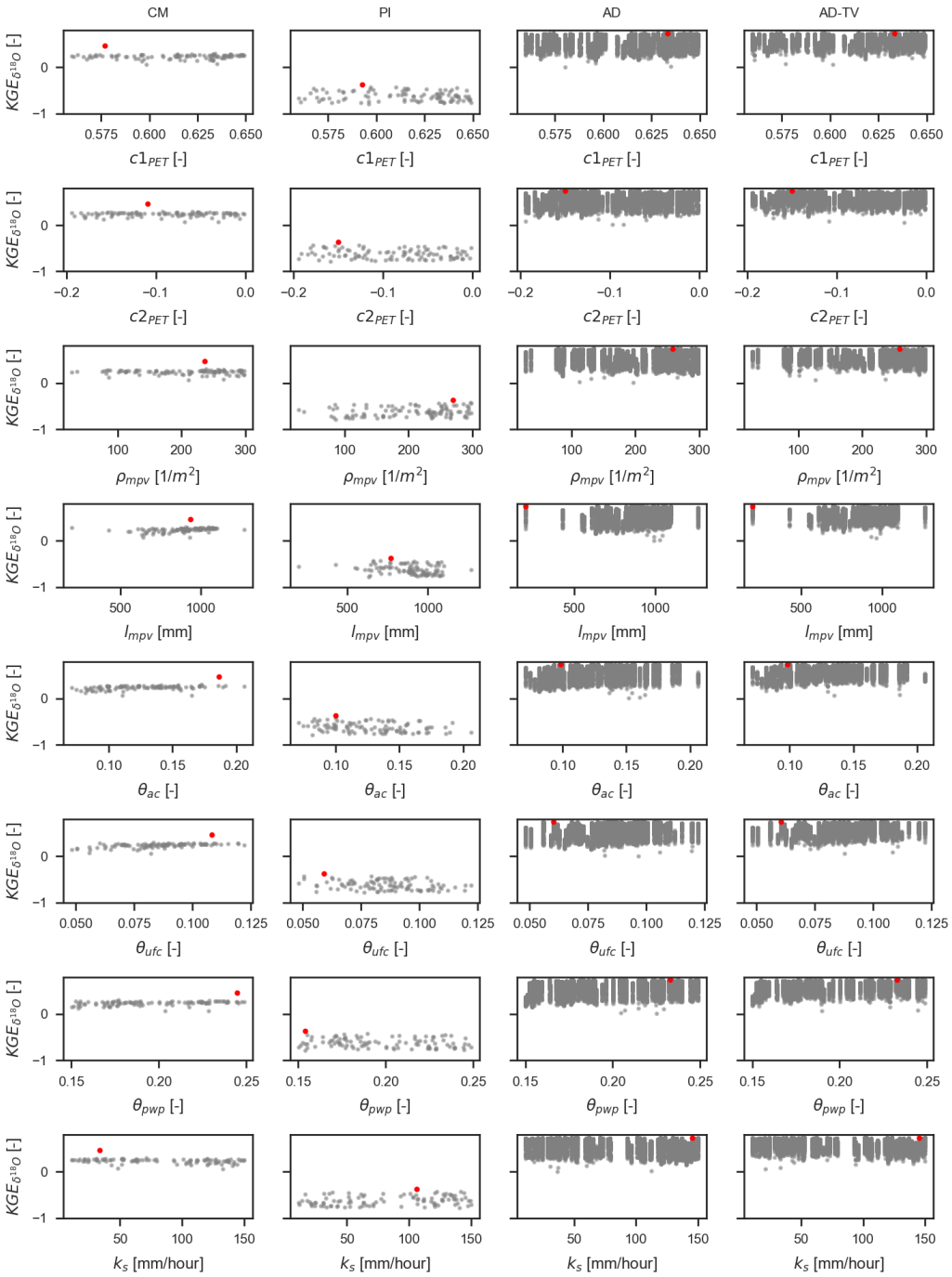

Figure S4. Dotty plots of hydrologic model parameters for Monte Carlo $\delta^{18}O$ simulations with RoGeR. Red dot indicates best simulations according to KGE.

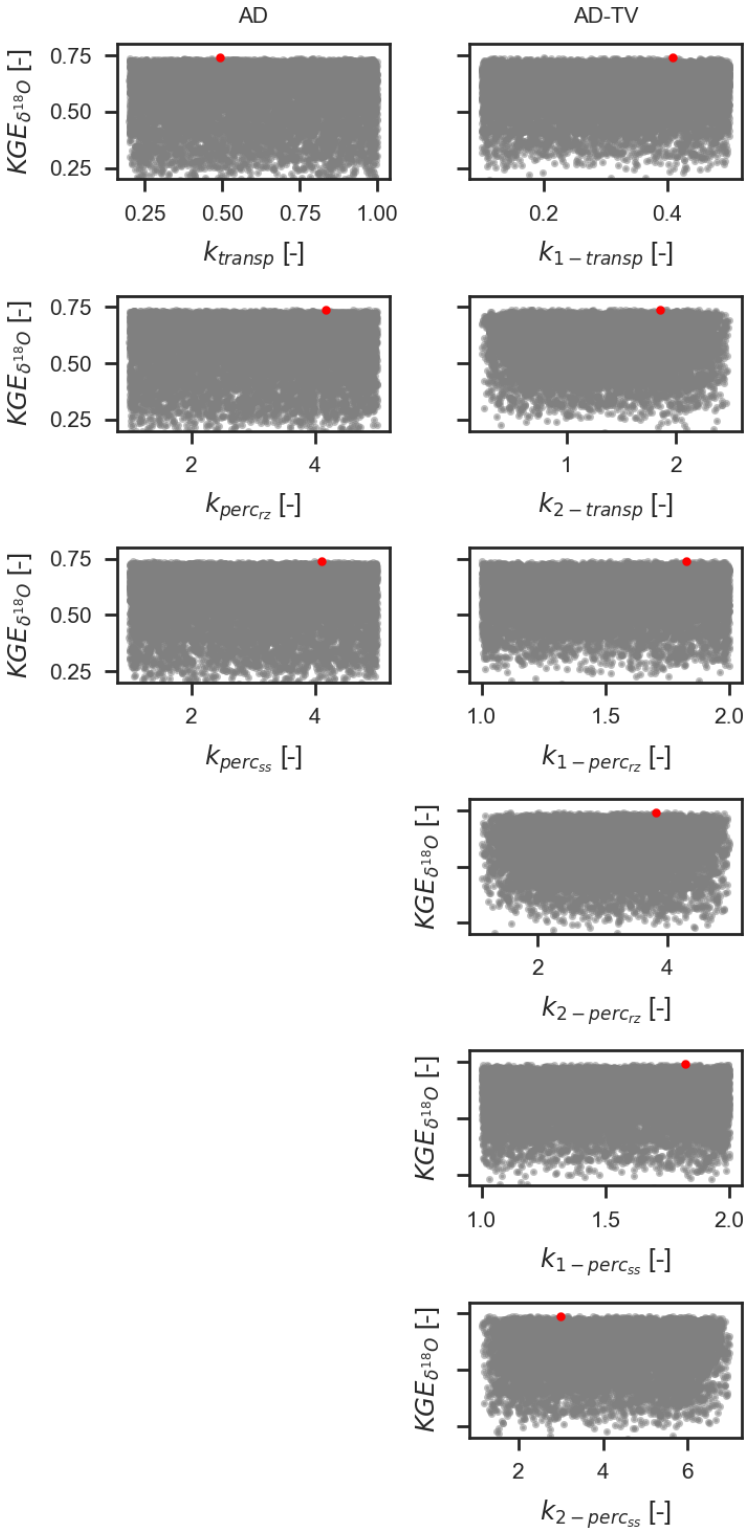

Figure S5. Dotty plots of SAS parameters for Monte Carlo $\delta^{18}O$ simulations with RoGeR. The red dot indicates best simulations according to KGE.

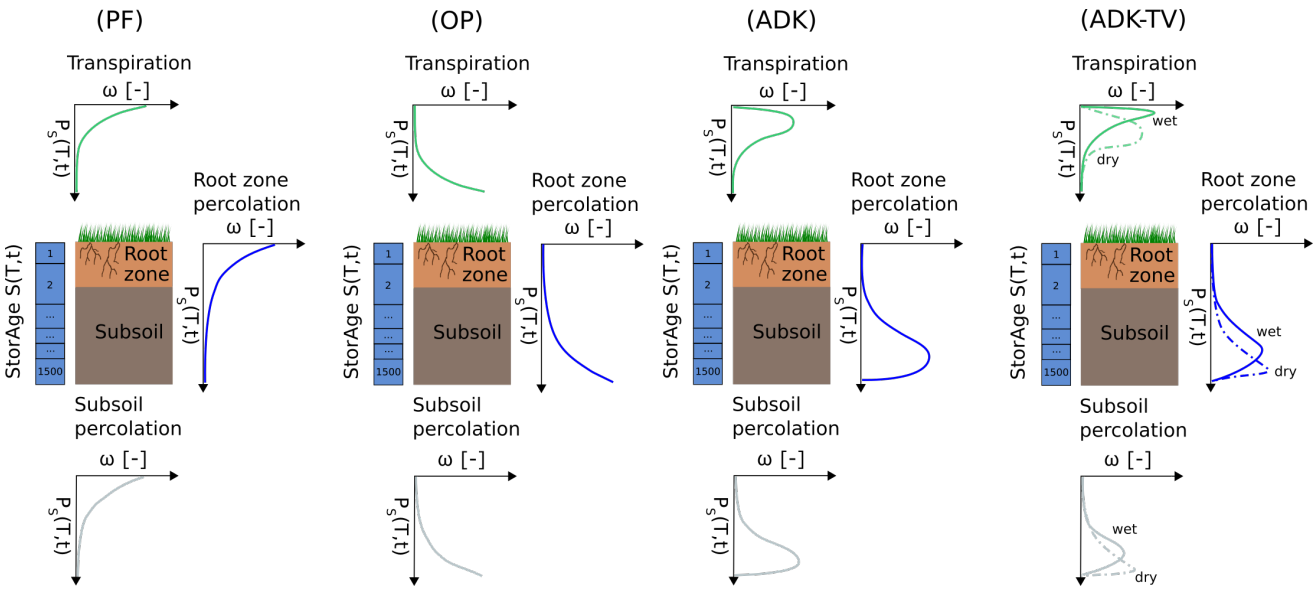

Figure S6. Additional transport model structures: Preferential transport model (PF), Old-preference transport model (OP), Advection-dispersion transport model using a Kumaraswamy distribution function (ADK) and Advection-dispersion transport model with time-variant SAS parameters using a Kumaraswamy distribution function (ADK-TV).

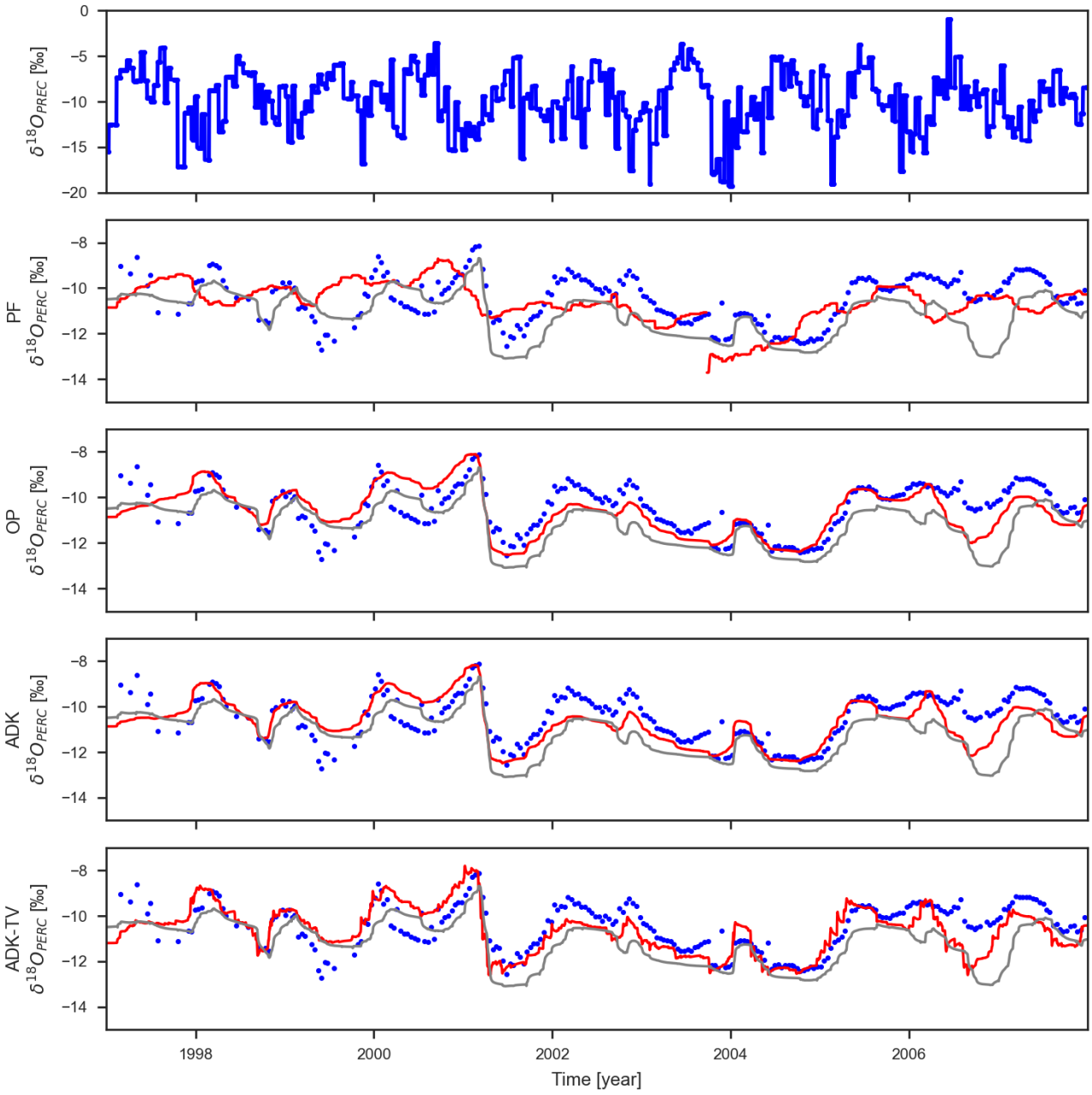

Figure S7. Observed $\delta^{18}O$ in precipitation and observed (blue) and simulated $\delta^{18}O$ in percolation with RoGeR (red) and HYDRUS-1D (grey). Values are shown for different model structures (see Figure S6).

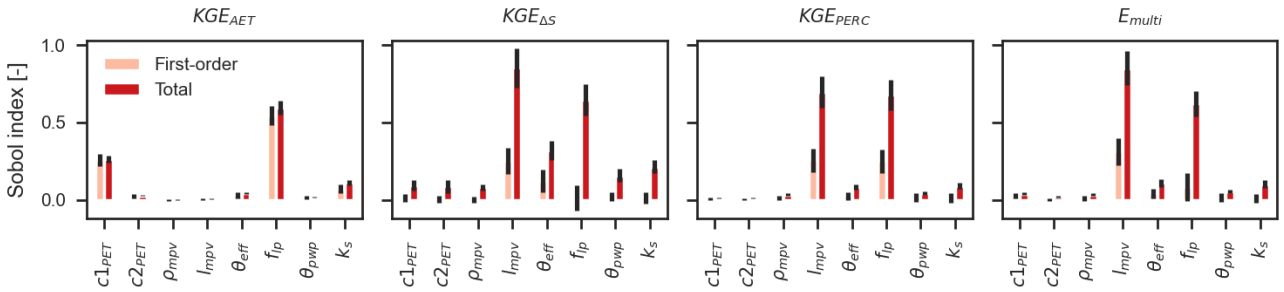

Figure S8. Sobol' indices of hydrologic model parameters calculated for KGE of evapotranspiration, storage change, percolation and multi-objective criteria.

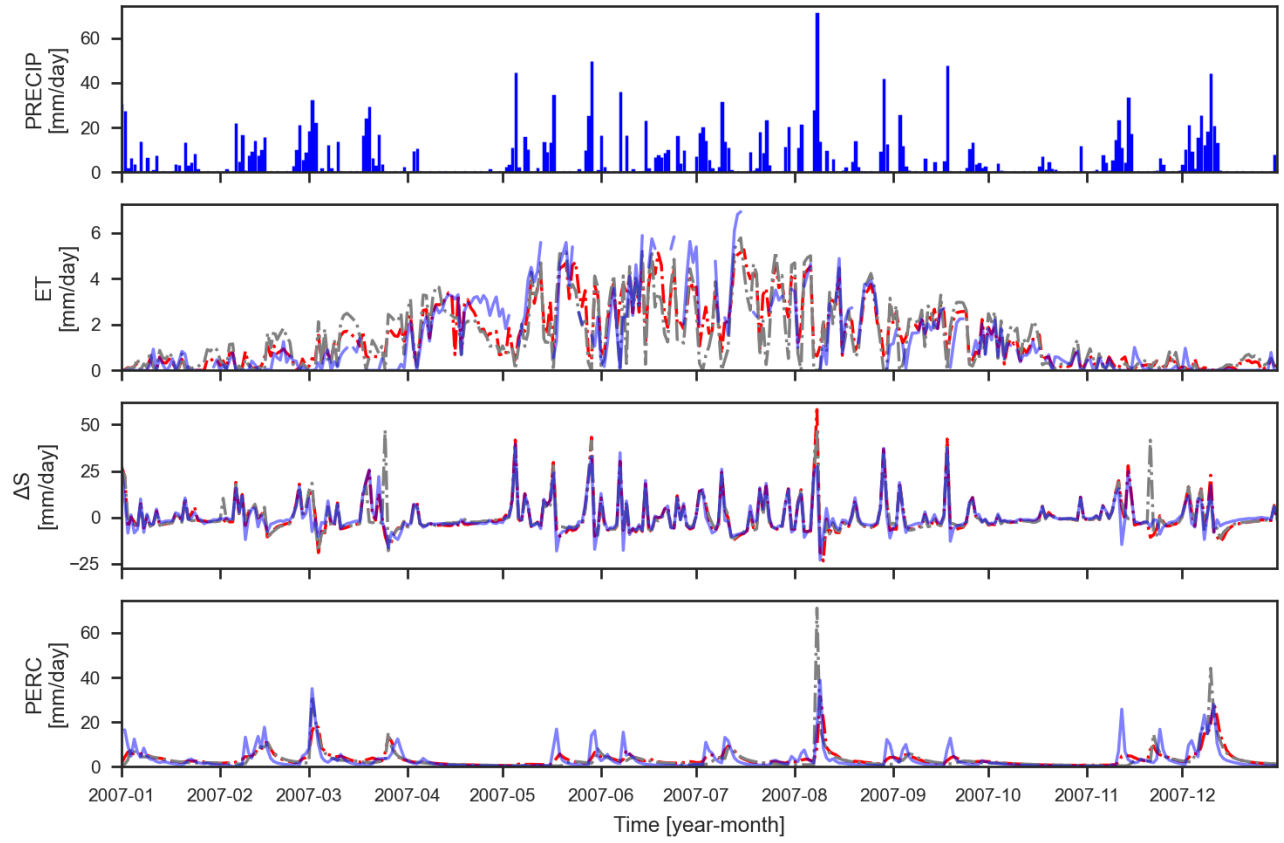

Figure S9. Comparison of observed (blue), simulated values with RoGeR (red) and simulated values with HYDRUS-1D (grey) in year 2007. Simulated values are shown for best parameter set according to E_{multi} or KGE_{multi}, respectively.

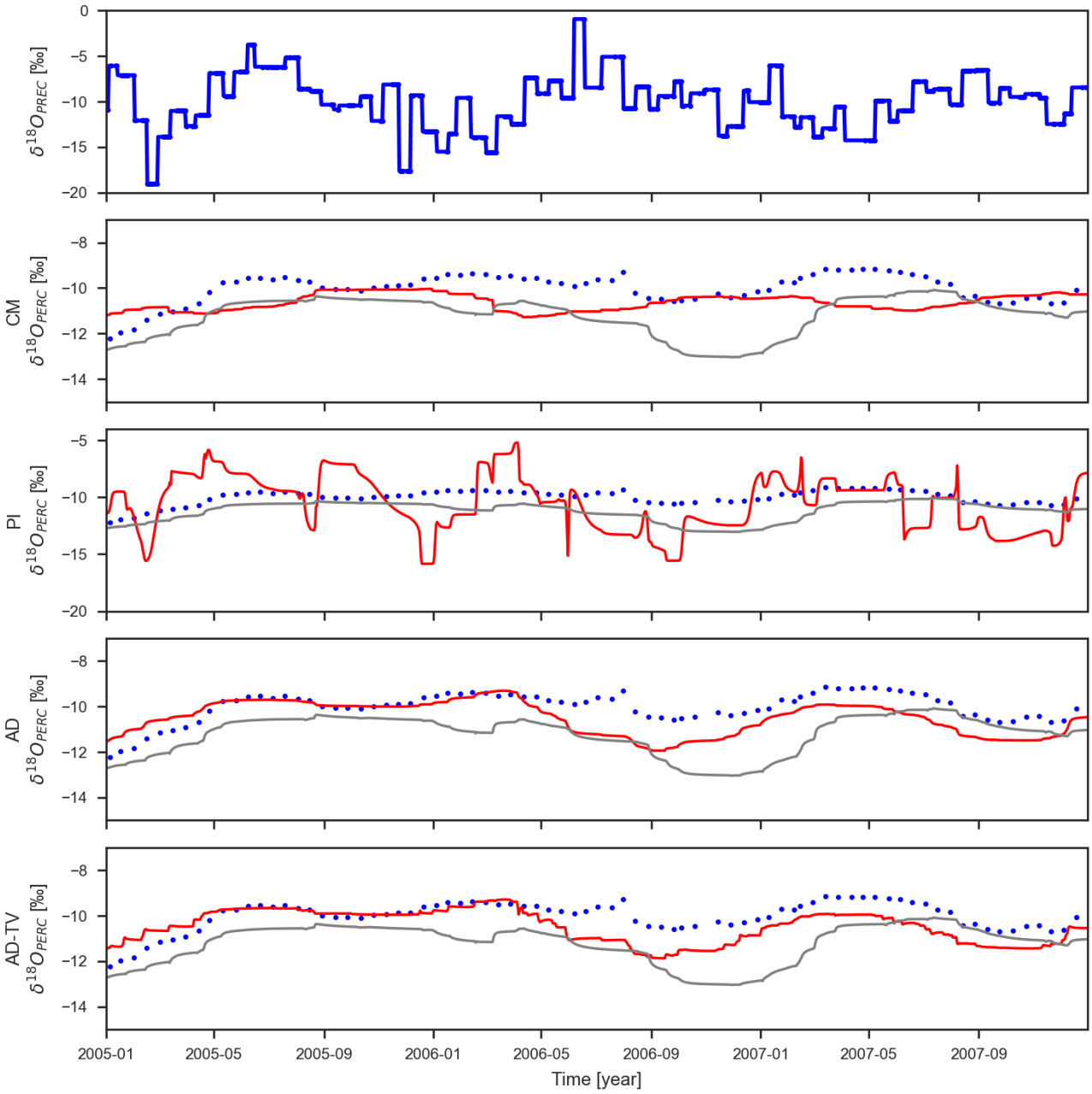

Figure S10. Comparison of observed (blue) and simulated $\delta^{18}O$ in percolation (red) in years 2005-2007. Simulated values are shown for best parameter set according to $KGE_{\delta^{18}O}$. The grey line indicates the benchmark simulation with HYDRUS-1D.

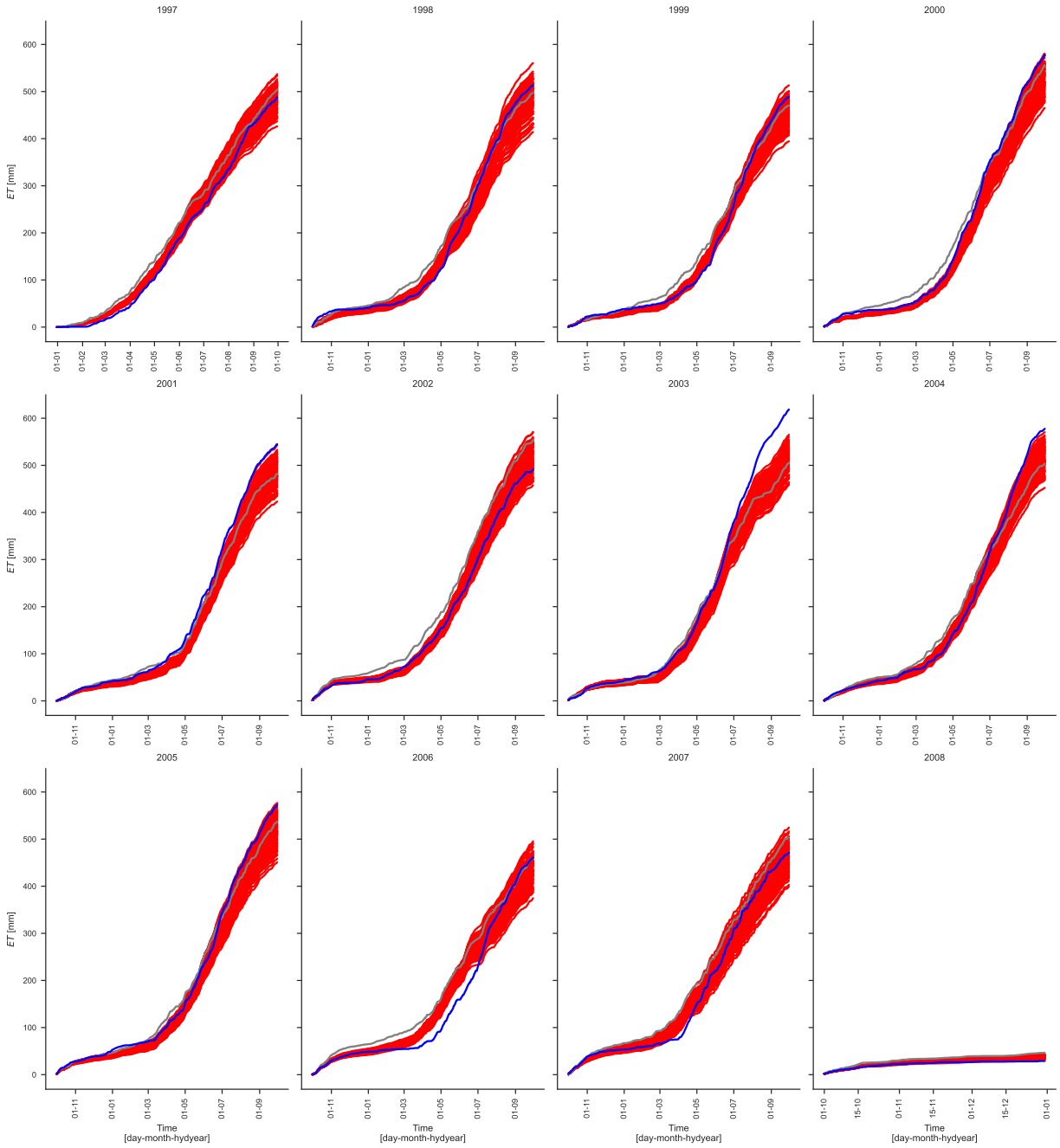

Figure S11. Comparison of cumulated observed evapotranspiration (blue) and simulated evapotranspiration (red) shown for best 100 simulations according to E_{multi}. Values are cumulated for each hydrologic year. The grey line indicates the benchmark simulation with HYDRUS-1D.

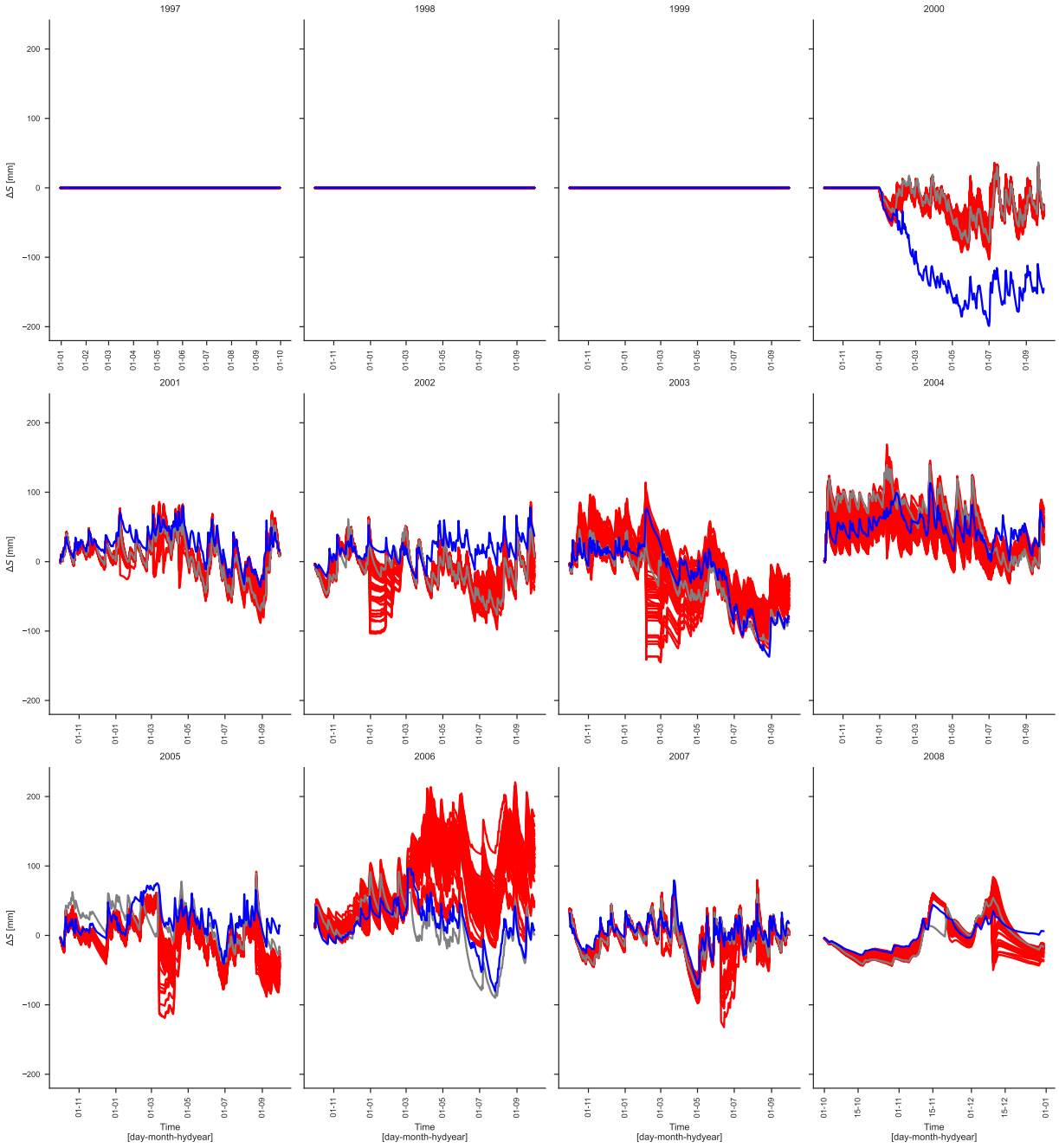

Figure S12. Comparison of cumulated storage change (blue) and simulated storage change (red) shown for best 100 simulations according to E_{multi}. Values are cumulated for each hydrologic year. The grey line indicates the benchmark simulation with HYDRUS-1D. From 1997 to 1999 no observations on storage change were available.

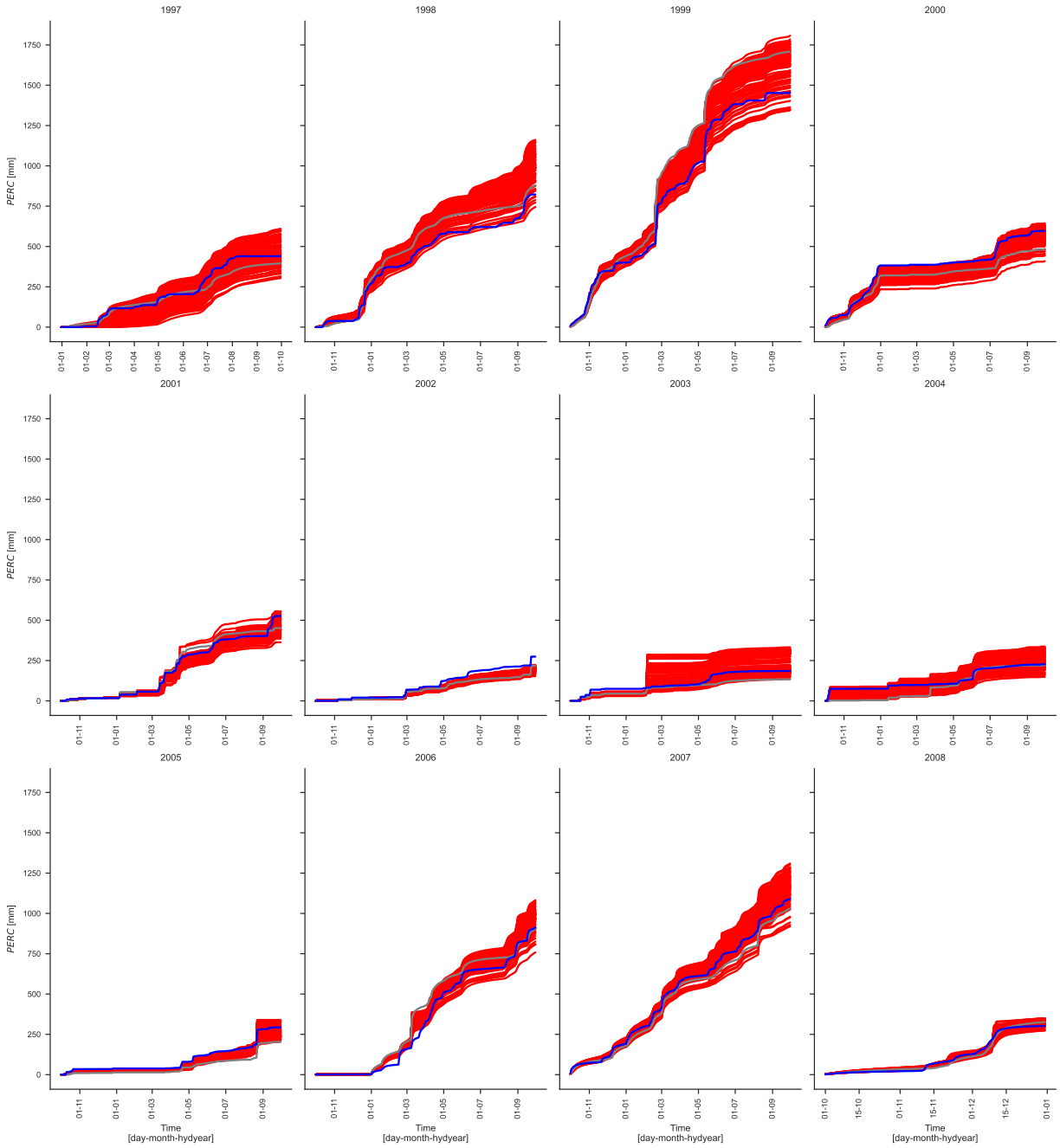

Figure S13. Comparison of cumulated percolation (blue) and simulated percolation (red) shown for best 100 simulations according to E_{multi}. Values are cumulated for each hydrologic year. The grey line indicates the benchmark simulation with HYDRUS-1D.

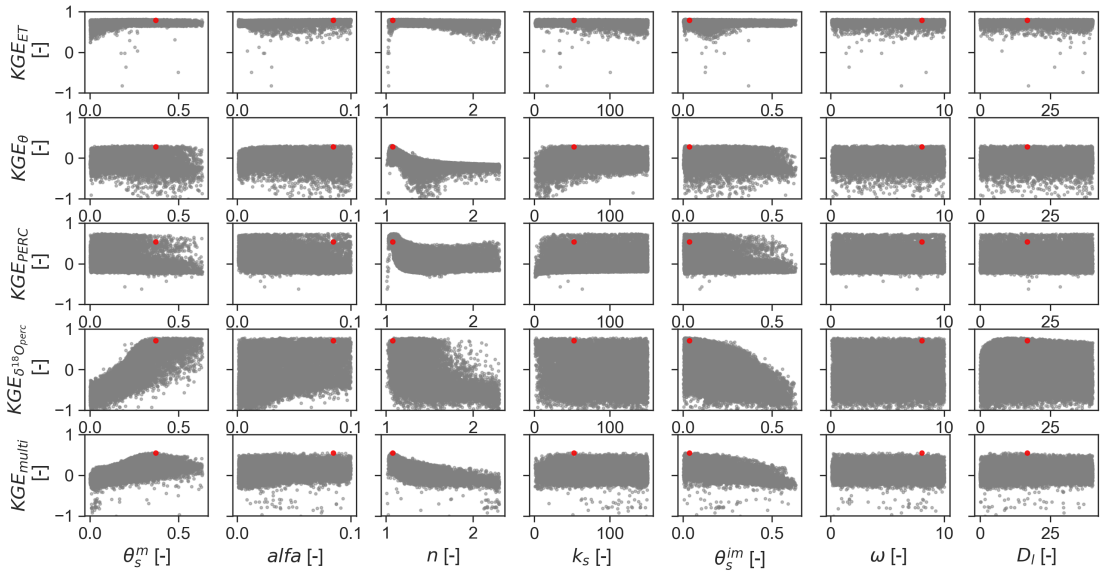

Figure S14. Dotty plots of Monte Carlo simulations with HYDRUS-1D. Red dot indicates best simulation according to KGE_{multi}.

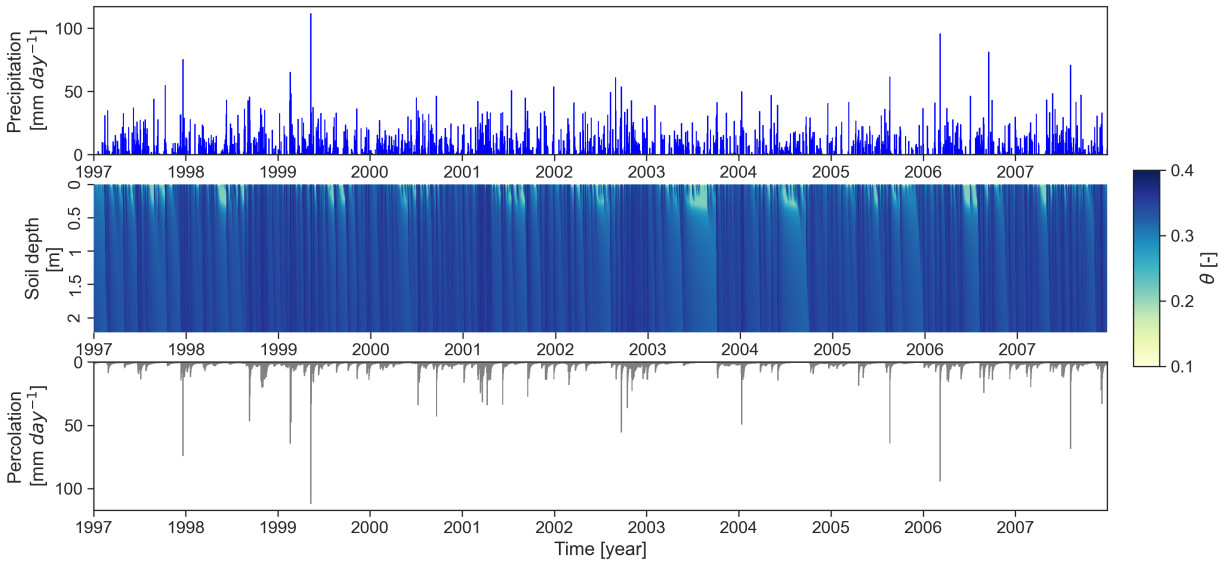

Figure S15. Precipitation, simulated soil water content and simulated percolation with HYDRUS-1D.

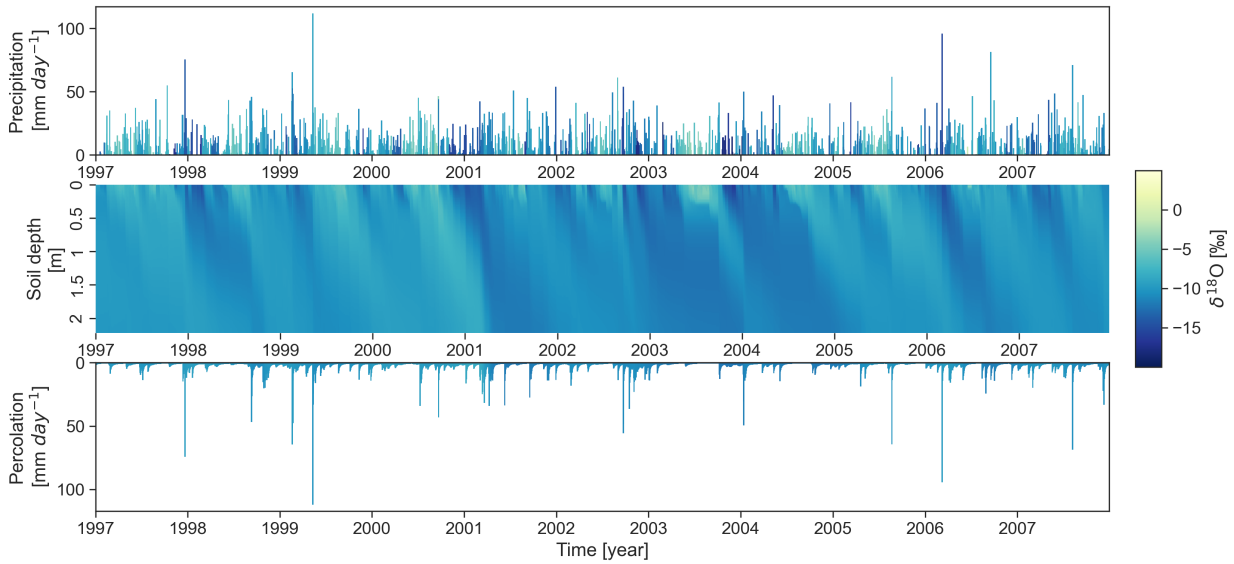

Figure S16. $\delta^{18}O$ of precipitation, simulated $\delta^{18}O$ of soil water and $\delta^{18}O$ of simulated percolation with HYDRUS-1D.

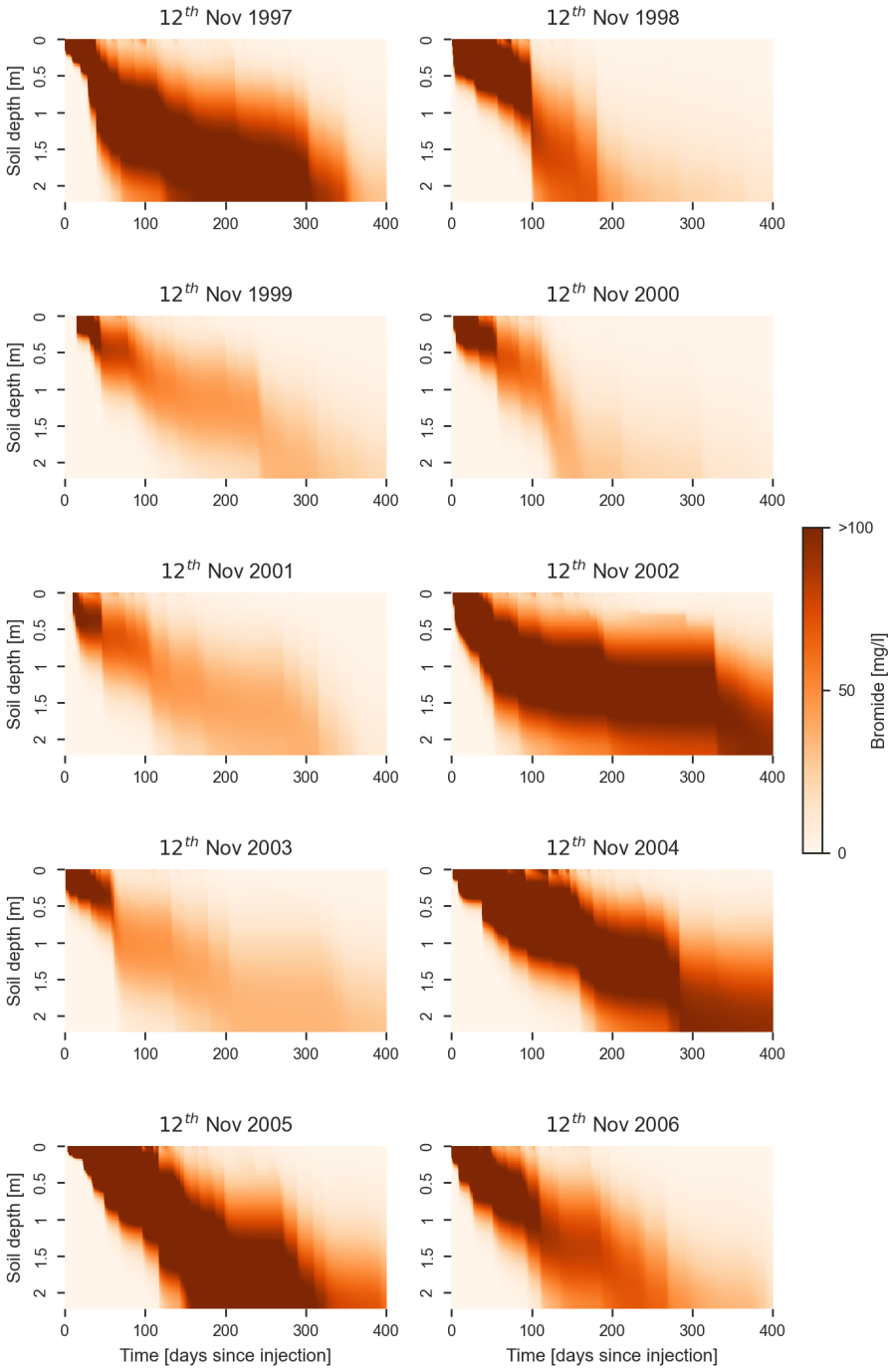

Figure S17. Simulated bromide concentrations of soil water with HYDRUS-1D

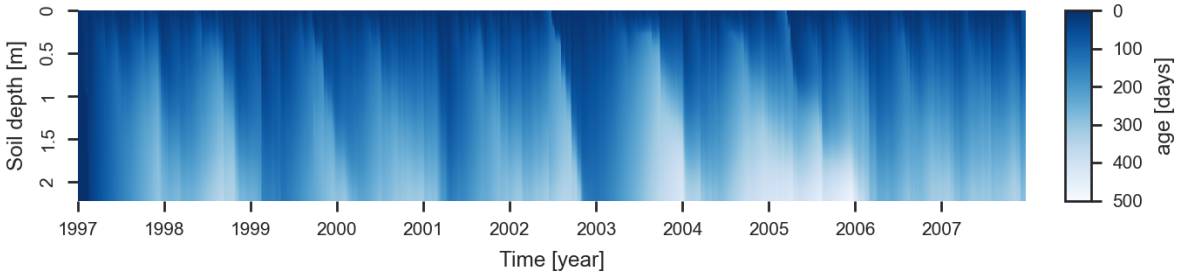

Figure S18. Mean residence time of soil water simulated with HYDRUS-1D.

Table S3. Parameters of HYDRUS-1D with dual-porosity domain

Model parameter		Unit	Parameter boundaries	Best parameter
Vertical discretization	Δz	cm	2	2
Soil depth	z_{soil}	cm	220	220
Effective porosity	θ_{eff}	-	0.15 - 0.65	0.47
Fraction of mobile region	f_m	-	0.01 - 0.99	0.86
Fraction of immobile region	f_{im}	-	1 - f_m	0.14
Residual water content for the mobile region	θ_r^m	-	0	0
Saturated water content for the mobile region	θ_s^m	-	$\theta_{eff} \cdot f_m$	0.40
Parameter in the soil water retention function	$alfa$	cm^{-1}	0.001 - 0.1	0.04
Exponent in the soil water retention function	n	-	1.01 - 2.3	1.07
Saturated hydraulic conductivity	k_s	cm day^{-1}	2.4 - 360	200.9
Pore-connectivity parameter	l	-	0.5	0.5
Residual water content for the immobile region	θ_r^{im}	-	0	0
Saturated water content for the immobile region	θ_s^{im}	-	$\theta_{eff} \cdot f_{im}$	0.07
First-order rate coefficient in the water mass transfer equation	ω	day^{-1}	0.1 - 10	2.54
Bulk density of porous medium	ρ	$g\ cm^{-3}$	1.5	1.5
Longitudinal dispersivity	D_l	cm	0 - 40	7.55
Dimensionless fraction of the adsorption sites	f_{mo}	-	1	1
Physical nonequilibrium[a]		-	0	0

[a] Set equal to 0 when the physical nonequilibrium option is not considered.